FLOW-INDUCED VIBRATION OF BELLOWS WITH INTERNAL CRYOGENIC FLUID FLOWS

by

C. R. Gerlach
R. L. Bass, III
J. L. Holster
E. C. Schroeder

Interim Technical Report No. 2
Contract No. NAS8-21133
Control No. DCN 1-7-52-20017 (IF)
SwRI Project No. 02-2119

Prepared for

National Aeronautics and Space Administration
George C. Marshall Space Flight Center
Marshall Space Flight Center, Alabama 35812

August 1970

N71-13081 (ACCESSION NUMBER) (THRU)
89 (PAGES) (CODE)
CR-102 935 (NASA CR OR TMX OR AD NUMBER) 12 (CATEGORY)
FACILITY FORM 602

SOUTHWEST RESEARCH INSTITUTE
SAN ANTONIO HOUSTON

Reproduced by
NATIONAL TECHNICAL
INFORMATION SERVICE
Springfield, Va. 22151

N71-13081

SOUTHWEST RESEARCH INSTITUTE
Post Office Drawer 28510, 8500 Culebra Road
San Antonio, Texas 78228

FLOW-INDUCED VIBRATION OF BELLOWS WITH INTERNAL CRYOGENIC FLUID FLOWS

by

C. R. Gerlach
R. L. Bass, III
J. L. Holster
E. C. Schroeder

Interim Technical Report No. 2
Contract No. NAS8-21133
Control No. DCN 1-7-52-20017 (IF)
SwRI Project No. 02-2119

Prepared for

National Aeronautics and Space Administration
George C. Marshall Space Flight Center
Marshall Space Flight Center, Alabama 35812

August 1970

Approved:

H. Norman Abramson, Director
Department of Mechanical Sciences

REPRODUCED BY
U.S. DEPARTMENT OF COMMERCE
NATIONAL TECHNICAL INFORMATION SERVICE

PRECEDING PAGE BLANK NOT FILMED

TABLE OF CONTENTS

Preceding page blank

Table of Contents...Cont'd.

I. INTRODUCTION

This report summarizes all work performed by Southwest Research Institute during the past one-year period to study the effect of cryogenic fluid flow on the flow-induced vibration of bellows. The work was conducted under Contract NAS8-21133, "Study of Minimum Pressure Loss in High Velocity Duct Systems," and results reported herein supplement earlier work described in Interim Technical Report No. 1 (Reference 1) published 16 July 1969 on the same contract. During this same time period, investigations of acoustical resonance phenomena, as they affect bellows vibrations, were also undertaken, and preliminary results will be presented in a subsequent report.

This study is being performed for the George C. Marshall Space Flight Center of the National Aeronautics and Space Administration, administered technically by the Propulsion and Vehicle Engineering Laboratory with Mr. R. H. Veitch serving as Technical Manager.

Objective and Scope of Work

The objective of this investigation is to perform a theoretical and experimental study of heat transfer with respect to its effect on the flow-induced response of bellows when gas is formed in the convolutes and/or frost or liquid accumulates on the bellows exterior. The following questions are typical of those discussed in this report:

(a) How does bellows response in liquid nitrogen (LN_2) compare to test results for water and air?

(b) In practical situations, can heat transfer change the physical properties of the fluid in the bellows convolutions sufficiently to influence the vortex excitation phenomena?

(c) If heat transfer does have an effect under certain conditions, can these conditions be predicted and how do they relate to the physical properties of the cryogenic liquid?

(d) What effect does the external buildup of ice, slush and liquid have on the problem?

(e) What influence do changes in convolution geometry have on a possible heat transfer effect?

(f) What is the most realistic, and/or severe, method of testing a bellows to account for possible heat transfer and external damping effects; that is, what test procedure will most likely show failure-prone bellows?

II. BACKGROUND DISCUSSION

II. 1 Introduction

The occurrence of flow-induced vibrations of metal bellows contained in fluid ducting systems has, for some time, been a problem for aerospace applications. There are known instances where flow-induced vibrations of bellows have resulted in fatigue failures which forced the premature shutdown of some critical fluid systems. The most common methods for correcting unsuccessful bellows installations have been either to install an internal liner, where possible, or to use multiple plys or thicknesses of metal when constructing the bellows. Unfortunately, increasing the number of metal plys has not always cured the flow-induced vibration problem, and the use of a bellow's liner generally leads to an increase in component weight and cost. A major obstacle prior to the initiation of the present effort was that the flow mechanism which causes bellows vibration had not been described or understood, so that flow-induced failures could be anticipated. From the standpoint of the designer, a desirable goal was to have available an analytical procedure allowing the prediction of critical fluid flow ranges for a given bellows configuration and, further, giving a method for estimating stress levels resulting from the flow excitation in these critical ranges.

Most of the current knowledge of bellows flow-induced vibrations is presented in detail in Reference 1 prepared under the current contract. This state-of-the-art of bellows vibrations was derived from experimental and analytical studies of free bellows, and flex hose, in a size range equal to or less than 2 inches internal diameter. This effort dealt primarily with water flows and has resulted in development of a very acceptable analytical model of bellows flow-induced vibrations. Still, the work is not complete in that, (a) the results have not been verified for bellows of sizes greater than 2 inches and for the entire range of geometries typical of current stage hardware practices, and (b) the results are not adequate for gas flows where acoustical resonances have been shown to have a significant influence; these areas are currently under investigation.

Another area of significant importance is where cryogenic liquids are the flow media, so that heat transfer and/or external damping play an important role. The importance of this subject was discovered from investigations into the cause of a flex hose failure (J-2 engine, ASI fuel line) on Saturn flight AS-502; this is reported by Daniels and Fargo in Reference 2. The results of these authors, however, left unanswered questions as to the relative importance of heat transfer as it affects the flow excitation process, and external damping caused by frost and liquid condensation on the bellows.

The present report discusses these two possible flow-excitation suppression mechanisms and, we feel, clears up the inconsistencies and unanswered questions brought forth in Reference 2.

II.2 Bellows Flow-Induced Vibration Model

Figure 1 illustrates the fluid and structural dynamics involved in bellows flow excitation. The process of periodic vortex formation and shedding causes a corresponding periodic pressure to be exerted on the convolutions. The amplitude of this alternating pressure is proportional to the free-stream stagnation pressure ($1/2\ \rho_f V^2$). So far as the bellows structure is concerned, the effect of this alternating pressure may be considered as a net force applied at the tip of each convolution, as shown in Figure 1. The amplitude of this force is assumed to be of the form

$$F = C_F A_P (1/2\ \rho_f V^2) \tag{1}$$

where C_F is a vortex force coefficient (a dimensionless coefficient) and A_P is the projected convolute height area over which the pressure acts (the fluctuating pressure producing the force).

If the frequency of the vortex shedding coincides with some bellows mode frequency, then a resonance will occur and the bellows convolutions will experience a vibratory displacement, as illustrated in Figure 1, of the form

$$x = \frac{C_m F Q}{K_A} \tag{2}$$

In equation (2), C_m is a dimensionless factor dependent on the bellows mode of vibration (mode factor), F is the vortex shedding force defined in Equation (1), K_A is the bellows overall spring rate, and Q is the dynamic amplification factor (damping). This convolution vibratory displacement x will cause a corresponding stress, and the magnitude of this stress is dependent on the convolution geometry, as illustrated in Figure 1.

Accepting this simple concept of bellows vibration resulting from a coupling with the vortex shedding, the problem of calculating resultant dynamic stress levels boils down to one of requiring a forehand knowledge of the various "factors" illustrated in Figure 1. The primary factors are: C_F, a vortex force coefficient; C_m a vibration mode factor; Q a dynamic

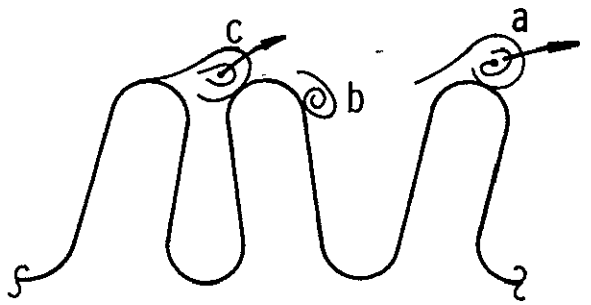

Vortex Shedding From Convolutions

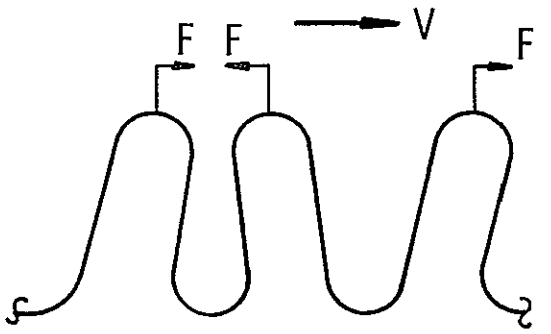

Vortex Force

$$F = C_F C_E A_p \left(\frac{1}{2} \rho V^2 \right)$$

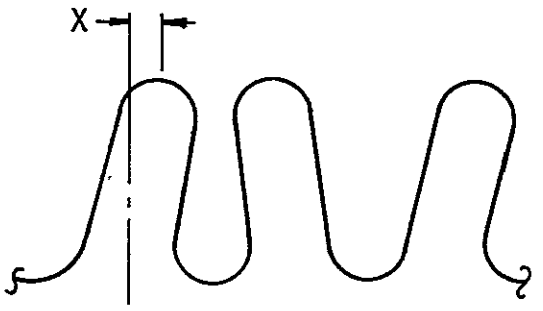

Convolution Displacement

$$x = \frac{C_m F Q}{k_A}$$

The resultant stress is

$$\text{Stress} = \frac{C_S E t x}{h^2}$$

In the above equations

C_F = vortex force coefficient
C_E = elbow factor
C_m = vibration mode factor
Q = dynamic amplification (damping)
C_S = geometric stress factor

2331

Figure 1. Illustration Of Stress Resulting From Vortex Force

amplification factor; and C_s, a geometric stress factor. Other factors may also be introduced to account for various unique situations. For example, when an elbow is located upstream of a bellows, this can have an effect and cause higher-than-normal stress levels for a given flow velocity. This can be accounted for by an "elbow factor" C_E, as indicated in Figure 1. If an acoustic resonance exists, this can change the picture, also.

Mode Factor C_m

In Reference 1, an analysis was presented showing that the mode factor C_m is of the form

$$C_m = \frac{1}{8N} \left\{ \frac{N}{N_c} + \sin \left(\frac{\pi N}{2N_c} \right) \right\} \tag{3}$$

This equation takes into account the fact that only one convolute per wavelength of the longitudinal vibration mode has an effective vortex shedding force imposed on it. Also, Equation (3) accounts for the form of the axial distribution of convolute displacement (mode shape).

Dynamic Amplification Factor Q

Our current knowledge of the dynamic amplification factor for bellows is fairly good for sizes up to about 2 inches. A large number of experiments have been conducted in which bellows were excited with an electromechanical shaker to determine response amplitude as a function of frequency. This data was then reduced to obtain Q values for a variety of bellows configurations, including 1, 2 and 3 ply, and with various internal fluids. This data was finally reduced to a single plot, shown in Figure 2, which gives Q values in terms of a unique and easily calculated "bellows operational parameter."

Vortex Force Coefficient C_F

Values for the vortex force coefficient have, to date, been obtained entirely from experiments. This is accomplished in a very straightforward manner by doing the following:

(a) The bellows is strain gaged and then "calibrated" to obtain force-deflection and strain-deflection curves.

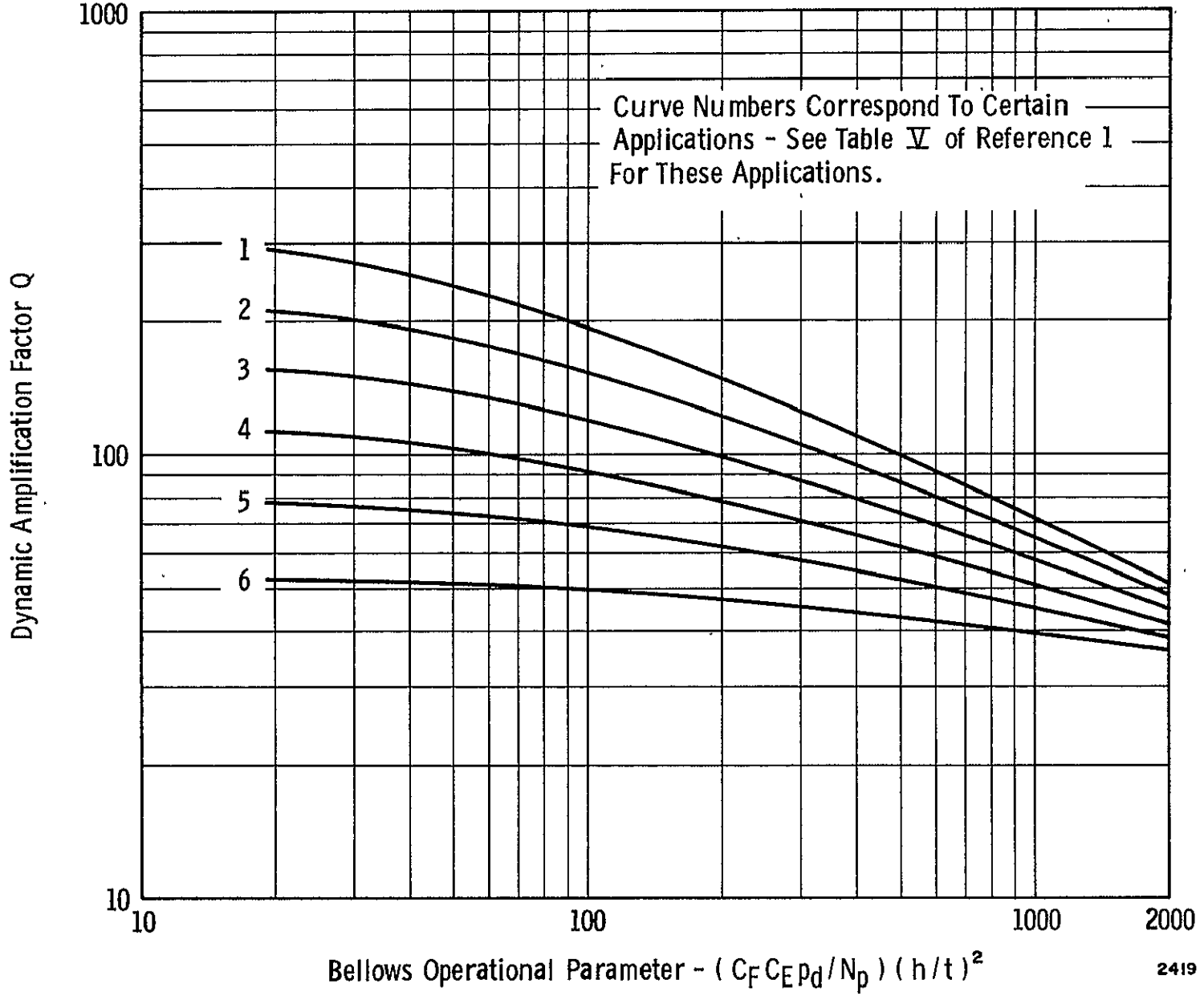

Figure 2. Dynamic Amplification Factors For Various Bellows Applications

(b) Next the bellows is mechanically excited on a shaker to obtain sufficient response data to yield a Q value. This step may be omitted if the bellows is close enough in configuration to bellows for which Q values have already been established.

(c) The bellows is next subjected to a flow test and dynamic strain versus flow velocity data is obtained.

(d) Finally, the data is reduced using the analytical model, represented by Equations (1) and (2), to obtain a value for C_F. This is easily done at this point since all quantities except C_F are known (x can be obtained from the observed dynamic strain data using the "calibration factor" for strain-deflection determined previously).

Figure 3 shows a summary of the vortex force coefficient data obtained to date for bellows of about 2 inches I.D.

II.3 Stress Indicator Parameter

As discussed in Reference 1, a special "Stress Indicator" has been developed to aid in rapidly judging the severity of bellows flow-induced vibrations. This parameter is essentially an approximation of the "Best Model" for bellows vibrations described briefly above, and is given by

$$\text{Stress Indicator} = \left(\frac{C_F Q}{N_P}\right)\left(\frac{h}{t}\right)^2\left(1/2\ \rho_f V^2\right) \qquad (4)$$

Using values for C_F and Q easily obtained from Figures 2 and 3, the stress indicator can quickly and easily be calculated for any situation.

Based on a number of bellows failures experienced in our laboratory and reported by others, a preliminary plot of bellows fatigue life as a function of the Stress Indicator has been compiled. This data is shown in Figure 4. Information of this type will undoubtedly prove very valuable to the designer, however, this plot has not yet been validated for larger bellows sizes and for the range of geometries typical of current stage hardware practices.

II.4 Heat Transfer Effects

Heat transfer effects as well as vortex, acoustic, geometric and cavitation influences must sometimes be considered in obtaining an understanding of the flow-induced vibrations in flexible metal bellows. The

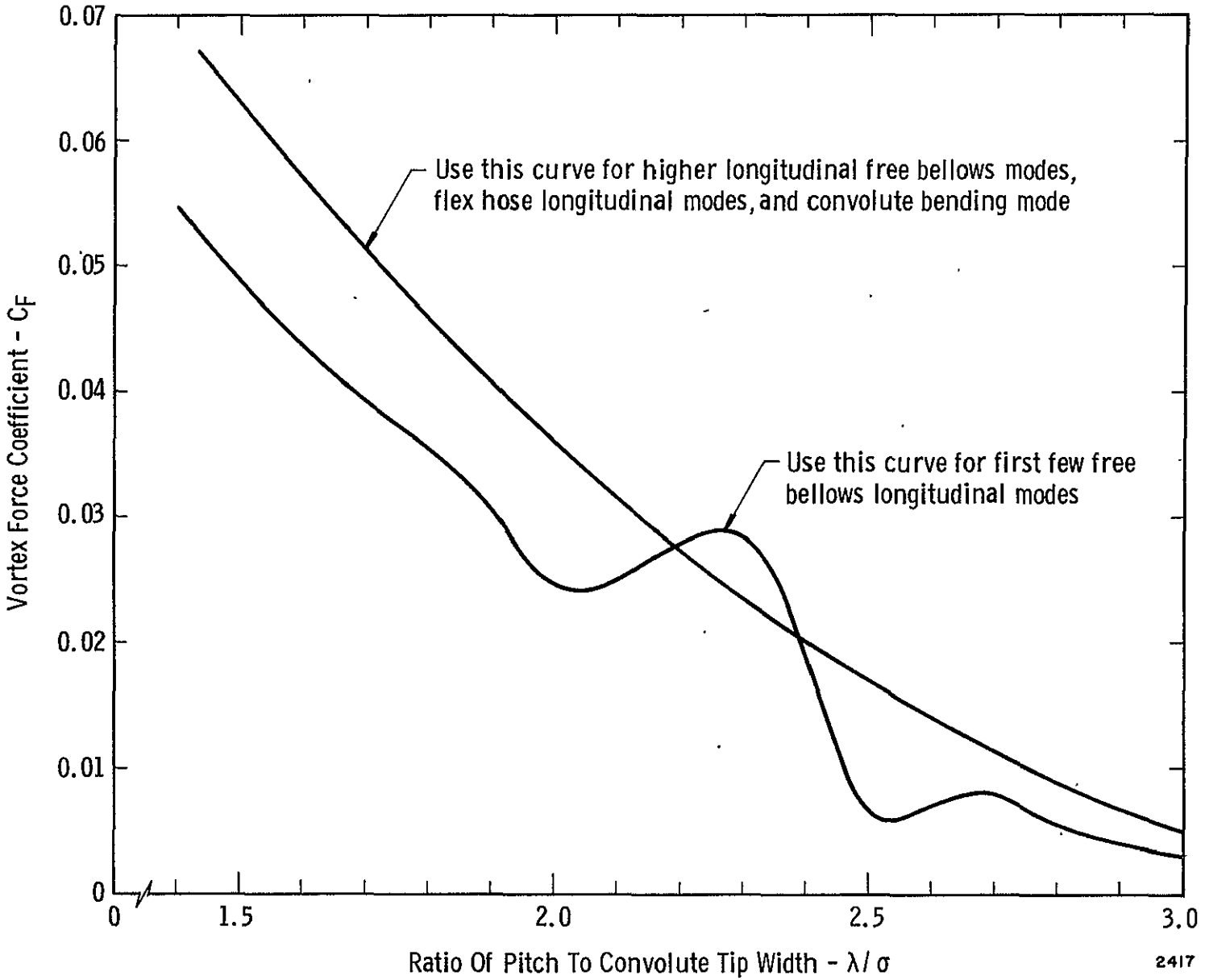

Figure 3. Summary Of Bellows Vortex Force Coefficient Experimental Data

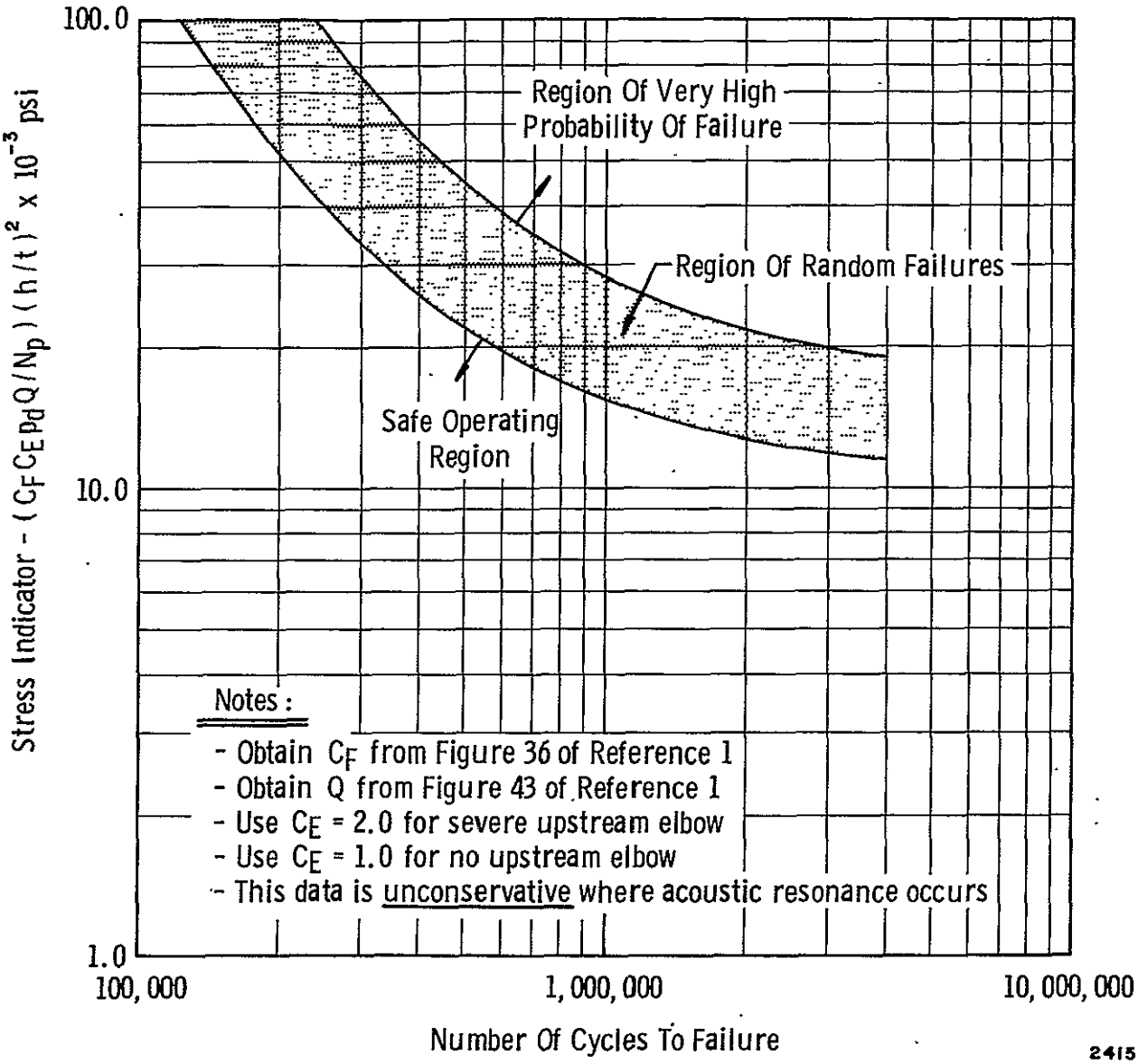

Figure 4. Preliminary Bellows Fatique Life Data

consequences of heat transfer in the case of cryogenic flow in bellows are of particular interest since large temperature differences exist between the flowing liquid and the bellows environment which could lead to a phase change near the inside bellows wall. Vapor formation will result in a "killing off" of the vortex shedding, and a change in the bellows flow response. Even low rates of heat transfer, which do not produce large scale boiling, may raise the vapor pressure near the wall so cavitation can occur and suppress the flow induced vibration. In addition to vapor effects on the flow induced vibration, frost buildup and liquid condensation on the outside bellows surface will affect the heating rate and add damping to the bellows structure, thus influencing its operating characteristics. Another question regarding bellows operation is the change in the bellows characteristics at extremely low temperatures in contrast to conditions tested in air and water at near ambient conditions. Once the bellows response to heat transfer is established, a more realistic evaluation of bellows performance in the field will be available in order to establish failure criteria under operating conditions.

The remainder of this report is devoted to discussion of results of our investigation of these various heat transfer effects.

III. EXPERIMENTAL FACILITY

III.1 Cryogenic Flow Loop

A special cryogenic flow loop was designed and fabricated for the purposes of this study. The loop is shown in Figures 5 and 6 before and after the insulation was installed. The pump is a standard centrifugal cryogenic unit, designed for liquid oxygen service, which was converted from electric motor drive to a hydraulic motor drive to provide a variable speed capability. The pump rating is 600 GPM at 110 ft total head when pumping liquid oxygen. The flow rate is measured with a turbine type flow meter which was calibrated in place with a pitot tube using water as the flow medium.

The flow loop has a total capacity of approximately 90 gallons. The system is filled from a 1500-gallon dewar which is installed adjacent to the laboratory. Any liquid remaining in the loop after completion of a test can be pumped back into the dewar.

Insulation of the loop consists of 2-inch thick styrofoam panels built into a box-like enclosure. A small amount of boiloff gas from the loop is vented into the enclosure to prevent any possible dangerous buildup of oxygen. The insulation is quite adequate for the short term tests such as those performed in this program. Liquid loss resulting from heat transfer was small compared to pumping loss. The styrofoam panels are easily removed when necessary for repair or modification of the loop.

The test section of the loop can be isolated by closing the upstream and downstream valves. The test piece can then be replaced without draining the system. The downstream valve can also be used to increase the back pressure in the test section during flow tests. System pressure can be controlled by manually venting gas or by setting an automatic relief valve.

III.2 Instrumentation

All bellows installed in the cryogenic flow loop described above were instrumented as illustrated in the schematic drawing shown in Figure 7. Four copper-constantane thermocouples were provided in order to monitor (1) the upstream fluid temperature, (2) downstream fluid temperature, (3) the bellows metal or skin temperature, and (4) the surrounding temperature of the environment in which the bellows were placed. All of these thermocouples were referenced to -320°F (boiling point of liquid nitrogen

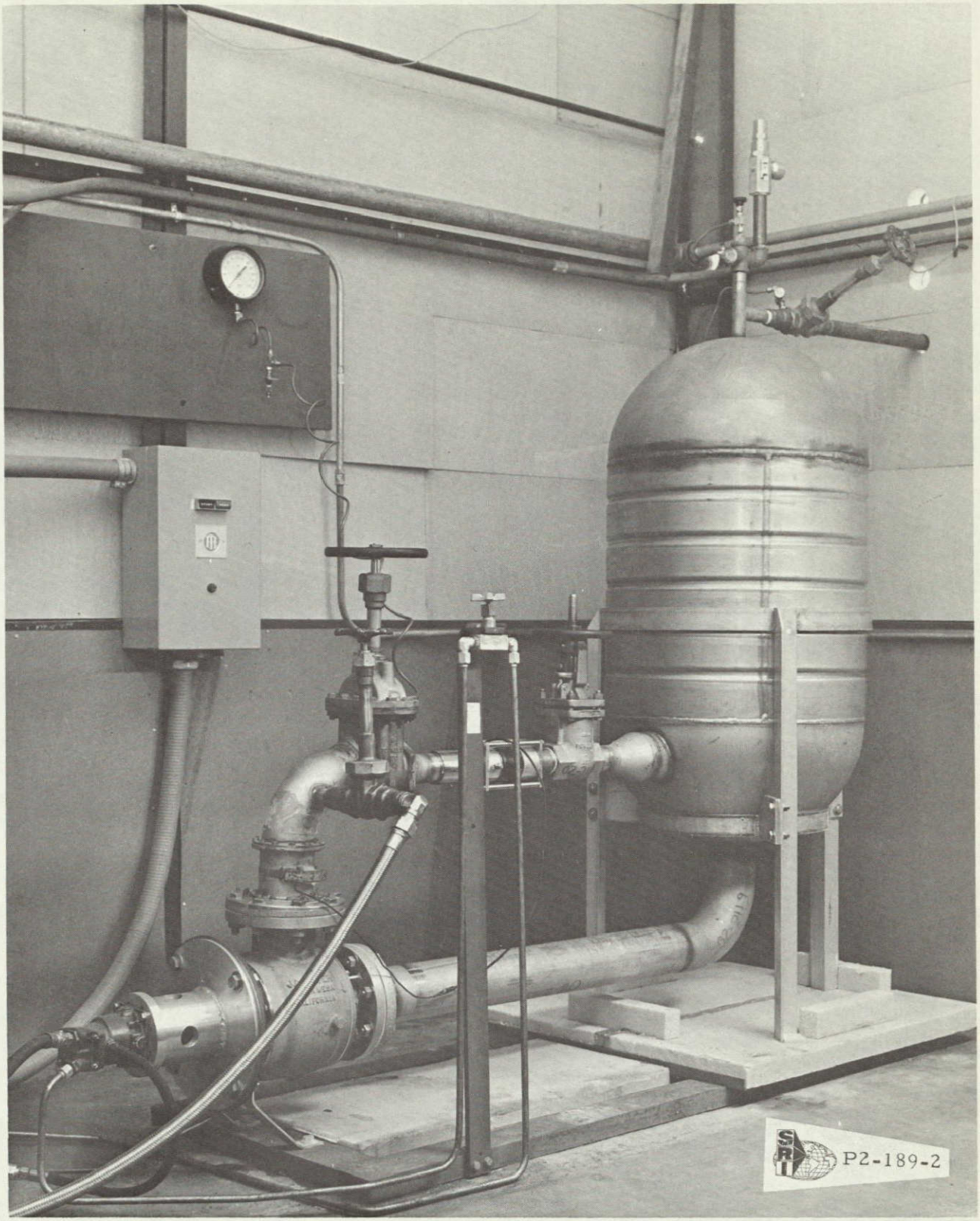

Figure 5. Cryogenic Flow Loop Without Insulation

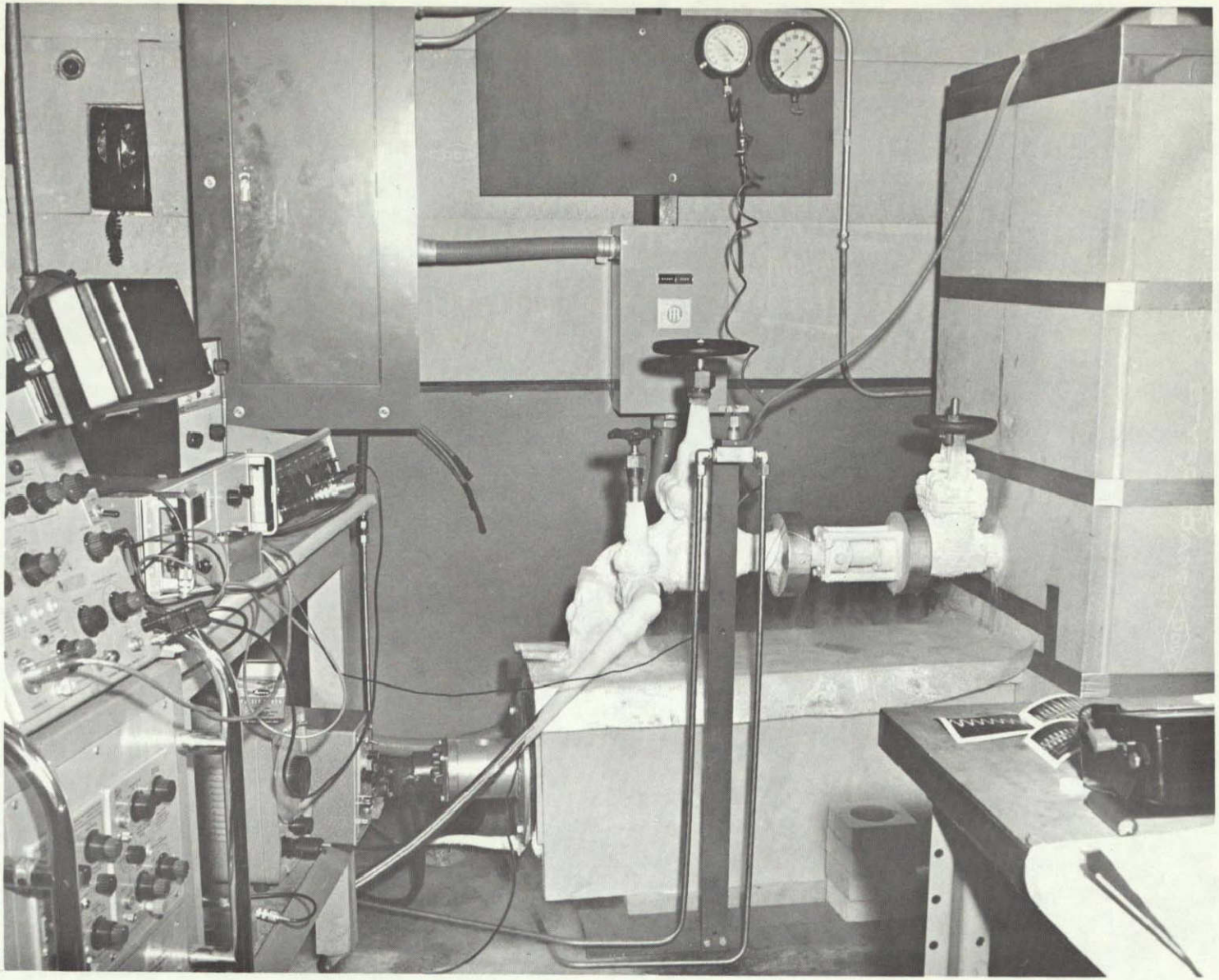

Figure 6. Cryogenic Flow Loop With Insulation

at standard conditions) in order to provide accurate results. A digital voltmeter was employed in conjunction with the thermocouples, and the accuracy was established to be $\pm$ 0.5 degrees F.

Bellows pressure was measured with a bourdon pressure gage, while the pressure drop across the bellows was measured with a mercury manometer. The static pressure of the system was measured with the same bourdon gage when the flow velocity was zero, and is referred to in the report as P_T (tank pressure or static system pressure). The downstream valve shown in Figure 7 was used to create the back pressure (P_B-P_T) required to excite the bellows vibration.

Dynamic strain was monitored through the use of 1/32-inch gages mounted on the first convolution tip of each bellows. Since the strain frequencies were expected to be relatively high, ordinary constantane foil type gages were used without temperature compensation. These gages are less expensive than those produced specifically for use at cryogenic temperatures, and they can readily be obtained in configurations which are convenient for bellows applications.

The fact that the apparent strain curve for constantane has a very large slope at cryogenic temperatures is of little consequence since the strain readout equipment was AC coupled, and the temperature changes were slow compared to the strain frequency.

The strain gages were installed with a 100% solids epoxy adhesive. Bellows surface preparation consisted of light sandblasting and application of a degreaser. The gages were positioned by the holding-tape technique, and the adhesive was cured under a light clamping force. Following strain gage installation, each bellows was tested to obtain static force-deflection and strain-deflection curves. This provided experimental spring rate values which allowed more accurate mode frequency calculations. The force-deflection and strain-deflection data for the six bellows tested in the cryogenic flow facility are shown in Figures 8 and 9.

At the cryogenic temperatures, considerable "zero drift" occurred with the strain gages, and the question was raised as to the reliability of the strain gage readings at these extreme temperatures under a dynamic situation. According to the manufacturers' specifications, the gage factor would change only 4% at these temperatures. As a check, one of the bellows was mounted on a mechanical shaker with one end fixed rigidly and the other free to move with the shaker (Figure 10). A dial deflection gage was used

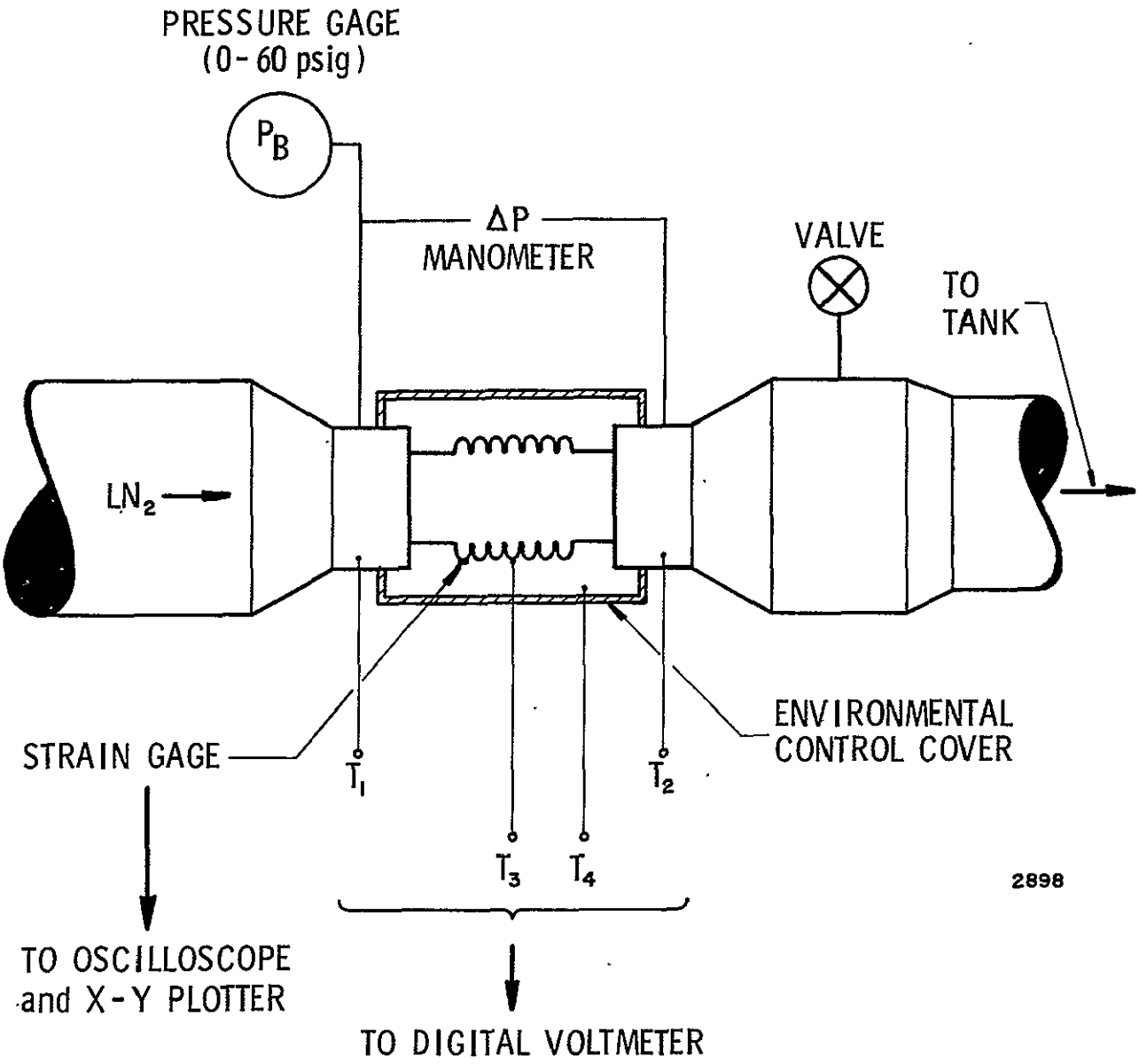

Figure 7. Instrumentation Schematic

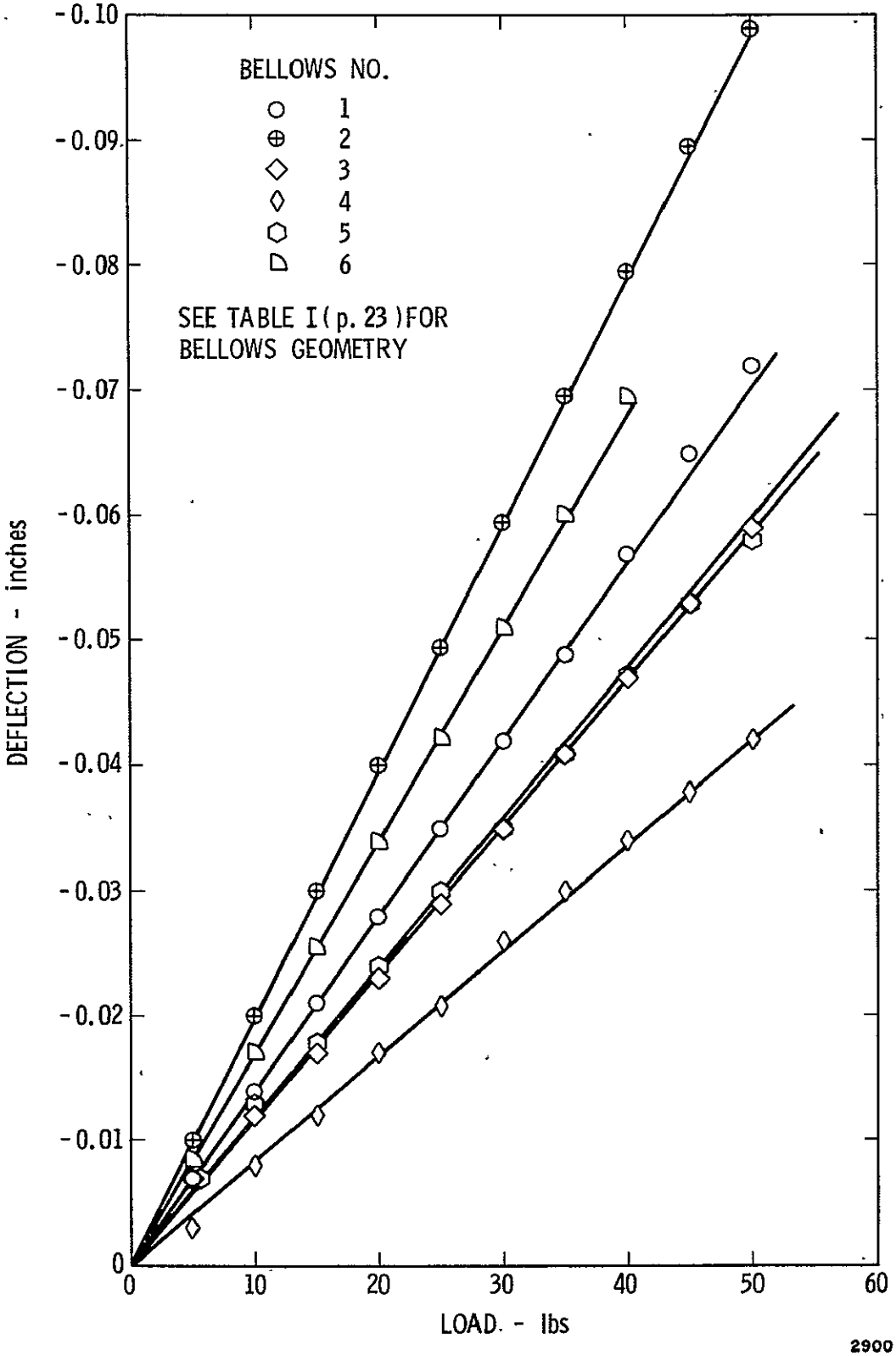

Figure 8. Load-Deflection Data For Test Bellows

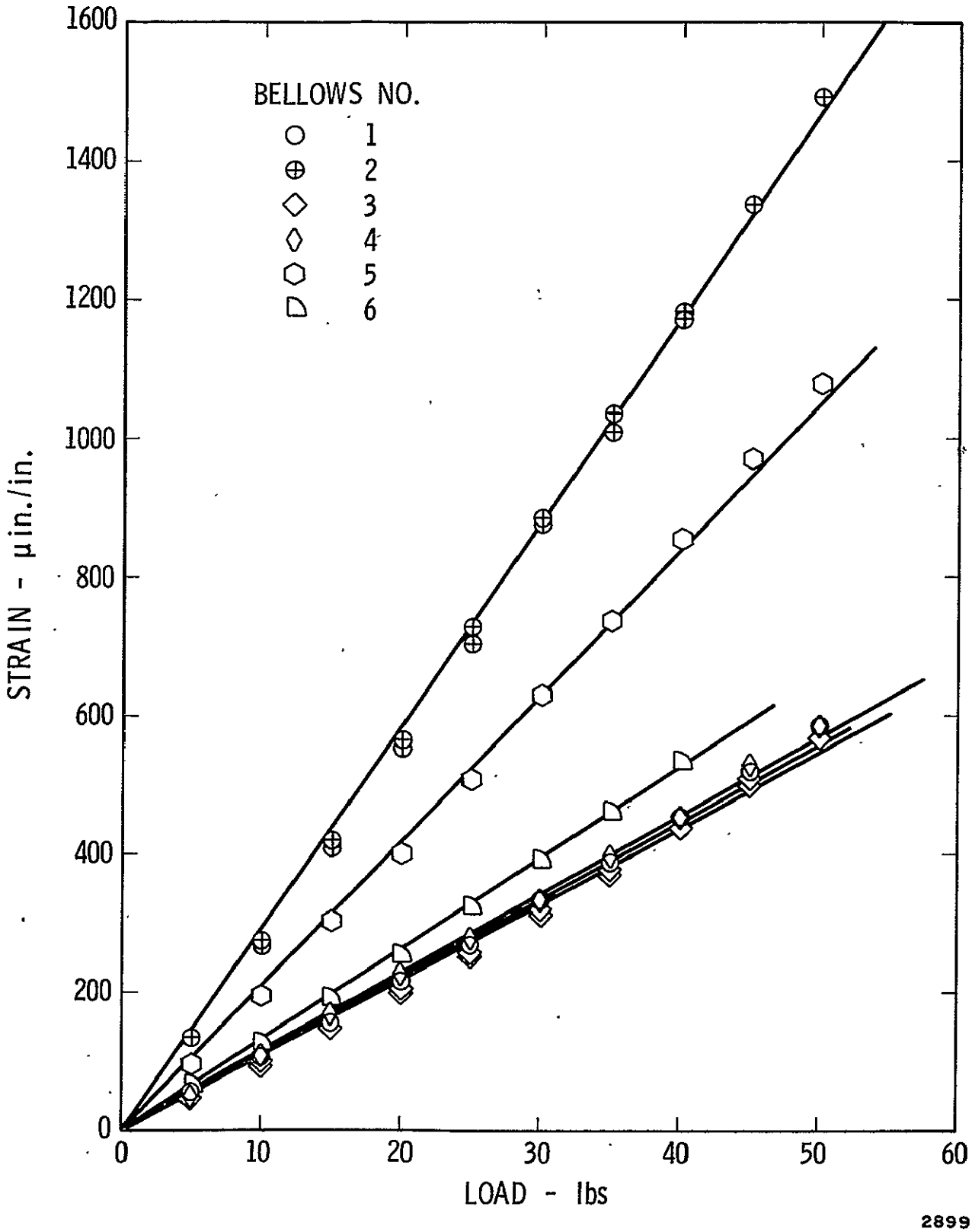

Figure 9. Strain-Load Calibration For Test Bellows

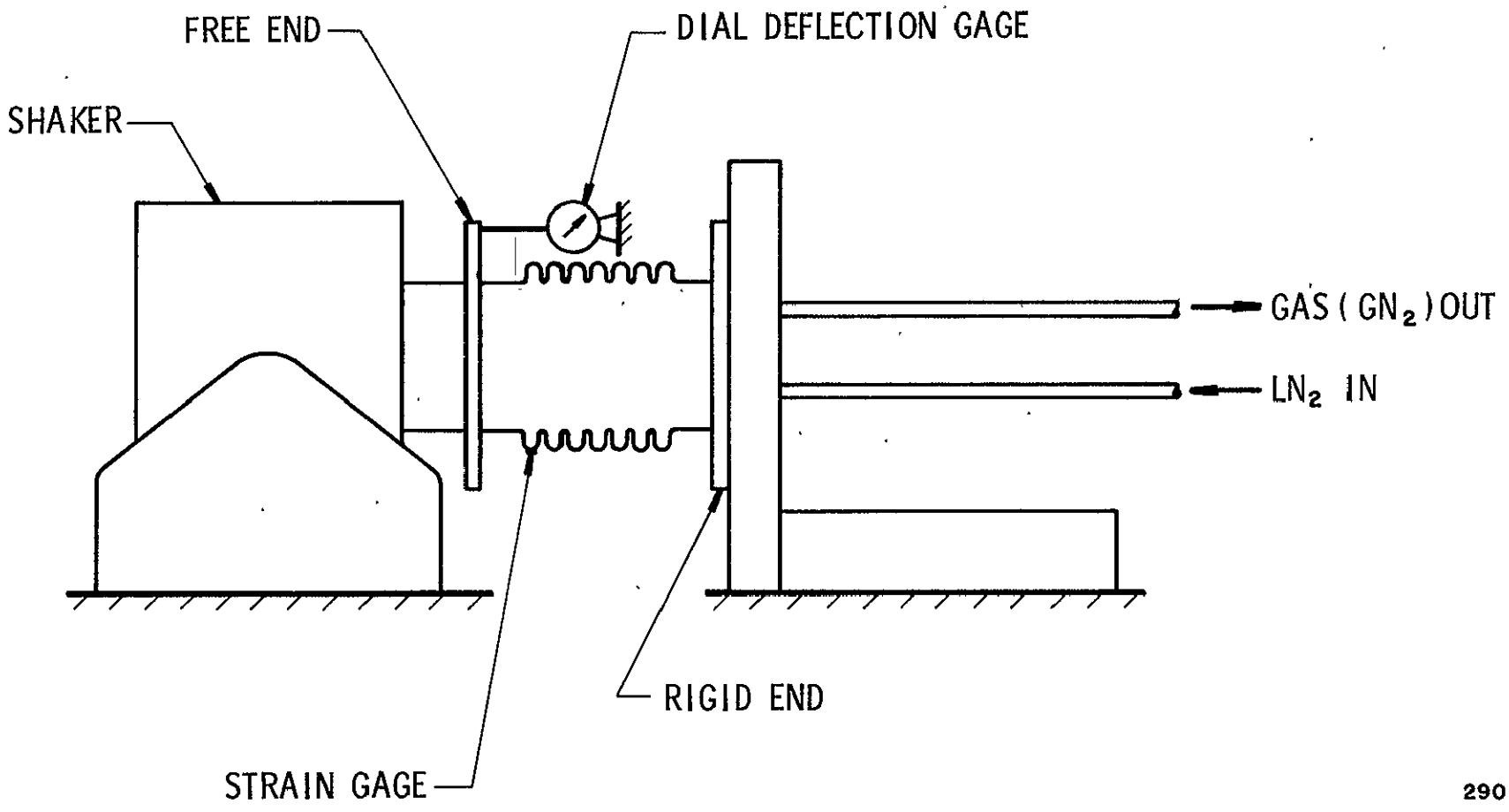

Figure 10. Strain Gage Temperature Calibration Set Up

to measure the movement of the free end while the shaker vibrated at a low frequency to simulate a dynamic loading on the bellows. This test was conducted with the bellows at room temperature, and again at -320°F by filling the bellows with boiling liquid nitrogen. The strain-deflection data for both temperatures is shown in Figure 11. The change in slope represents a change in gage factor of 4.5% at the cryogenic temperature which is very near the manufacturers specifications, therefore the dynamic strain data was verified for the low temperature conditions encountered in the tests.

The strain gage readout circuit consisted of a standard DC powered bridge which was AC coupled to an audio-frequency amplifier. The strain signal was displayed on an oscilloscope, and also plotted as a function of fluid velocity on an X-Y recorder. The DC equivalent of peak-to-peak strain was recorded as the ordinate, and the fluid velocity was recorded as the abscissa. A DC signal directly proportional to fluid velocity was obtained by connecting the turbine meter output to a frequency-DC converter.

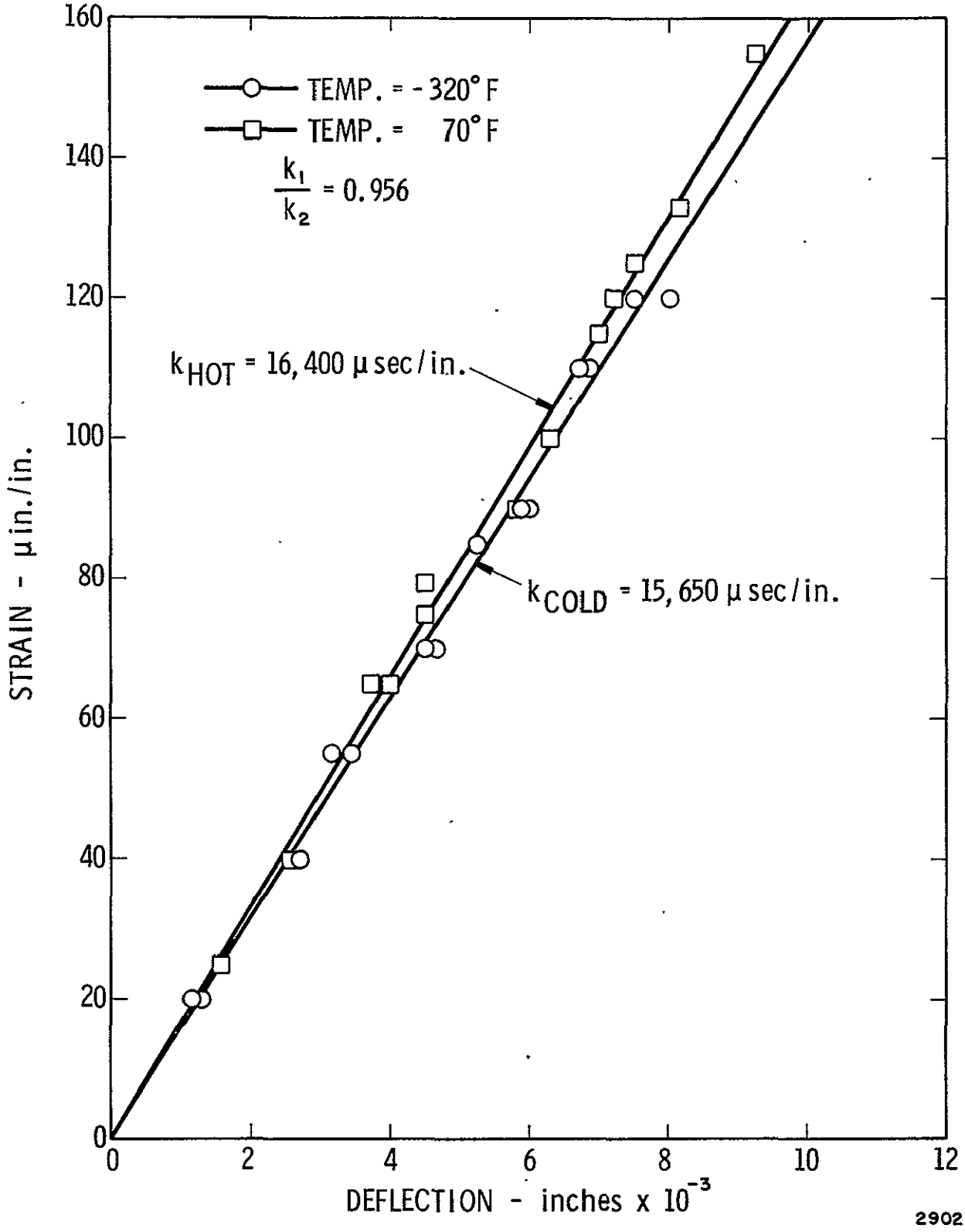

Figure 11. Strain Gage Calibration versus Temperature

IV. EXPERIMENTAL RESULTS

IV.1 Introduction

The cryogenic flow loop described in the previous section was utilized to study bellows flow excitation for a number of fluid and surrounding conditions. Initially, a number of exploratory tests were conducted simply to get a feel for the overall problem. Following this, detailed tests of various kinds were conducted. To obtain a comparison of bellows response with LN_2 versus water, a series of tests were conducted with identical bellows using both mediums, but with heat transfer effects maintained at a minimum. Heat transfer effects with LN_2 were then studied by controlling the bellows environmental conditions (temperature, frost buildup and convection rate) and recording the strain levels at different flow rates and pressures. Finally, pressure drop data was obtained under varying heating rates and operating conditions to yield additional information on bellows operating characteristics. The results of these tests are discussed in the following sections.

IV.2 Description of Test Bellows

Throughout this study, six different test bellows were employed. Dimensional data for these bellows is given in Table I.

Bellows #1, #2, and #6 have basically the same convolute geometry, except the pitch has been varied from the original configuration (#6) by stretching in one case (#1) and compressing in the other case (#2). Similarly, bellows #3, #4, and #5 have essentially the same geometry except for the pitch and were derived by the stretch and compression technique. Figure 12 illustrates a bellows identical to those from which specimens #3, #4, and #5 were made, and shows the effect of the stretch and compression.

IV.3 Initial Test Results and Effect of Back Pressure

When the testing of bellows with liquid nitrogen was first begun, it was observed that no matter what tank or system pressure the flow loop was operated at, the bellows would not vibrate except at the higher velocities, where low-level vibration of the higher frequency modes occurred. It was assumed that since the liquid nitrogen was so near the liquid-vapor line, a very small reduction in pressure, or increase in temperature, would cause cavitation, and hence, reduce or kill the vortex shedding excitation mechanism. (This assumption was later proved to be correct and is discussed in greater

Table I

Dimensional Data

Bellows #1 (Long 2.22)		Bellows #2 (Short 2.22)	
I.D. = 1.49	h = .312	I.D. = 1.49	h = .36
O.D. = 2.22	λ = .345	O.D. = 2.22	λ = .187
Dm = 1.85	σ = .125	Dm = 1.85	σ = .125
N_c = 7	t = .013	N_c = 7	t = .013
N_p = 1	LL = 2.75	N_p = 1	LL = 1.5
Bellows #3 (2.02 Nom)		Bellows #4 (Long 2.02)	
I.D. = 1.46	h = .27	I.D. = 1.46	h = .25
O.D. = 2.02	λ = .22	O.D. = 2.02	λ = .282
Dm = 1.74	σ = .144	Dm = 1.74	σ = .144
N_c = 8	t = .013	N_c = 8	t = .013
N_p = 1	LL = 1.52	N_p = 1	LL = 1.95
Bellows #5 (2.02 short)		Bellows #6 (2.22 N)	
I.D. = 1.46	h = .28	I.D. = 1.49	h = .345
O.D. = 2.02	λ = .156	O.D. = 2.22	λ = .250
Dm = 1.74	σ = .125	Dm = 1.85	σ = .125
N_c = 8	t = .013	N_c = 7	t = .013
N_p = 1	LL = 1.25	N_p = 1	LL = 2.0

ID	=	internal diameter
OD	=	outside diameter
D_m	=	mean diameter
N_c	=	number of convolutes
N_p	=	number of plys
h	=	convolute height
λ	=	convolute pitch
σ	=	convolute tip width (internal)
t	=	ply thickness
LL	=	live length

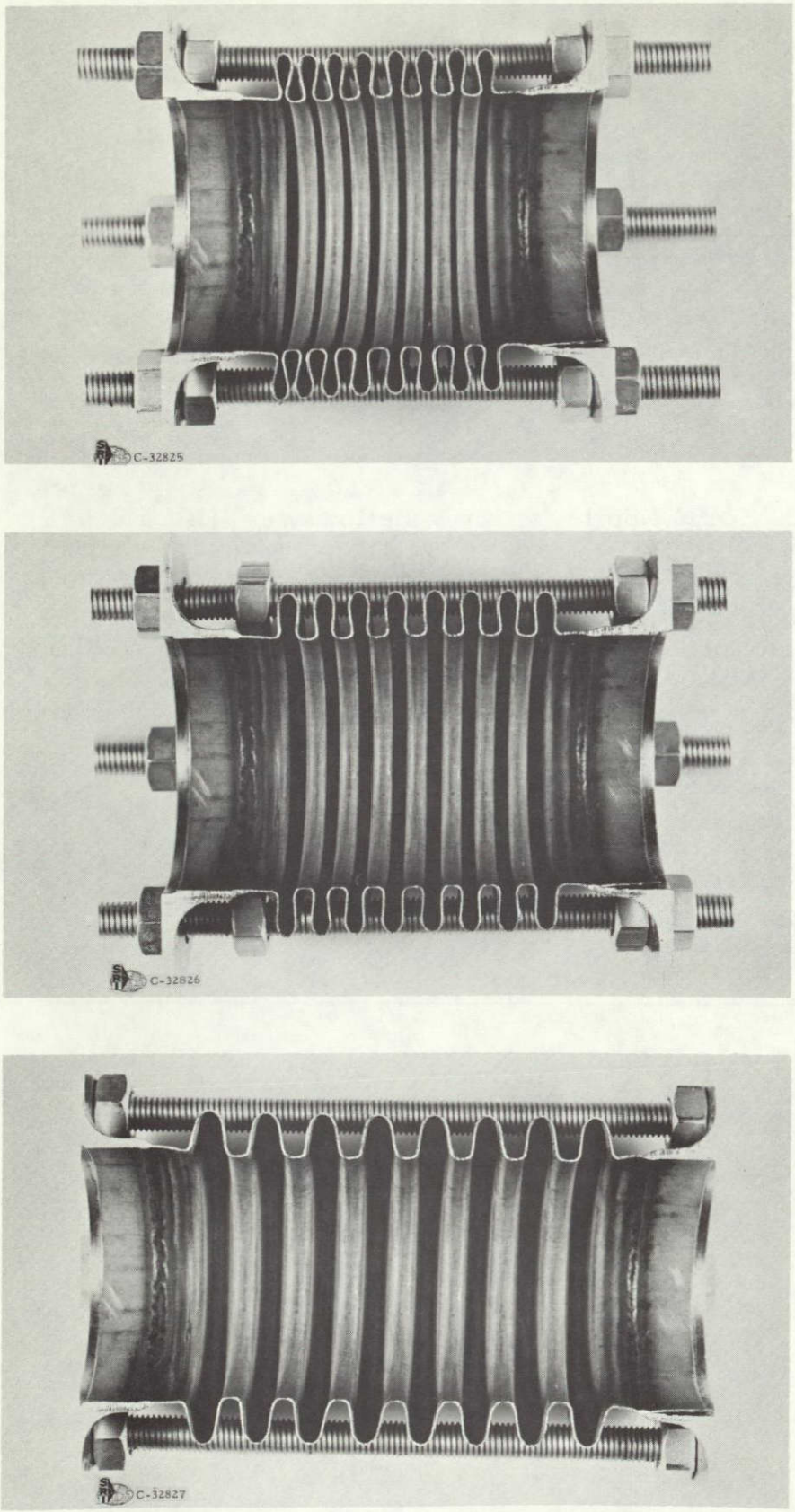

Figure 12. Photographs Of Stretched And Compressed Bellows

detail in a later section of this report.) The first attempt to correct this condition and produce stronger flow excitation was to close a valve on the tank and let the pressure of the system build up. However, it soon became obvious that this was simply moving the fluid state to a point further along the liquid-vapor line, since the temperature was also increasing with the pressure (along the equilibrium or liquid vapor line). In order to increase the pressure at the bellows, and hopefully induce vibrations of the lower modes, a valve was installed into the loop (Figure 7) downstream of the bellows. This valve was used to restrict the flow and cause an increase in pressure in the bellows greater than the system pressure. This allowed an increase in pressure and only slight, if any, temperature increase in the bellows or test section. Therefore, the state of the fluid in the bellows could be arbitrarily adjusted away from the liquid-vapor line.

By closing the downstream valve in increments, successive increases in the bellows pressure was produced. The effect of increasing this back pressure can be seen in Figures 13 through 18 which present the maximum strain level recorded versus the bellows pressure at various values of the tank system pressure (P_T) for the six test items. In all cases it can be seen that the strain increases with increasing back pressure (P_B-P_T) up to a maximum where it levels off and becomes invariant with further increases in bellows pressure. More information of this phenomena is provided in a later section where the effects of heat transfer into the bellows is discussed.

IV.4 Comparison of Liquid Nitrogen to Water - Heat Transfer Effects Minimized

To provide a direct comparison of flow induced vibration phenomena with LN_2 and water, a series of tests were conducted in which heat transfer effects were minimized as much as was practical. The resultant data should, therefore, reflect basically any possible difference in the vibrations because of differences in the two flow media or because of bellows material property changes with temperature. To reveal possible geometry effects, all six test bellows were used for this series of tests.

Flow-induced vibration test results for the six bellows, with both water and LN_2 flows, are given in Figures 19 through 24. In all cases the data shown is for the first or lowest frequency longitudinal mode. In obtaining the LN_2 data, each bellows was run with a back pressure sufficient to minimize possible cavitation suppression of the vortex shedding. Also the bellows exterior was subjected to a cold GN_2 purge to prevent frost or liquid condensation which might cause unwanted external damping.

The test data presented in Figures 19, 20 and 21 show excellent agreement of the peak flow-induced strain levels for the two test liquids. In each case, the maximum strain is greater for water flow than for the

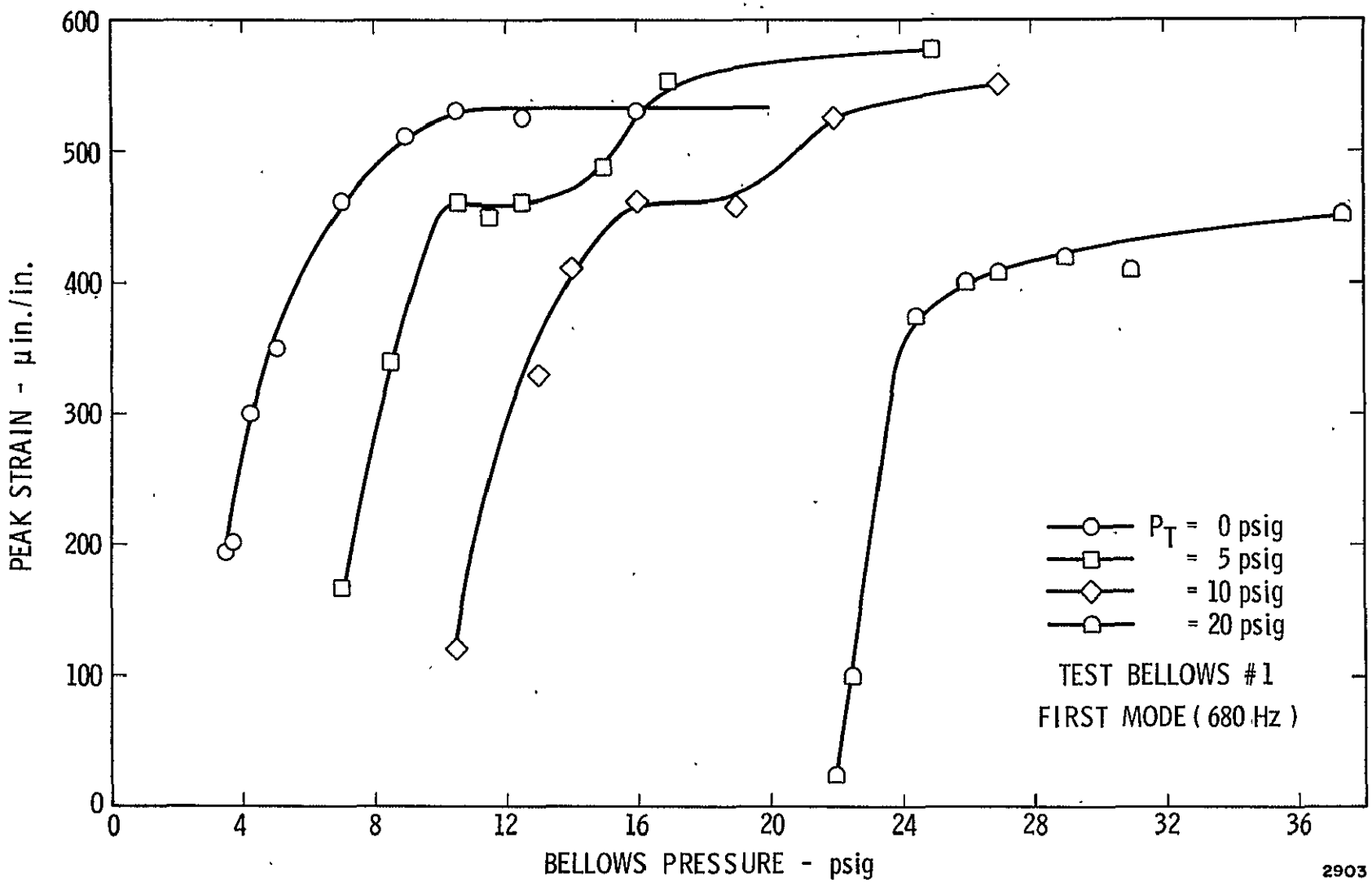

Figure 13. Pressure Sensitivity Of Flow Excited Bellows (# 1) With LN_2 Flow

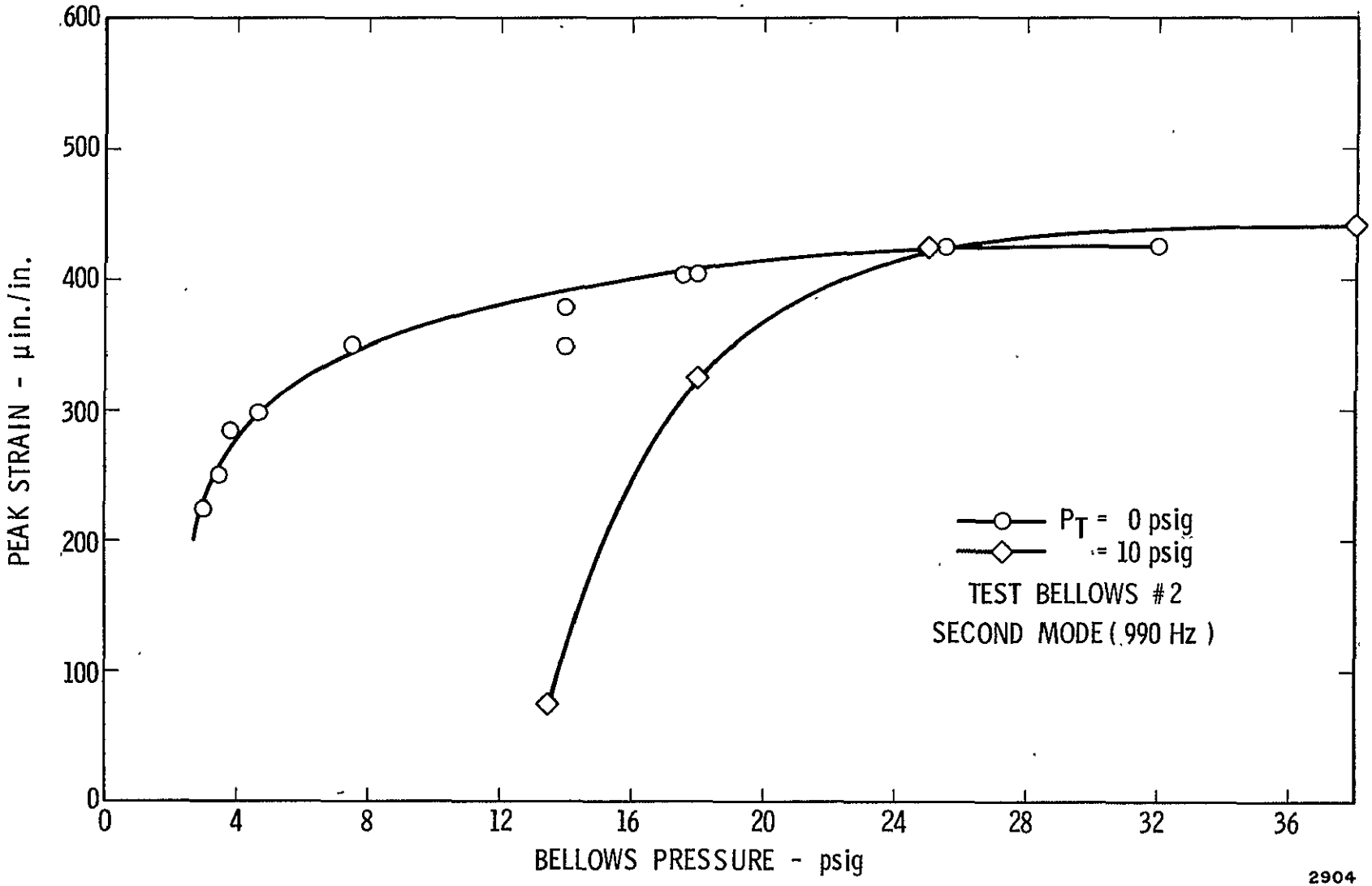

Figure 14. Pressure Sensitivity Of Flow Excited Bellows (# 2) With LN_2 Flow

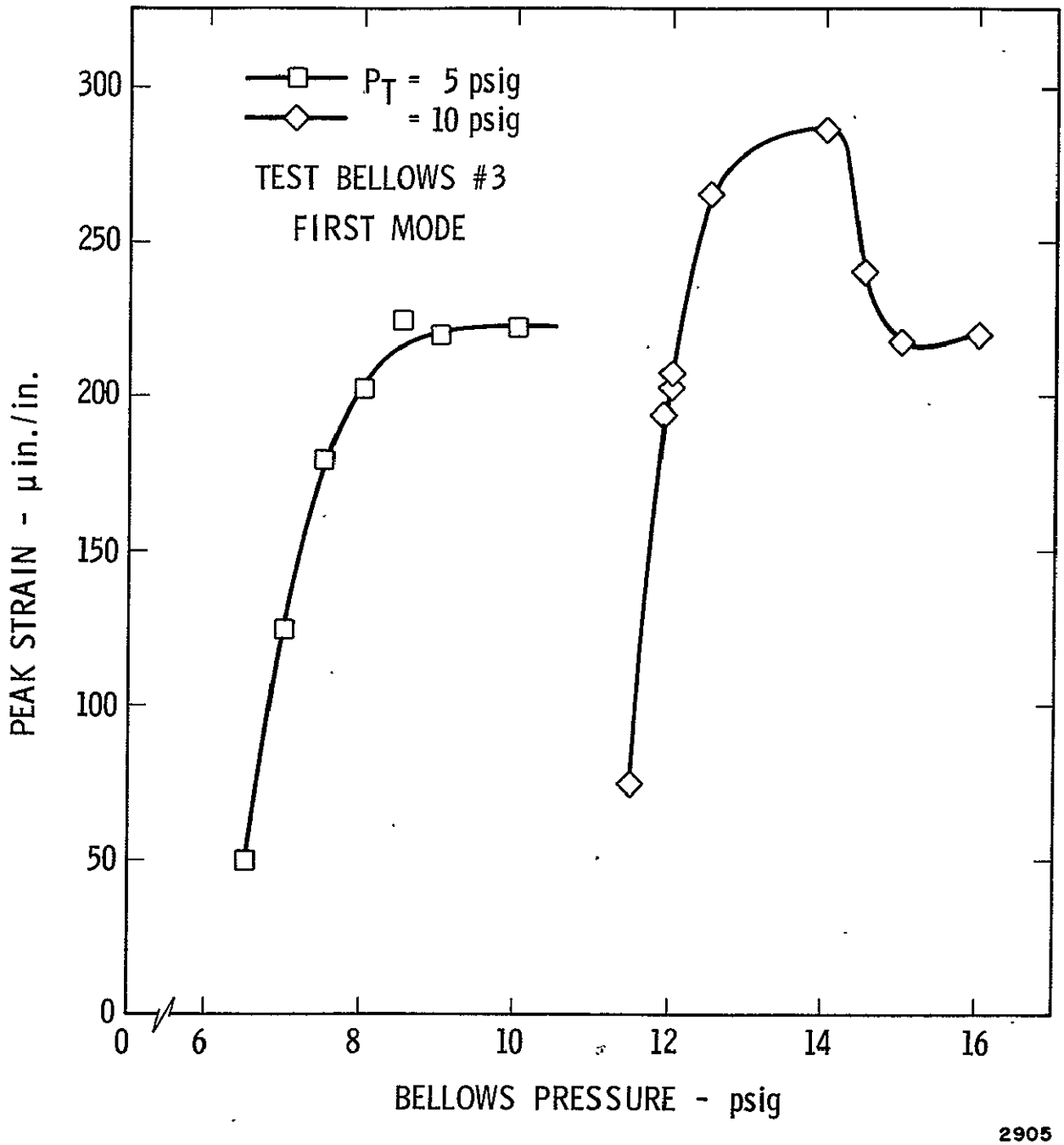

Figure 15. Pressure Sensitivity Of Flow Excited Bellows (# 3) With LN_2 Flow

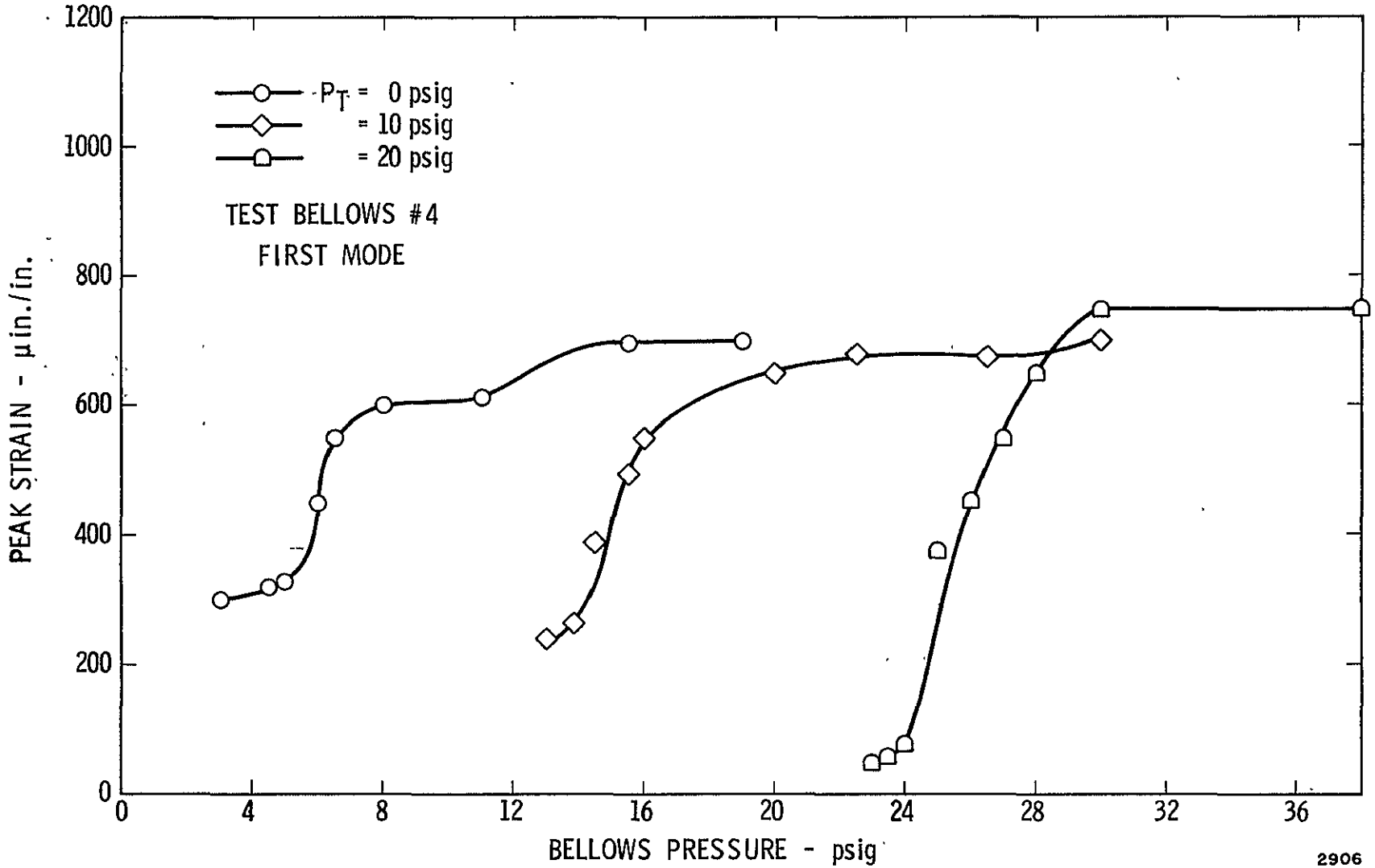

Figure 16. Pressure Sensitivity Of Flow Excited Bellows (# 4) With LN_2 Flow

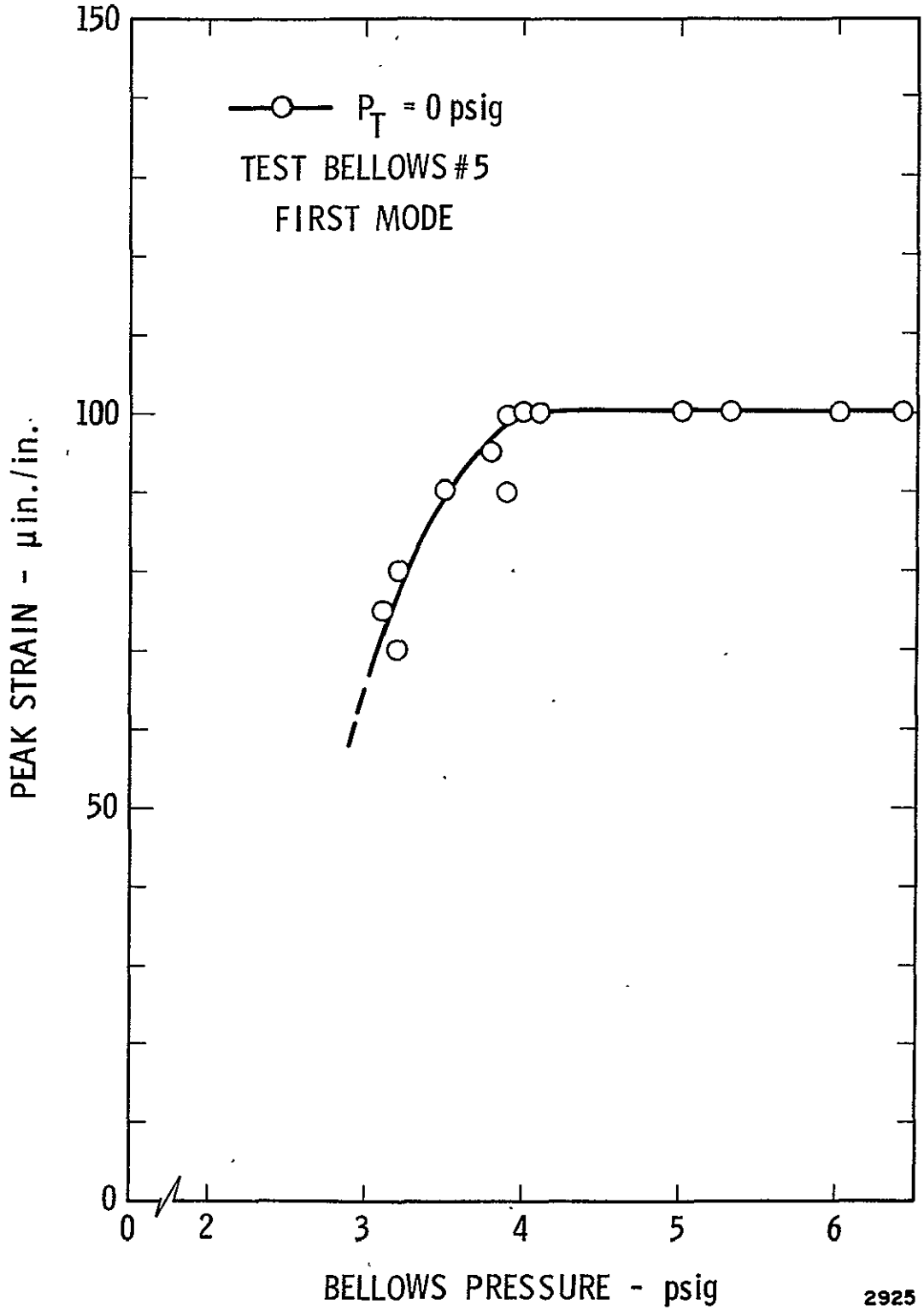

Figure 17. Pressure Sensitivity Of Flow Excited Bellows (#5) With LN_2 Flow

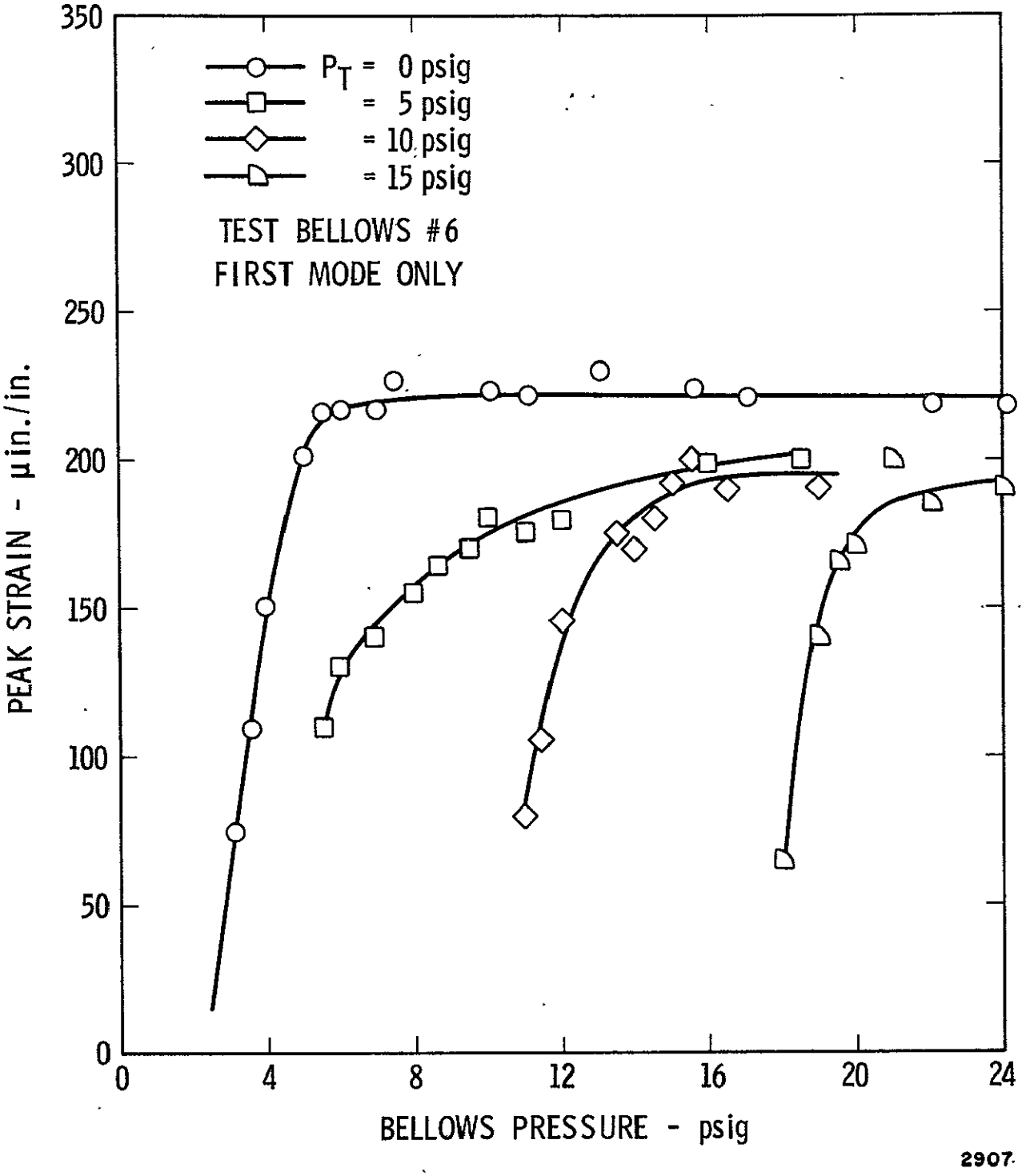

Figure 18. Pressure Sensitivity Of Flow Excited Bellows (# 6) With LN_2 Flow

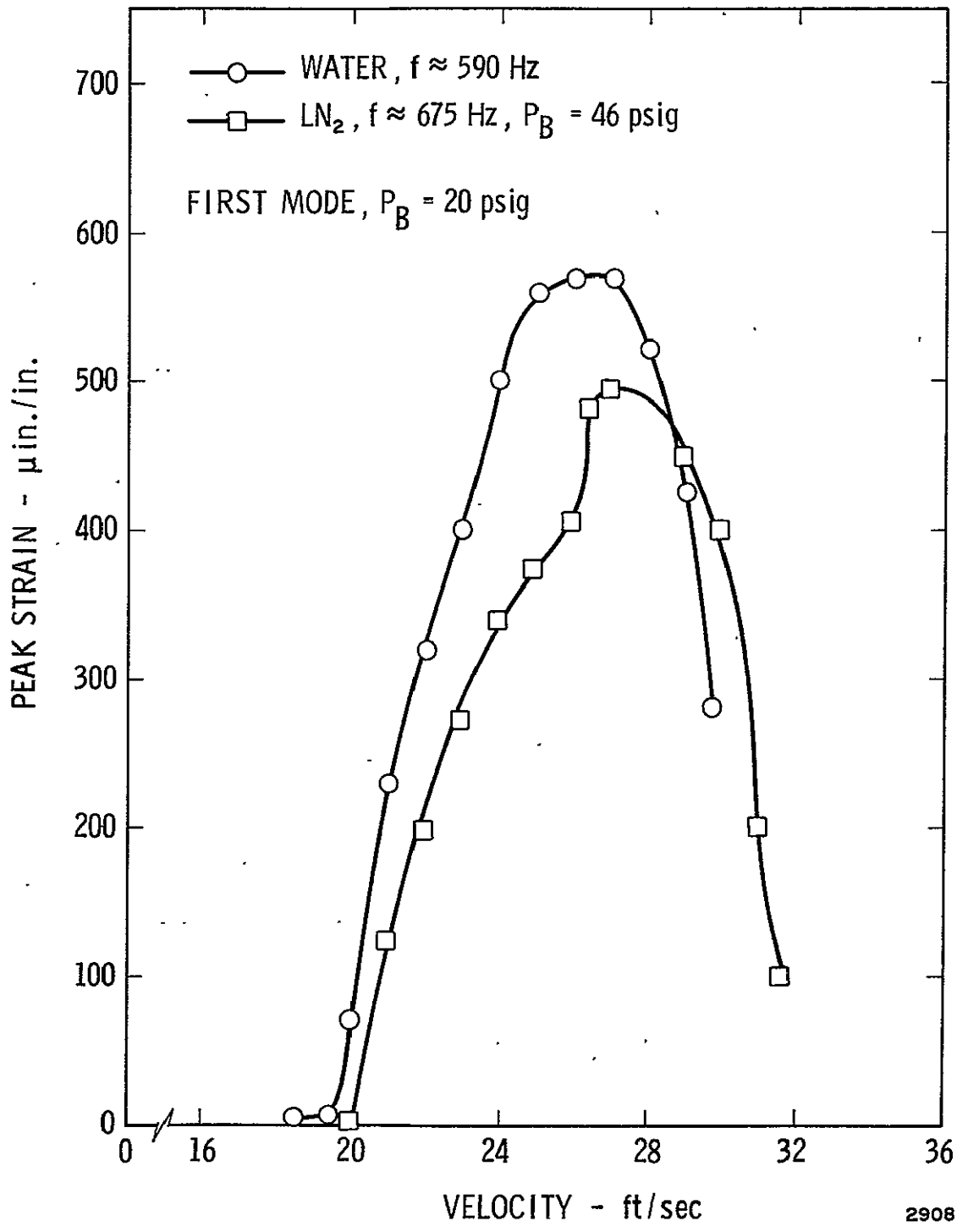

Figure 19. Comparison Of Flow-Induced Vibration With Water And LN_2, Bellows #1

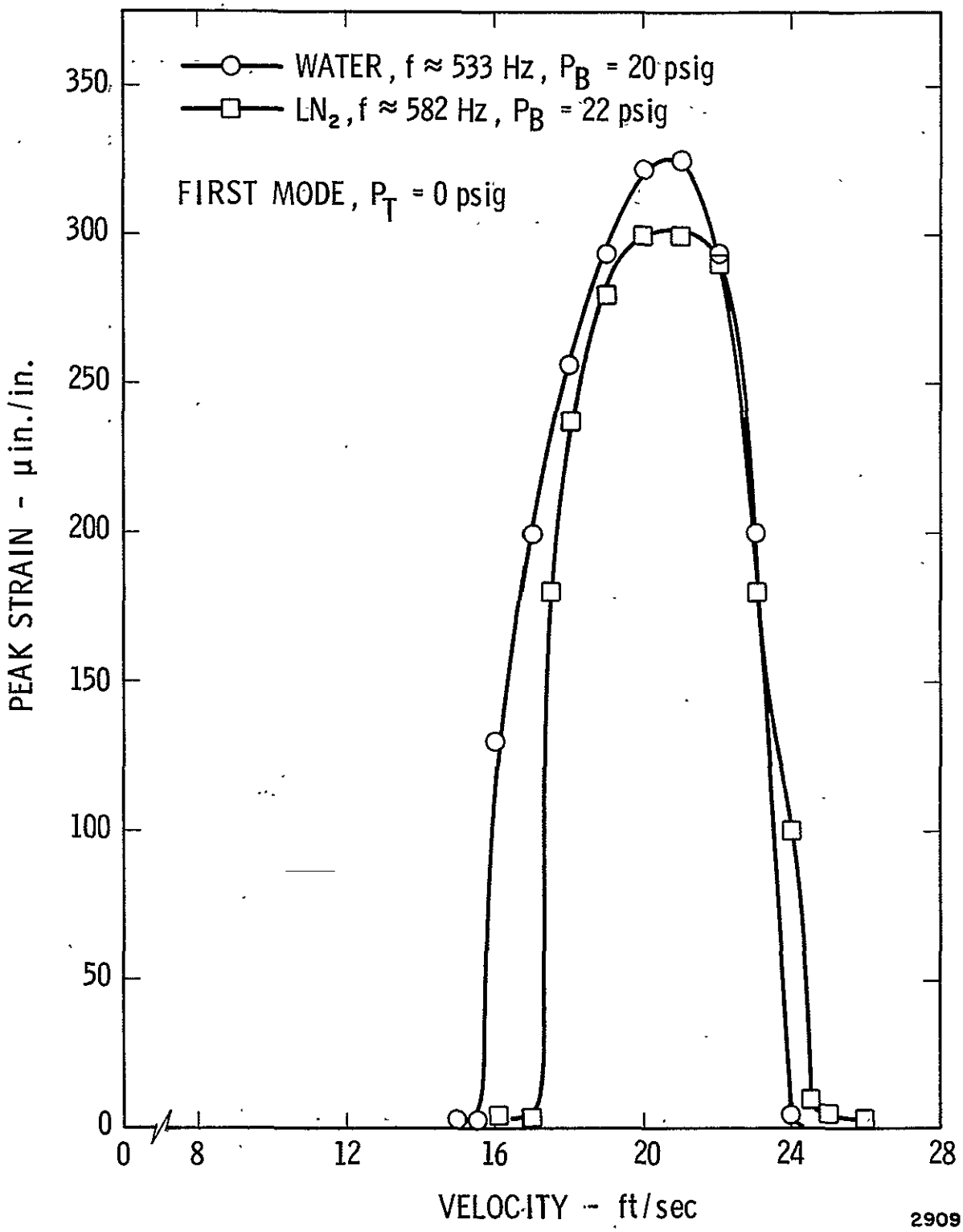

Figure 20. Comparison Of Flow-Induced Vibration With Water And LN_2, Bellows #6

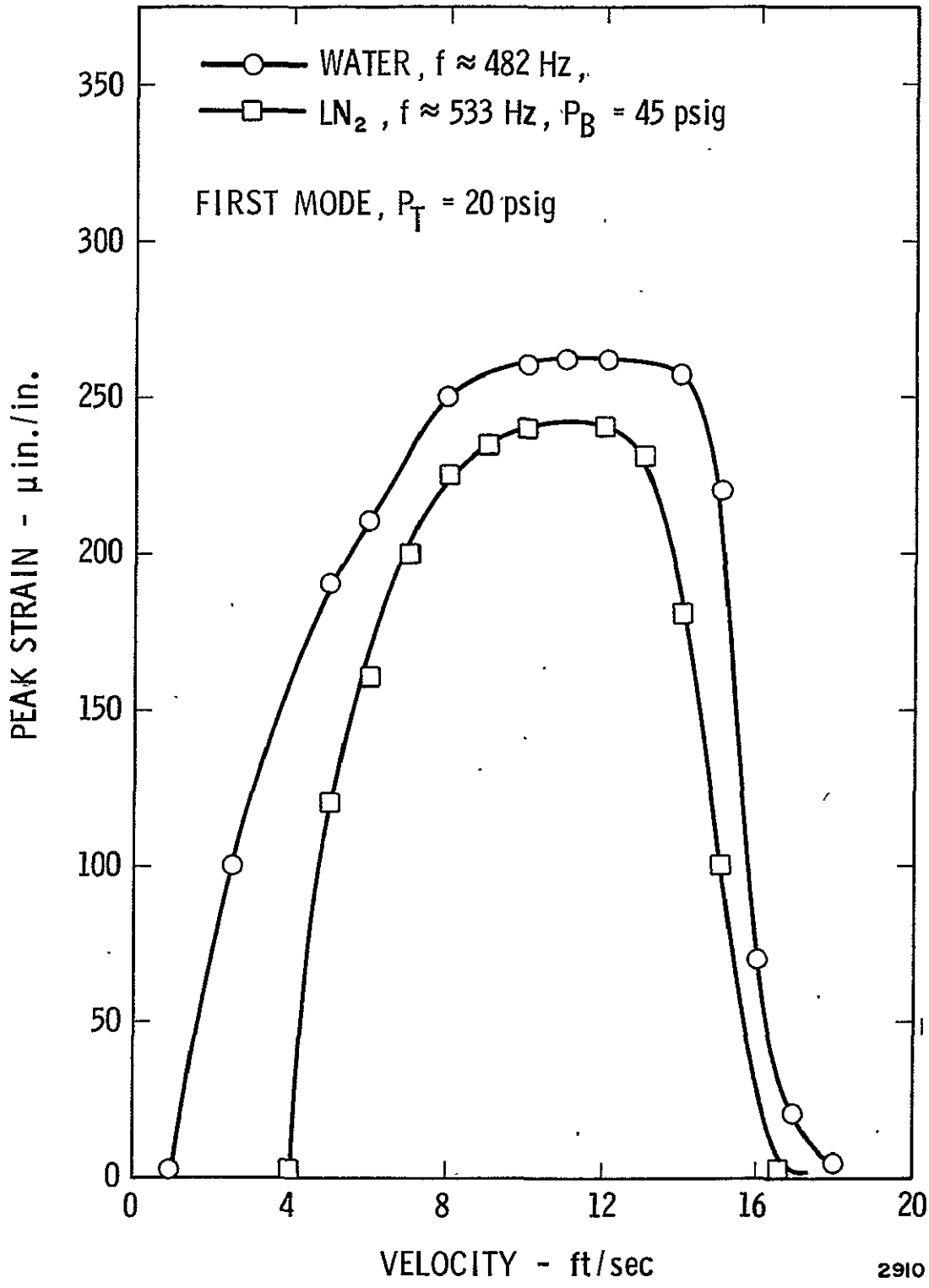

Figure 21. Comparison Of Flow-Induced Vibration With Water And LN_2, Bellows #2

LN_2 flow. This is to be expected since the LN_2 was less dense than the water, hence the vortex shedding excitation force, which is proportional to $1/2\,\rho\,V^2$, was less. The results given in Figures 19, 20 and 21 were for one series of bellows having essentially the same convolute geometry, except for the pitch.

Figures 22, 23 and 24 show a comparison of flow-induced vibration data for the second series of bellows with similar convolute geometry, except for pitch. This data does not show as good a correlation of the LN_2 and water results as did the results for the first bellows series (Figures 19, 20 and 21). The primary disagreement is in the velocity at which the peak strain occurs, since the LN_2 results peak at a velocity which is about 10 percent higher than the peak for the water data. Still, the agreement is good enough that we can conclude there are no major discrepancies between flow-induced vibration results for water and LN_2, if no cavitation suppression occurs and no external damping media is allowed to form.

Based on these results, we conclude that the theory presented in Reference 1 is valid for cryogenic fluids, as well as water, except for the limitations noted above which reduce the dynamic strain levels, hence are suppression effects. The remainder of this report is devoted to further discussion of results of studies of the suppression effects.

IV.5 Bellows Response With Heat Transfer

Initial studies with a two-dimensional clear plastic flow channel and bellows segment* revealed that the vortex shedding phenomena responsible for bellows flow induced vibrations could be completely suppressed by vapor addition in the convolute sections. This suppression was accomplished by passing water through the channel at the proper velocity for vibration and then blowing small air bubbles into the convolutes. The vortex shedding and bellows vibration was easily observed by injecting ink upstream of the convoluted segment, and viewing the shedding with a strobe light set near the shedding frequency. Once this condition was established, air bubbles injected into the convolutes completely killed off the shedding process and the convolute vibrations ceased. This observation led to the conclusion that if vapor, created by either cavitation, heat transfer, or a combined cavitation/heat transfer effect, was formed in a bellows flowing a liquid, then the flow induced response could be altered.

* This bellows flow visualization model is further described in Reference 1, page 12.

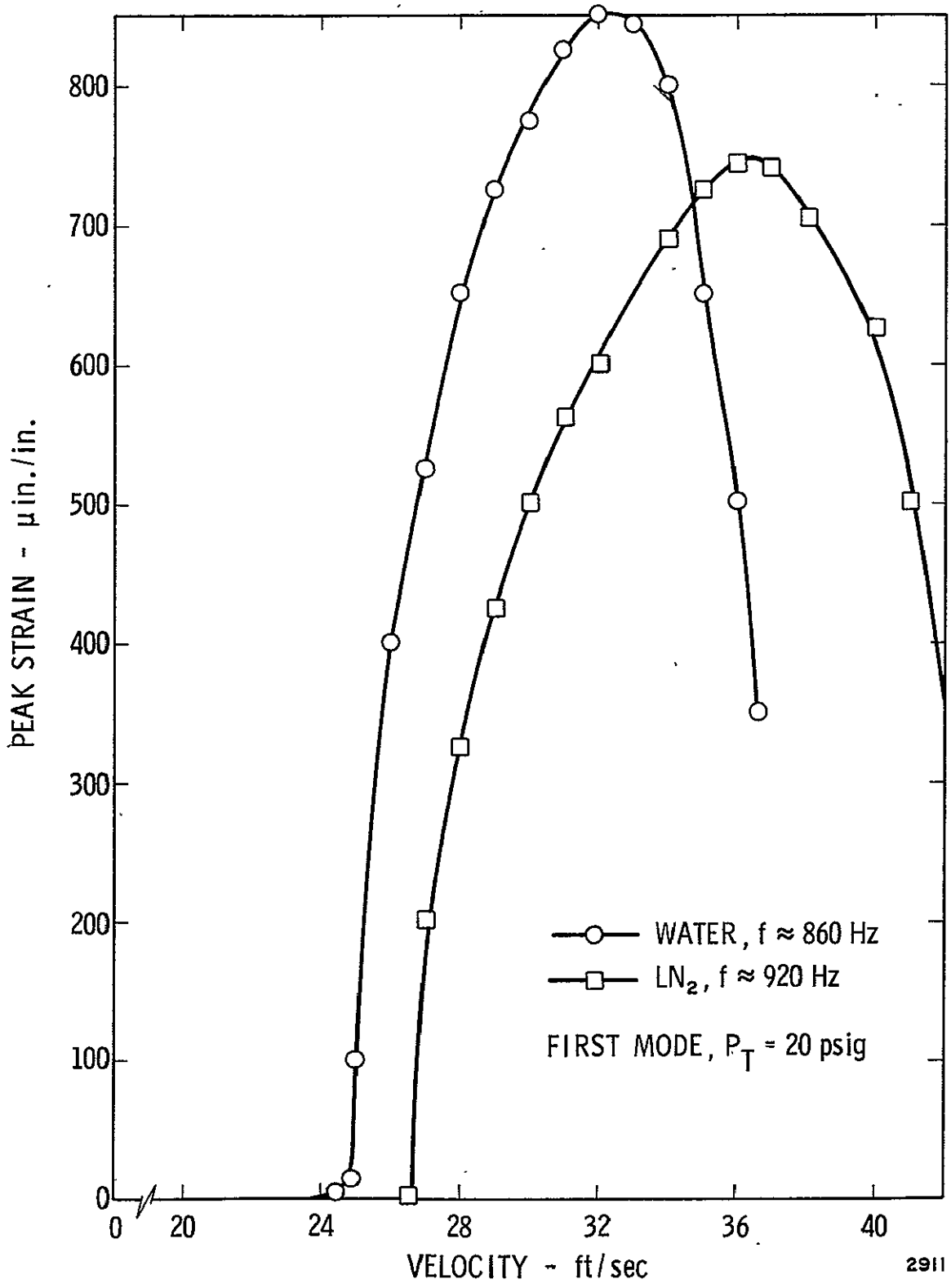

Figure 22. Comparison Of Flow-Induced Vibration With Water And LN_2, Bellows #4

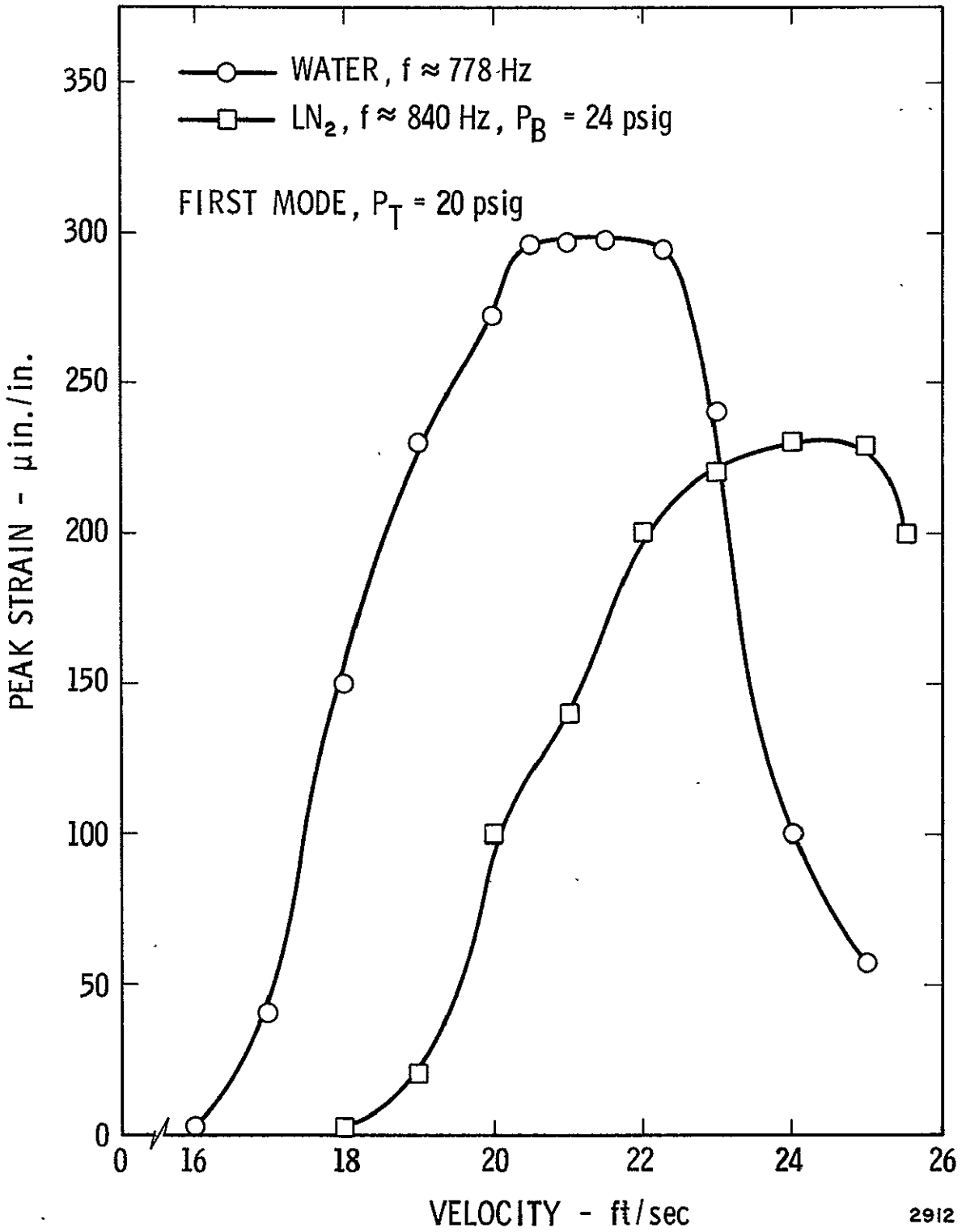

Figure 23. Comparison Of Flow-Induced Vibration With Water And LN_2, Bellows #3

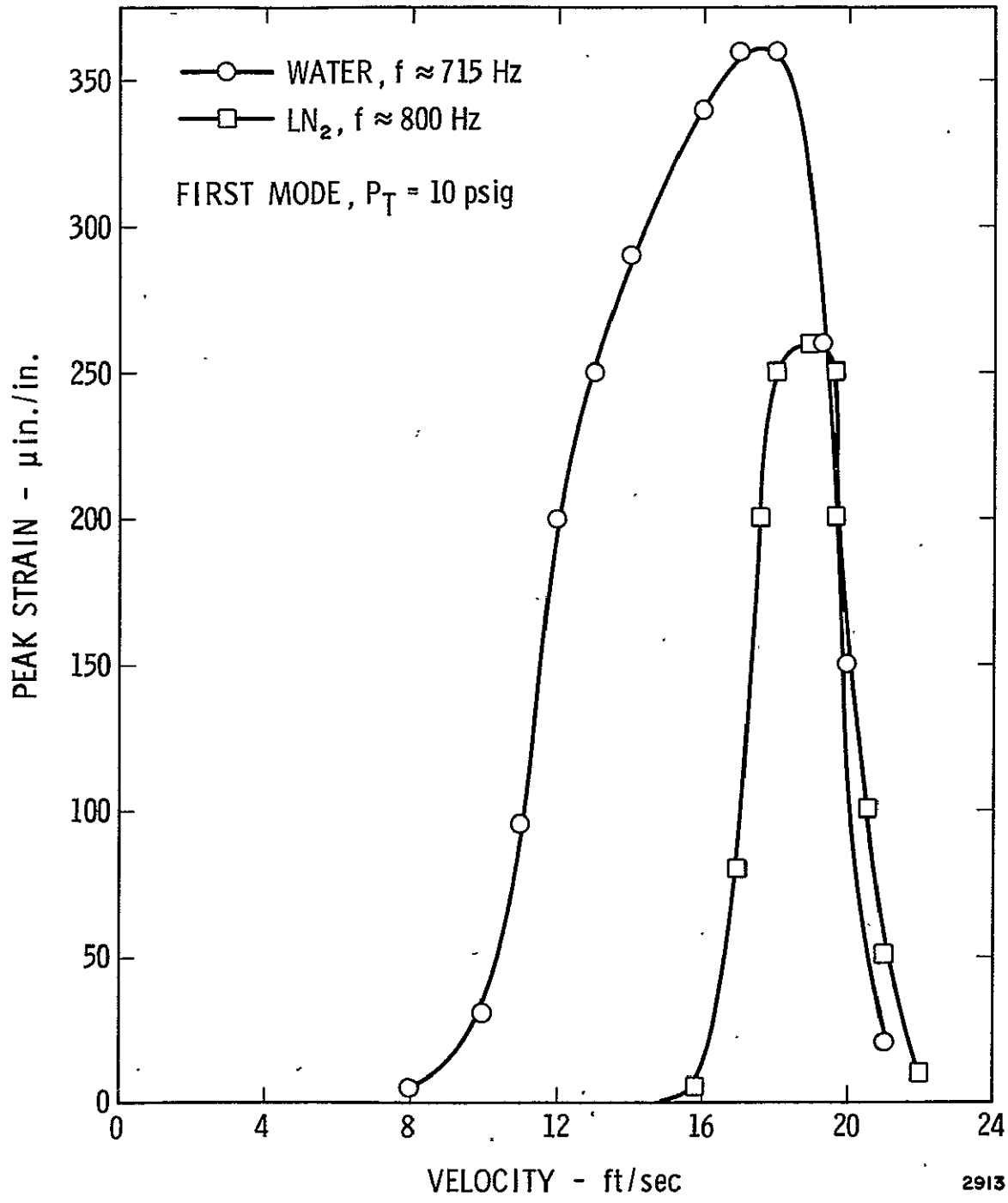

Figure 24. Comparison Of Flow-Induced Vibration With Water And LN_2, Bellows #5

To provide initial quantitative information of the effects of heat addition during operation of flow excited bellows, a duct was designed to surround the bellows completely so that hot air could be passed over the convolutes. A thermocouple was located at both the entrance and exit of this duct so that the change in air temperature could be recorded as it passed over the cold bellows containing flowing LN_2. From thermodynamics, the heat added or removed per-unit mass of a gas at constant pressure is given by

$$d\dot{Q}^* = c_p dT \tag{5}$$

where c_p is the specific heat at constant pressure of gas (air). For a flowing gas losing heat between arbitrary points 1 and 2, Equation (5) becomes

$$\dot{Q}^* = \dot{w}\, c_p\, (T_2 - T_1) \tag{6}$$

where $\dot{w}$ is the weight flow per unit time. This expression represents the heat input per unit time into the bellows section. In the experiment, the heating air weight flow, $\dot{w}$, was produced by a blower with a 20 amp heating element located at the entrance of the duct, and was calibrated by measuring the velocity and, hence, mass flow at the duct entrance. Since some of the heat was lost into the duct itself and not all absorbed by the bellows, a calibration of heat ($\dot{Q}^*_d$) lost to the duct alone was also made. This value was always subtracted from the total heat lost per unit time, $\dot{Q}^*$, to obtain the actual heat per unit time added to the bellows section alone, $\dot{Q}^*_B$, or

$$\dot{Q}^*_B = \dot{Q}^*_T - \dot{Q}^*_{duct} \tag{7}$$

With the flow loop operating at a velocity which produced maximum excitation of the first mode of the bellows, the heating rate was increased with time, and the resulting strain or stress amplitude was recorded. Typical results are shown in Figure 25, and these results indicate that increasing the heating rate produced a corresponding decrease in strain until a point was reached where the vibration was completely suppressed. Therefore, it was concluded that heat transfer did affect bellows response in a manner similar to vapor addition in the two dimensional visualization flow channel.

Bellows usually operate under conditions of approximately steady state heat transfer, therefore the results in Figure 25 for transient heating are not typical of bellows environmental conditions but do indicate the possible effects from heat transfer. Since vapor formation in the bellows

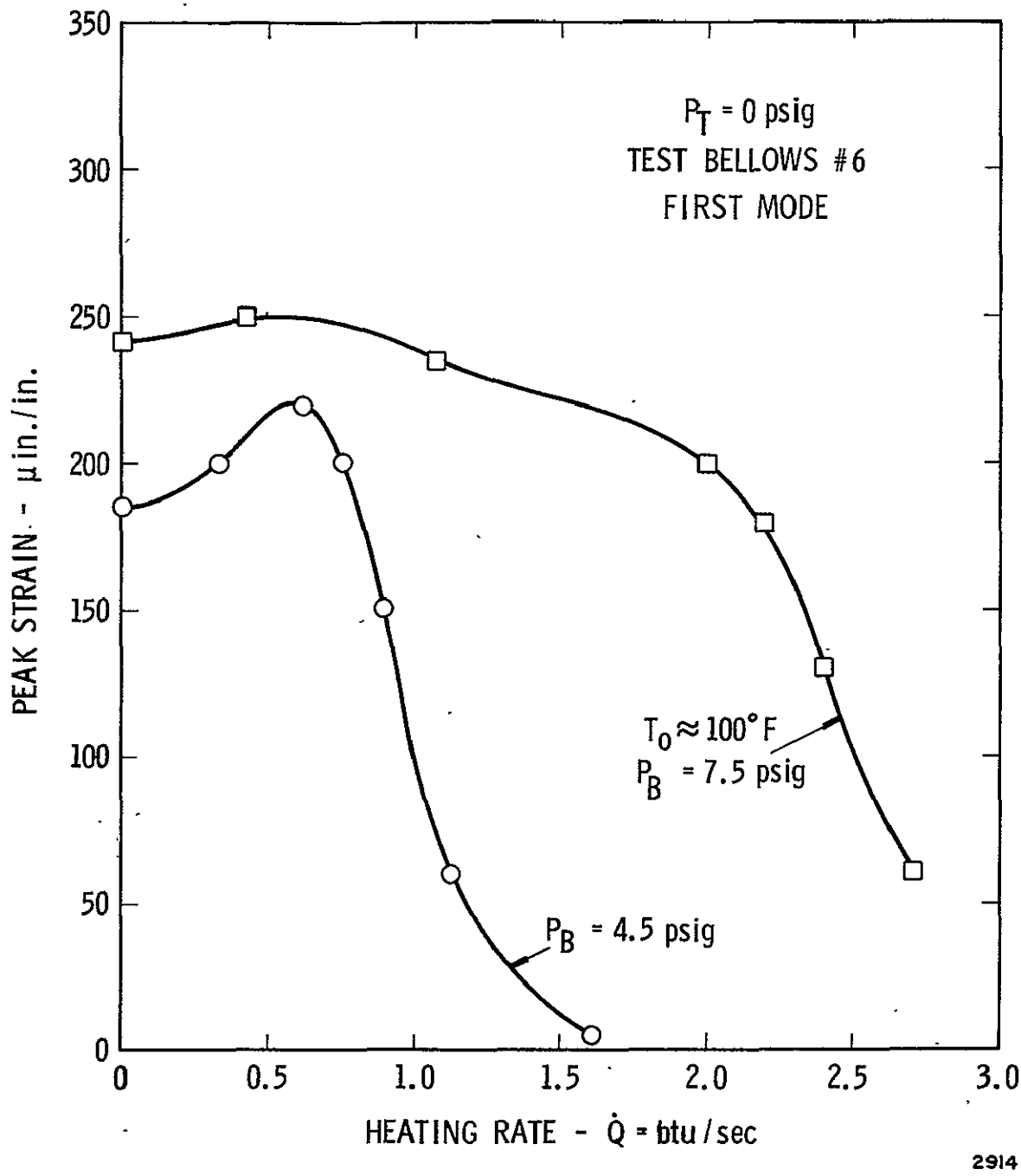

Figure 25. Effect Of Heating Rate On Maximum Strain Level

convolutes will be affected by operating pressure, (compare the results for P_B = 7.5 versus 4.5 in Figure 25) a test was conducted to determine the effect of bellows pressure on strain response with constant heat input. To produce these conditions, a bellows with flow excitation of its first mode was surrounded with cold GN_2 to maintain constant heat transfer, and the operating pressure was varied from 0 to 25 psig. Figure 26 shows the test results. This data is similar to that shown in Figures 13 to 18 for various bellows geometries. The strain response versus operating pressure shown in Figure 26 indicates that there is some minimum pressure at which the bellows will vibrate and produce maximum flow-induced strain. This pressure is indicated as P_{Bmax} in Figure 26 and is, then, the lowest operating pressure at which maximum strain will occur. As the pressure is decreased below P_{Bmax} the strain amplitude decreases rapidly until zero strain is recorded at P_{Bmin}, the highest operating pressure for no flow-induced vibration. Below P_{Bmin} no condition of flow excitation is observed. Therefore, under conditions of constant heat transfer there is a minimum operating pressure which will allow flow excitation to occur and produce vibrational strains in the bellows structure.

To better define the effects of heat transfer on P_{Bmax} and P_{Bmin}, additional experimental results were obtained at different levels of heating. Four conditions of heating were obtained by producing four levels of environmental temperatures, in the following ways:

(a) Surrounding the bellows with cold N_2 gas, $T_0 = -200^\circ F$

(b) Surrounding the bellows with cold N_2 gas-air, $T_0 = -145^\circ F$

(c) Surrounding the bellows with air, $T_0 = 45^\circ F$

(d) Surrounding the bellows with heated air, $T_0 = 285^\circ F$

For each of the four conditions of T_0, the bellows was operated at flow velocities corresponding to peak excitation of the first vibrational mode, and strain data was obtained over a range of operating pressures. The free stream temperature was $-320^\circ F$ (saturation temperature at 1 ATM in LN_2) for each heating level, and no frost was allowed to build up on the bellows external surface. At each test condition thermocouples recorded environment, skin and stream temperature. The results in Figure 27 show that as additional heat is added to the bellows, i.e., increasing T_0, the values of P_{Bmax} and P_{Bmin} are also increased. The same trend with increasing T_s is also shown in Figure 28 for a condition where the environmental temperature was held constant, and four levels of stream temperature

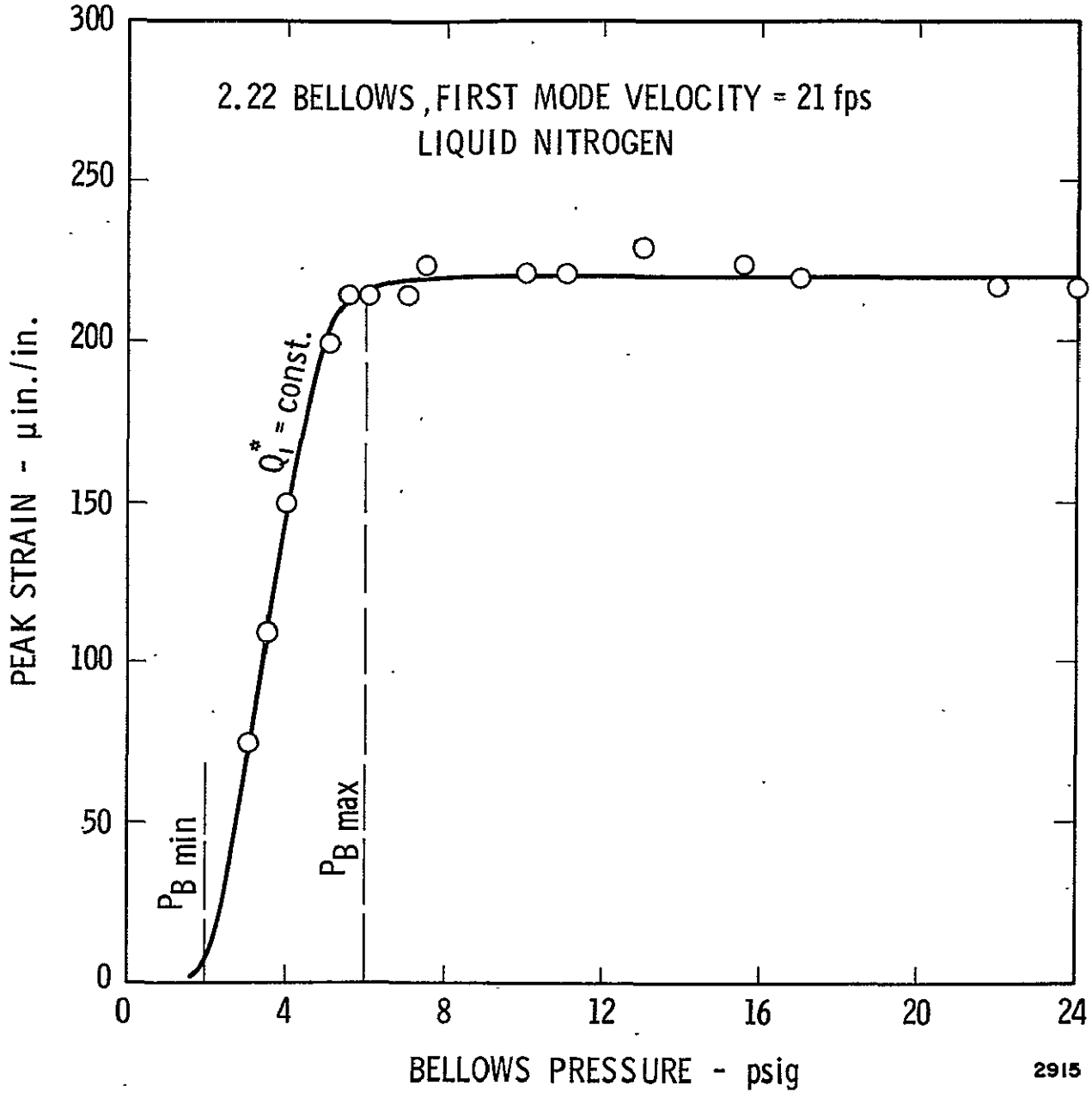

Figure 26. Effect Of Increasing Bellows Pressure On Maximum Strain Level

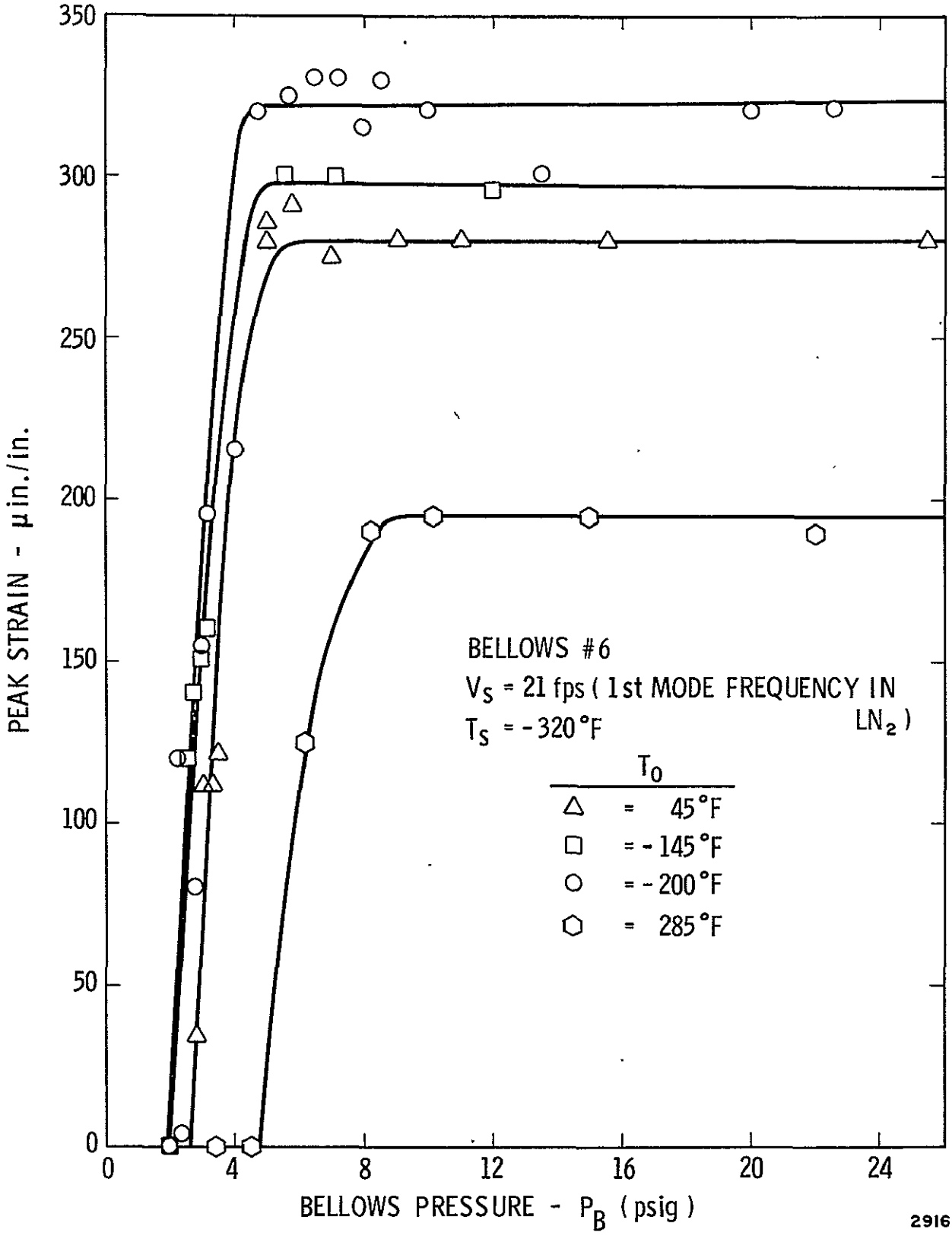

Figure 27. Effects Of Heat Transfer On Bellows Pressure At Zero And Maximum Strain With Different Environmental Temperatures

were used. The stream temperatures were increased by allowing the static LN_2 tank pressure to increase, which raised the system LN_2 temperature before it flowed through the bellows. The higher stream temperatures resulted in higher operating pressures required to insure peak strain.

The results in Figure 28 indicate that increased levels of heat transfer result in vapor formation at the low-operating pressures, hence producing a damping or complete suppression of the flow excitation. Increasing the operating pressure to P_{Bmax} will cause a recovery of the flow induced dynamic strain. The effect of an increased heat transfer rate is a corresponding shift of P_{Bmax} or P_{Bmin} with increasing stream temperature. Thus operating pressure must be increased to suppress vapor formation and maintain peak strain if

(a) The liquid is flowing at a given stream temperature and additional heat is transferred through the bellows wall raising the inside wall temperature and causing vapor formation in the convolutes, or

(b) The liquid stream temperature is increased by some change in operating conditions upstream of the bellows.

The bellows flow velocity required to produce peak flow-induced strain remained unchanged with changing heat transfer rates. The results in Figure 29 reveal this fact for the first mode frequency, which shows the peak excitation resulted at approximately 21 fps for all four environmental temperatures. An investigation of the theoretical bellows frequency change with large temperature changes supports the experimental results, showing no frequency shift should occur with different levels of bellows temperature. That is, the bellows frequency (1) is given by

$$fo = \frac{1}{2\pi} \left(\frac{k}{m}\right)^{1/2} \tag{8}$$

where k is the bellows spring rate and m an elemental model mass composed of fluid and metal contributing terms. Large changes in temperatures will affect the spring rate k because of changes in Young's modulus, and will affect the model mass by changing the fluid mass from a liquid to a gas. However, these effects on the natural frequency are negligible, as the frequency decreases only 3 percent for changes in Young's modulus for stainless steel over a temperature range from -300°F to 100°F, while mass changes produced by the liquid vaporizing creates a frequency increase of 5 percent. The combined effect of both a change in Young's modulus and the model mass is a 2 percent increase in the bellows frequency for the 400°F temperature change. This change is considered insignificant since peak strain occurs over a band of frequencies larger than $\pm$ 2 percent of the mean.

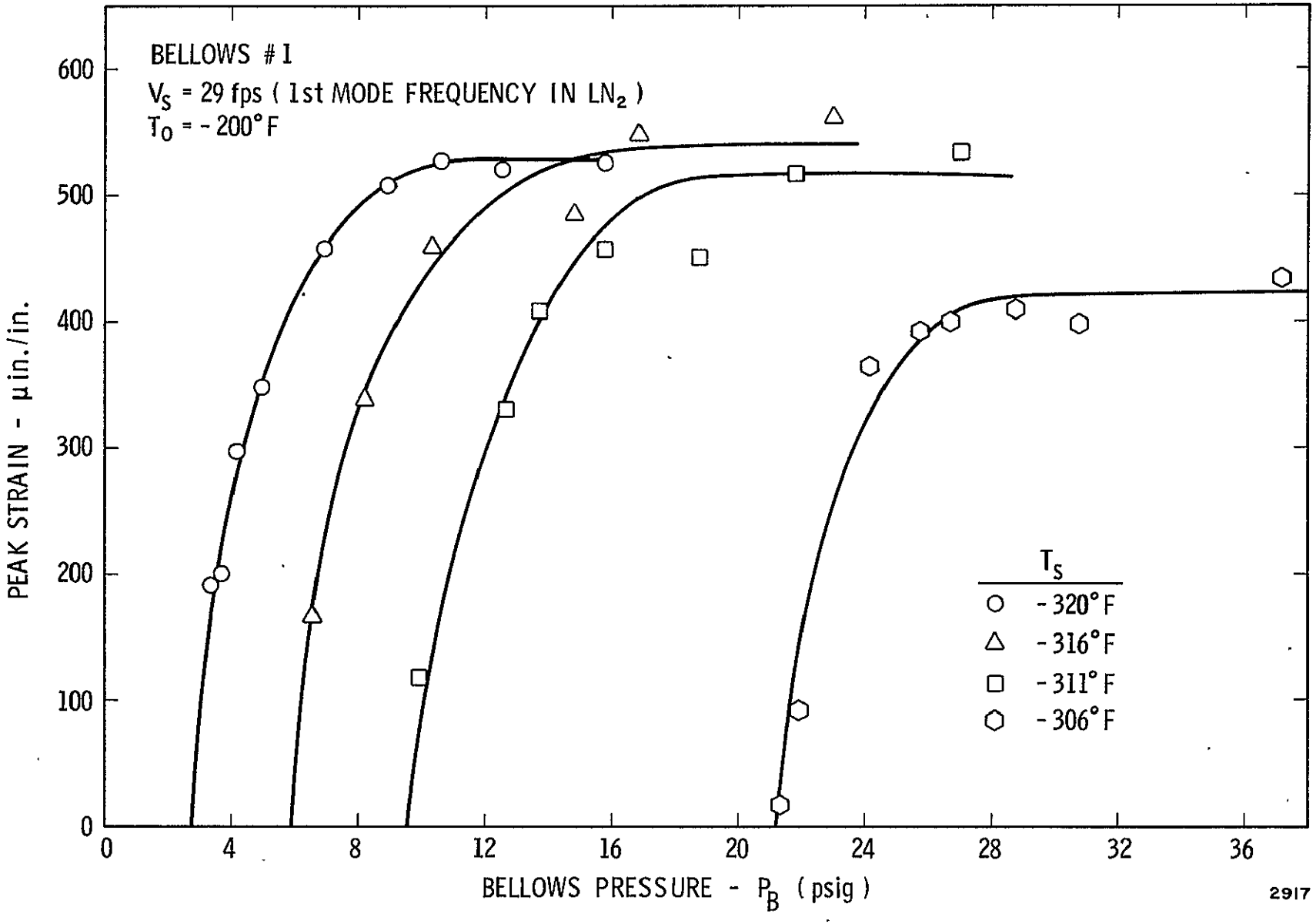

Figure 28. Effects Of Heat Transfer On Bellows Pressure At Zero And Maximum Strain With Different Stream Temperature

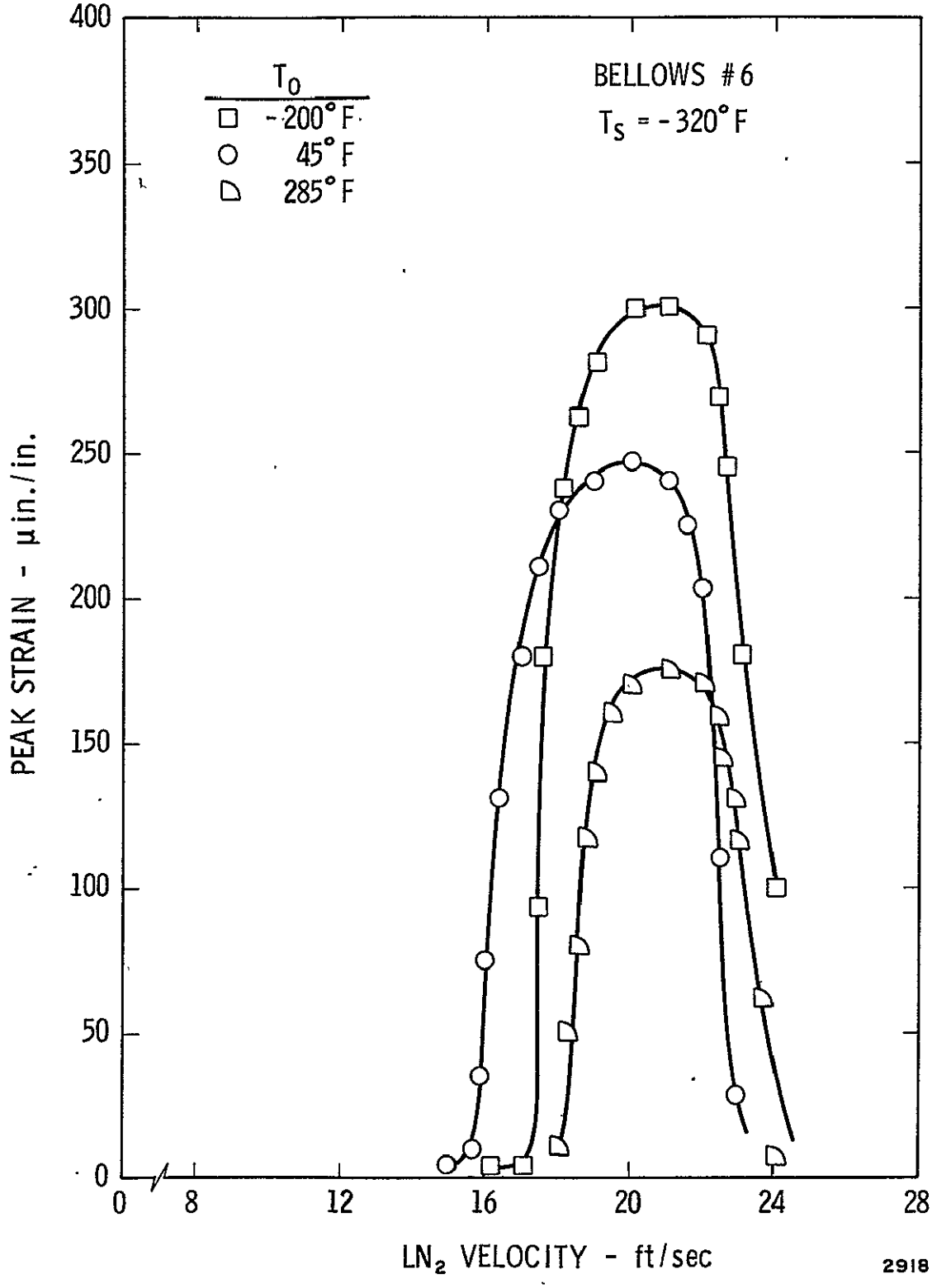

Figure 29. Effect Of Environmental Temperature On First Mode Frequency

IV.6 Pressure Drop Data

The pressure drop across the bellows was recorded during tests to establish heat transfer effects with LN_2. The results of the pressure drop versus operating pressure are presented in Figure 30 for the case of $T_0 = -200^{\circ}F$. Results at the other test environmental conditions indicate the same trend in pressure drop across the bellows. The results in Figure 30 show that below P_{Bmin} an increase in pressure causes a decrease in pressure drop resulting from a reduction in the vapor formation in the flowing LN_2. Near P_{Bmin} additional increases in pressure cause enough suppression of the vapor phase so that vortex shedding begins to occur, and this causes disturbances in the flow and an increase in the pressure drop. Increasing pressure from P_{Bmin} to P_{Bmax} creates an increase in the pressure drop as the vibrational amplitudes build to a maximum. Increasing the pressure above P_{Bmax} results in decreasing the pressure drop since vibrational effects remain constant but the flow media progressing further into the liquid phase. Although results were not obtained at pressures higher than 20 psig, it is expected that the pressure drop would level off at the higher pressures and remain at a constant value.

The pressure drop data presented here indicates that bellows heating will not only create a change in the vibrational characteristics of bellows but will also alter their pressure drop characteristics.

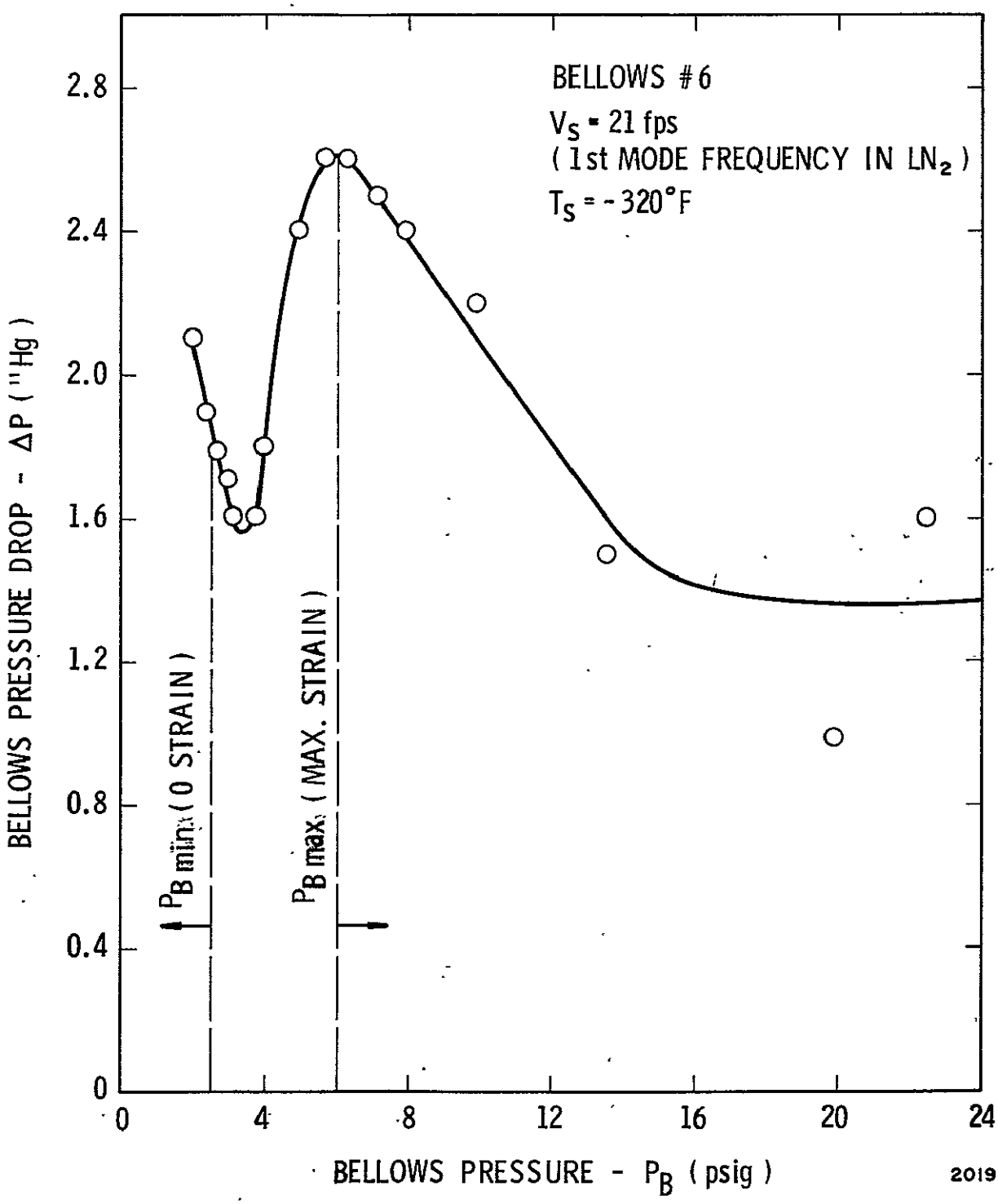

Figure 30. Bellows Pressure Drop versus Operating Pressure

V. HEAT TRANSFER ANALYSIS

V.1 Introduction

The experimental results presented in the preceding section indicate that heat transfer to a flowing cryogen through a bellows wall can change the flow-induced response of the bellows by altering the vortex shedding phenomena. A concept of how this likely occurs is illustrated in Figure 31. For a condition of no heat transfer, the vortex shedding phenomena will behave as illustrated in Figure 31a. If, however, the fluid is heated somewhat, and the internal pressure is low enough, then cavitation in the vortex formation and shedding region can occur, and this will tend to reduce the vortex force; see Figure 31b. For even greater heating inputs, local boiling can occur in the convolutes as well, as shown in Figure 31c; this likely corresponds to a condition of complete suppression of the vortex shedding phenomena.

In order to gain a better understanding of the heat transfer effects, and to obtain a method for predicting the operating conditions at which the bellows response characteristics are altered, a heat transfer model has been developed. The model may be used to predict temperature distributions across the bellows between the environment and the flowing medium. A knowledge of this distribution, combined with a defining cavitation number, allows the operating pressures at the initial points of maximum and minimum dynamic strain to be correlated and predicted. The effect of frost formation on these pressures is also obtained, and a limiting frost thickness is determined for different environmental conditions.

V.2 Heat Transfer Model Development

Geometry

The bellows geometry, Figure 32, for purposes of setting up a heat transfer model, was assumed to be a thin walled cylinder of radius, r_m, equal to the mean radius of the bellows and of length ℓ corresponding to the actual expanded length along the convoluted surface. This length is given in terms of the bellows geometric parameters as

$$\ell = 2N_c \left(\frac{Do-Di}{2}\right) + \left(2N_c - 1\right) \sigma , \qquad (9)$$

and the corresponding wall area is

$$A_w = 2\pi r_m \ell$$

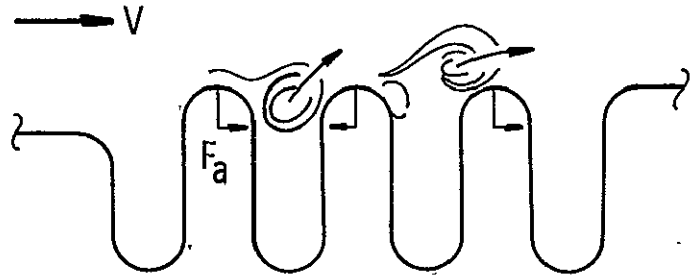

(a) NO HEAT INPUT - CONVENTIONAL VORTEX PHENOMENA

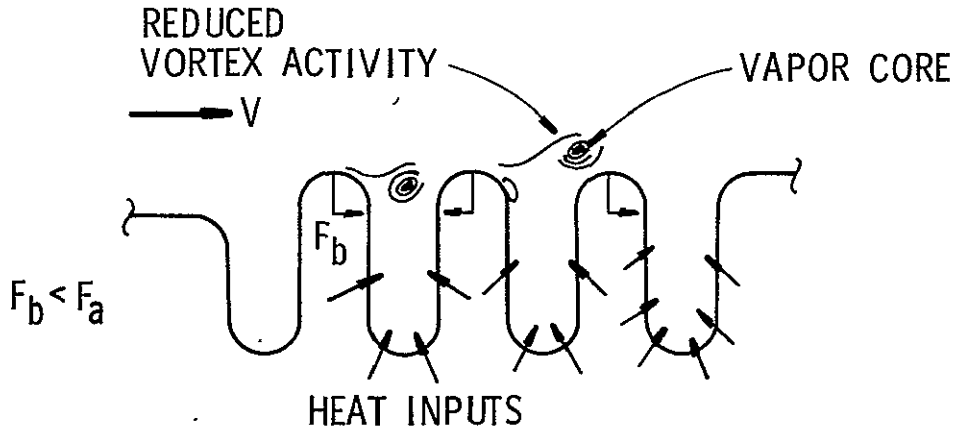

(b) EXTERNAL HEATING - VAPOR CORE IN VORTEXES

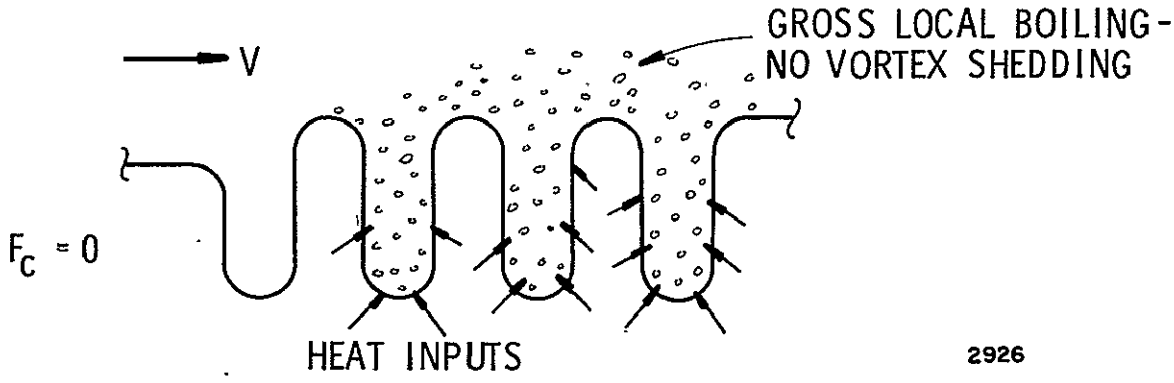

(c) EXTERNAL HEATING - GROSS BOILING

Figure 31. Illustration Of Heating Effect On Bellows Vortex Shedding Flow Excitation

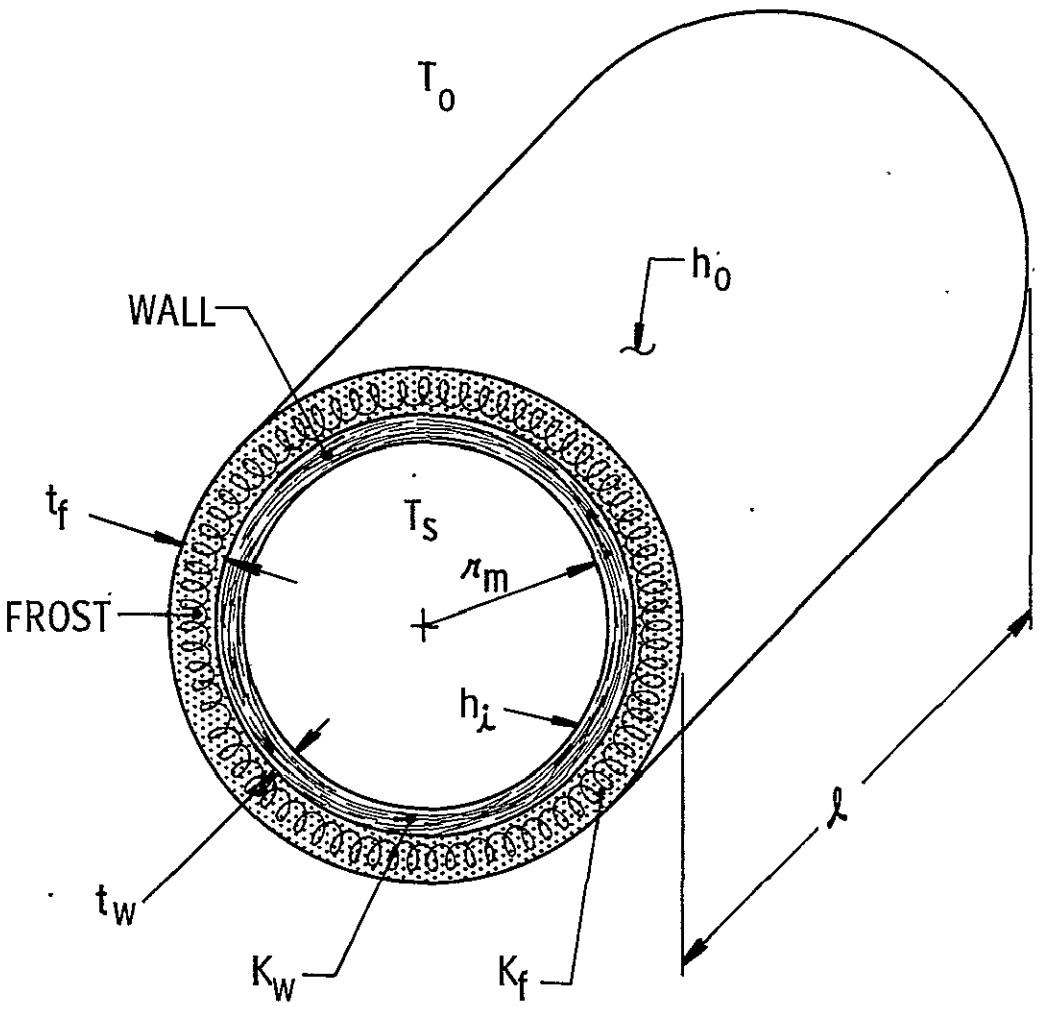

$$r_m = \frac{r_i + r_o}{2}$$

$$\ell = N_c \left(\frac{r_o - r_i}{2}\right) + (2N_c - 1)\ \sigma$$

$$A_{wi} = 2\pi r_m \ell$$

$$A_{wo} = 2\pi\ (r_m + t_w + t_f)\ell$$

Figure 32. Bellows Geometry For Transfer Model

2928

Heat Transfer

The heat transfer was assumed to be one-dimensional steady-state conduction and convection in the radial direction of the thin-walled cylinder, with no conduction along its length.

The heat transferred between the bellows environment, at temperature T_0, and the flowing liquid at T_s is given by

$$\dot{Q}^* = \frac{T_0 - T_s}{\Sigma R} \tag{10}$$

where

$$\Sigma R = R_1 + R_2 + R_3 + R_4$$

which is the total resistance to heat transfer caused by the thermal potential, $T_0 - T_s$. The resistances are defined as follows:

$$R_1 = \frac{1}{A_{wo}\, h_o} \tag{11}$$

which is the convection resistance between the environment and the outside surface (frost or wall).

$$R_2 = \left[\ln\left(\frac{r_m + t_w + t_f}{r_m + t_w}\right)\right]\left(\frac{1}{2\pi\ell\, K_f}\right) \tag{12}$$

is the conduction resistance of the frost at thickness t_f and having a thermal conductivity K_f;

$$R_3 = \left[\ln\left(\frac{r_m + t_w}{r_m}\right)\right]\left(\frac{1}{2\pi\ell\, K_w}\right) \tag{13}$$

is the conduction resistance of the wall at thickness t_w and with thermal conductivity K_w;

and

$$R_4 = \frac{1}{h_i A_{wi}} \tag{14}$$

is the convection resistance between the inside wall and the free stream.

In order to utilize these equations to obtain heating rates and temperatures, a knowledge of the inside and outside convection coefficients, h_i and h_o, must be known as well as the bellows geometry, and thermal conductivity, K_w, and the frost conditions, t_f and K_f. The most difficult parameter to estimate is the inside heat transfer coefficient, h_i, which depends on the state of the LN_2 in the convolutes. That is, can the heat transfer between the inside wall and the stream be described as

(a) Forced convection with minimum boiling ($T_{wi} - T_s < 5^o$)

(b) Forced nucleate boiling ($5^o < T_{wi} - T_s < 20^o$)

(c) Forced unstable film boiling ($20 < T_{wi} - T_s < 60^o$), or

(d) Forced film boiling ($T_{wi} - T_s > 60^o$) ?

The temperature ranges given above are for pool (static fluid) boiling, but a review of experimental data of forced flow boiling heat transfer to cryogenic fluids indicates that these ranges are approximately correct for forced flow boiling also. While a tremendous amount of work has been done on pool boiling of liquids, few correlations exist for forced flow boiling heat transfer. Some experimental work and a few analytical studies are available as a guide.

If Case (a) represents the heat transfer in the convolutes then the work of Nunner (3) can be used to estimate h_i, thus

$$\frac{Nu_d}{Re_d Pr^1} = \frac{0.0384\,(Re_d)^{-1/4}}{1 + A\,(Re_d)^{-1/8}\,(P_r{}^1 - 1)} \tag{15}$$

where

$$P_r{}^1 = P_r\,(f/f_o)$$
$$A = 1.5\,(P_r{}^1)^{-1/6} \tag{16}$$

and the bellows friction factor, f^*, and that for a smooth pipe, f_o^*, are determined for the bellows Reynolds number, Re_d.

If Case (b) is valid where nucleate boiling dominates, then from Reference 4, h_i is given by

$$\frac{C_p(T_{wi} - T_s)}{h_{fg}} = a \left\{ \frac{h_i(T_{wi} - T_s)}{\mu_\ell\, h_{fg}} \right\}^{1/3} \cdot \left\{ \frac{\tau}{g(\rho_\ell - \rho_v)} \right\}^{1/6} P_r{}^{1.7} \tag{17}$$

where $0.0022 < a < 0.015$.

For Case (c) Bromley (5) estimated h_i by

$$h_i = C \left\{ \frac{V_\infty K_v \rho_v \lambda^1}{D_w (T_{wi} - T_s)} \right\}^{1/2} \tag{18}$$

where

$$\lambda^1 = h_{fg} \left\{ 1 + \frac{0.4 (T_w - T_s) C_{pv}}{h_{fg}} \right\}$$

and C = 2.7 for forced flow over horizontal tubes.

Once the state of the fluid in the convolutes has been determined then either Equation (15), (17) or (18) may be used in the analysis. If unstable film boiling exists ($20 < Tw-Ts < 60^oF$) no analytical method is available, and an extrapolation between nucleate and film boiling must be used.

The outside convection coefficient, h_o, can be determined from correlations for the forced flow of air over cylinders, by

$$\frac{h_o D_o}{K_{air}} = C \left(\frac{V_{air} D_o}{\nu_{air}} \right)^m \tag{19}$$

where C and m are functions of Reynolds number, or from the literature when natural convection is considered. Typical values of h_o for natural convection of air to cylinders range from 1 to 5 Btu/hr ft^2 ^oF.

Pressure at Peak and Zero Strain

With the heat transfer model in hand, the bellows inside wall temperature can be determined by

$$T_{wi} = T_s + \overset{*}{Q} R_4 \tag{20}$$

Knowing T_{wi}, an estimate of the bellows operating pressure at peak and zero strain can be obtained from a set of cavitation numbers defined as

$$\sigma_m = \frac{P_{Bmax} - P_v @ T_{wi}}{q_\infty} \qquad \text{(Cavitation number at peak strain)} \tag{21}$$

$$\sigma_o = \frac{P_{Bmin} - P_v @ T_{wi}}{q_\infty} \qquad \text{(Cavitation number at zero strain)} \qquad (22)$$

where P_v at T_{wi} is the vapor pressure corresponding to the inside wall temperature and q_∞ is the dynamic stream pressure. The vapor pressure, P_v, is given by the relation (Reference 6)

$$\text{Log}_{10}\ P_v\ (\text{ATM}) = A_1 + A_2/T_{wi} + A_3\ T_{wi} + A_4\ T_{wi}^2 + A_6\ T_{wi}^3 + A_6\ T_{wi}^4 + A_7\ T_{wi}^5 \qquad (23)$$

where
$$A_1 = 5.27805(10^{-1})$$
$$A_2 = 3.0507339(10^{-2})$$
$$A_3 = 1.6441101(10^{-1})$$
$$A_4 = 3.1389205(10^{-3})$$
$$A_5 = 2.9857103(10^{-5})$$
$$A_6 = 1.4238458(10^{-7})$$
$$A_7 = 2.7375282(10^{-10})$$

and T_{wi} in ^oK.

The cavitation numbers at peak and zero strain, together with the inside wall temperature, LN_2 flow velocity and density, allow P_{Bmax} and P_{Bmin} to be calculated.

To determine P_{Bmin} and P_{Bmax} for a given bellows operating and environmental condition:

(a) Calculate T_{wi} from heat transfer analysis.

(b) Determine P_v at T_{wi}

(c) Calculate P_{Bmin} from σ_o (determined experimentally)

(d) Calculate P_{Bmax} from σ_m (determined experimentally)

The experimentally determined cavitation numbers are presented in the next section.

V.3 Results

Cavitation Numbers at Peak and Zero Strain

The model presented in the preceding section requires a knowledge of the cavitation number in order that an estimate of the operating pressures at peak and zero strain may be made. The experimental P_{Bmax} and P_{Bmin} data presented in Figures 27 and 28, together with the heat transfer model (which yields P_v at T_{wi}) allowed σ_o and σ_m to be determined. To utilize the heat transfer equations, the inside convection coefficient h_i was determined from Equation (15), and the outside coefficient h_o was assumed to be 4 Btu/hr ft^2 ^oF. Use of Equation (15) to determine h_i was based on the fact that experimental values of outside bellows skin temperature obtained in the testing revealed that the wall temperature remained near the stream temperature. This indicates that the inside heat transfer is the result of forced convection. A value of 4 Btu/hr ft^2 ^oF was chosen for h_o since the bellows environment was calm, but bellows vibrations caused some agitation of the air near the convolutes. Work on natural convection from vibrating wires (7) indicates that the assumption of h_o = 4 Btu/hr ft^2 ^oF is valid. Fluid and thermal properties in Equation (15) were evaluated at the stream temperature. Usually, an evaluation of properties is made at some stream temperature between stream and wall values. This requires an accurate guess of T_{mean}, or use of an iteration procedure until the guessed and calculated values correspond. Since wall and stream temperature values were within a few degrees, using the stream temperature to determine h_i should result in negligible error.

Vapor pressures corresponding to T_{wi} calculated from the model, and combined with experimental values of P_{Bmax} and P_{Bmin} were used to determine σ_o and σ_m from Equations (21) and (22). The results are presented in Figure 33. The average cavitation number at initial maximum strain (σ_m at P_{Bmax}) for the eight experimental conditions is 2.25. The cavitation number at initial zero strain (σ_o at P_{Bmin}) is 0.4 for the eight experimental conditions. These cavitation numbers are reasonable considering initial cavitation usually occurs when the cavitation number is reduced to near one, and gross cavitation occurs between zero and one. These results indicate that when operating conditions are such that the cavitation number nears σ_m initial cavitation begins and vortex shedding is damped; see Figure 31b. When σ_o is approached, vortex shedding is completely suppressed; see Figure 31c.

Operating Pressures for Different Environmental Conditions

The cavitation numbers given in the previous section, together with the heat transfer analysis have been used to predict P_{Bmax} and P_{Bmin} under more general conditions than those tested. The computations were made by

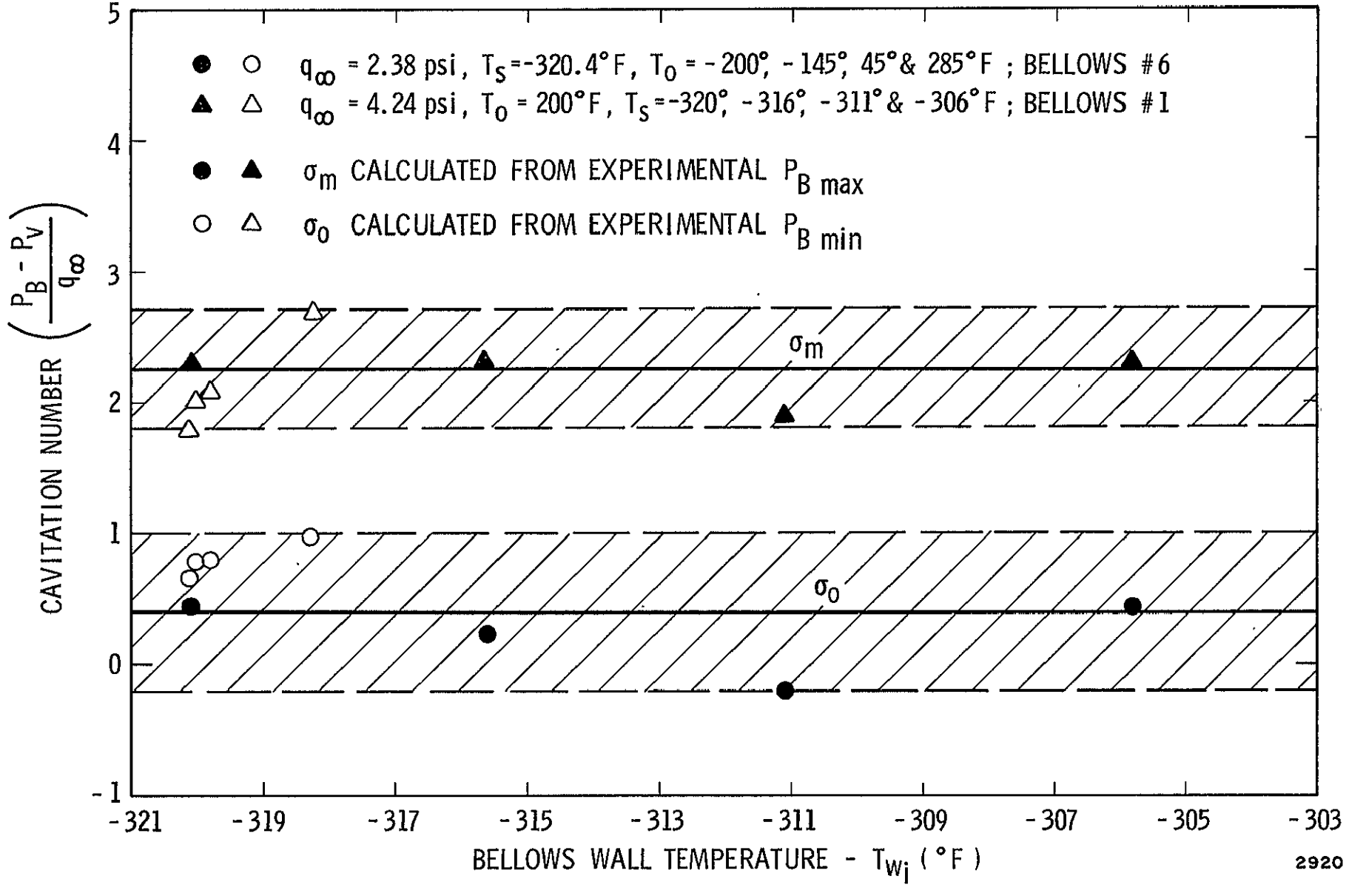

Figure 33. Experimental Cavitation Numbers At Maximum Strain (σ_m) And At Zero Strain (σ_0)

a digital computer, since the equations are cumbersome and not conducive to hand calculations. A listing of the program is provided in the Appendix. The computation proceeds as follows:

(a) Bellows geometry and LN_2 flow velocity and temperature are introduced into the program.

(b) Equation (15) is used to determine h_i with LN_2 properties evaluated at T_s.

(c) Environmental temperature T_0, outside convective coefficient h_o and frost thickness t_f were allowed to vary.

(d) Frost thermal conductivity (8) is assumed to be 0.030 Btu/hr ft ^oF, and bellows wall conductivity 10.0 Btu/hr ft ^oF for stainless steel.

(e) Equations (11) and (14) are used to determine the heat transfer resistances.

(f) Equation (10) is used to calculate the heat transfer.

(g) Equation (20) is used to obtain T_{wi} and Equation (23) to determine P_v.

(h) P_{Bmin} is then determined from Equation (22) for σ_o range of 0 to 1.0 and P_{Bmax} for σ_m from 1.75 to 2.75.

(i) P_{Bmax} and P_{Bmin} are determined for a range of T_0 from -200 to 280^oF and for h_o varying between 2 and 20 Btu/hr ft^2 ^oF (from natural to forced convection on the outside bellows surface). Frost thickness is varied from 0 to 1 inch at each condition of T_0 and h_o.

The results of the previous calculation procedure indicate that the largest resistance to heat transfer from the environment to the fluid flowing in a bellows occurs from the outside convection characteristics and from the insulating effect from the frost. The thin bellows wall offers little resistance to heat flow, and the inside convection resistance is small because of the forced flow over the rough convoluted surface. Since the inside convection resistance is small, the inside wall temperature remains only a few degrees above the stream value, and use of Equation (15) remains

valid. Equation (15) is also considered ideal for estimating h_i since it was shown to fit experimental data taken on pipes artificially roughened by attaching various size rings to the inside surface. The rings would be directly analogous to the convoluted section of a bellows. The friction factor, f^* used in Equation (15) was determined from previous friction factor data (1) obtained for 2-inch diameter bellows over a range of Reynolds numbers.

No Frost Formation

The results of this analysis are presented in Figures 34 and 35 for a 2-inch diameter bellows flowing LN_2 at a velocity of 21 fps, corresponding to the first mode frequency, and with no frost formation on the bellows exterior surface. The values of P_{Bmax} and P_{Bmin} were determined from σ_o and σ_m equal to 0.4 and 2.25, respectively. The results indicate that

(a) Increasing the outside convection coefficient from 2 to 12 Btu/hr ft ^oF, with a constant environmental and stream temperature, causes a corresponding increase in the value of P_{Bmax} and P_{Bmin}. The range on h_o represents natural convection (h_o = 4 Btu/hr ft^2 ^oF) to forced convection at h_o = 12 Btu/hr ft^2 ^oF, representing a wind velocity of 40 mph from Equation (19).

(b) Increasing T_0 at a constant h_o and T_s also results in a corresponding increase in P_{Bmax} and P_{Bmin}.

Frost Formation

The effects of frost formation are presented in Figures 36 and 37 for the same bellows and flow conditions as for the no-frost case. In this case environmental temperature is held constant at 80^oF and the effects of frost thickness with varying outside convection conditions are presented. The limiting frost thickness is determined by examining the frost temperature at the outside surface as given by

$$T_{fo} = T_{wi} + \dot{Q}^* R_2$$

Once the frost thickness has increased to a point where the temperature drop across the frost is such that T_{fo} = 32^oF, then no additional frost buildup will occur. The limiting thickness will depend on the total heat

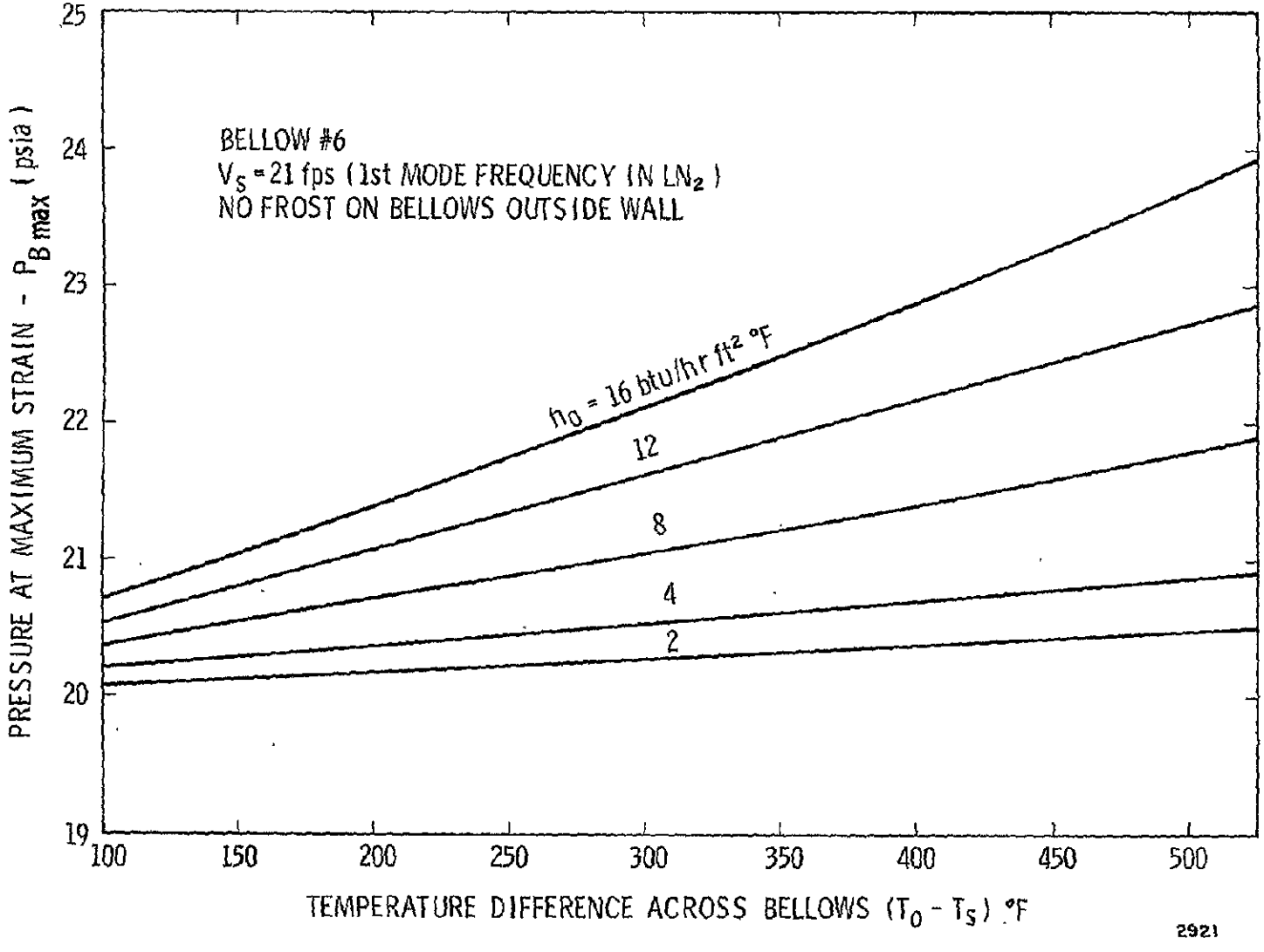

Figure 34. Bellows Pressure At Maximum Strain With No Frost On Wall

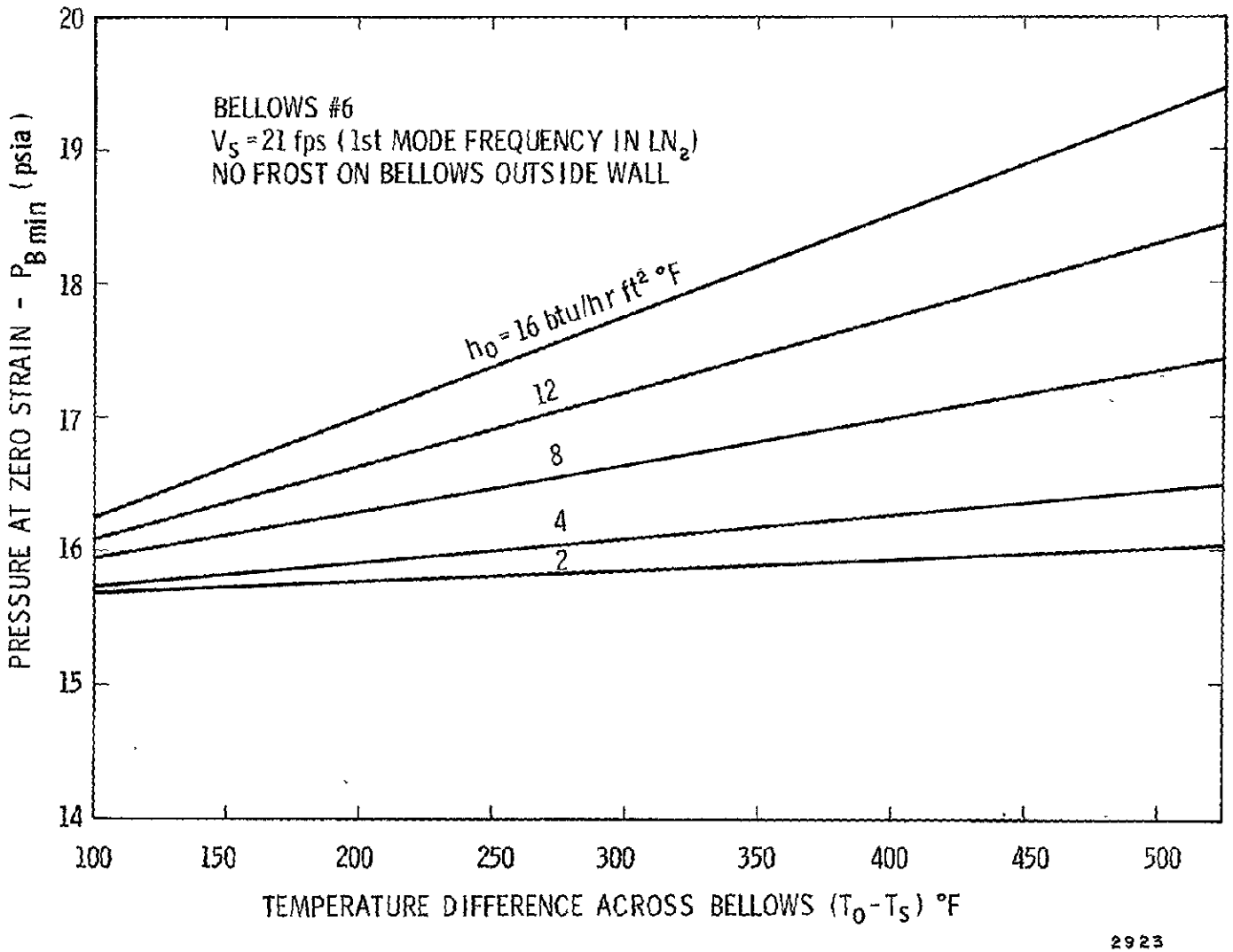

Figure 35. Bellows Pressure At Zero Strain With No Frost On Wall

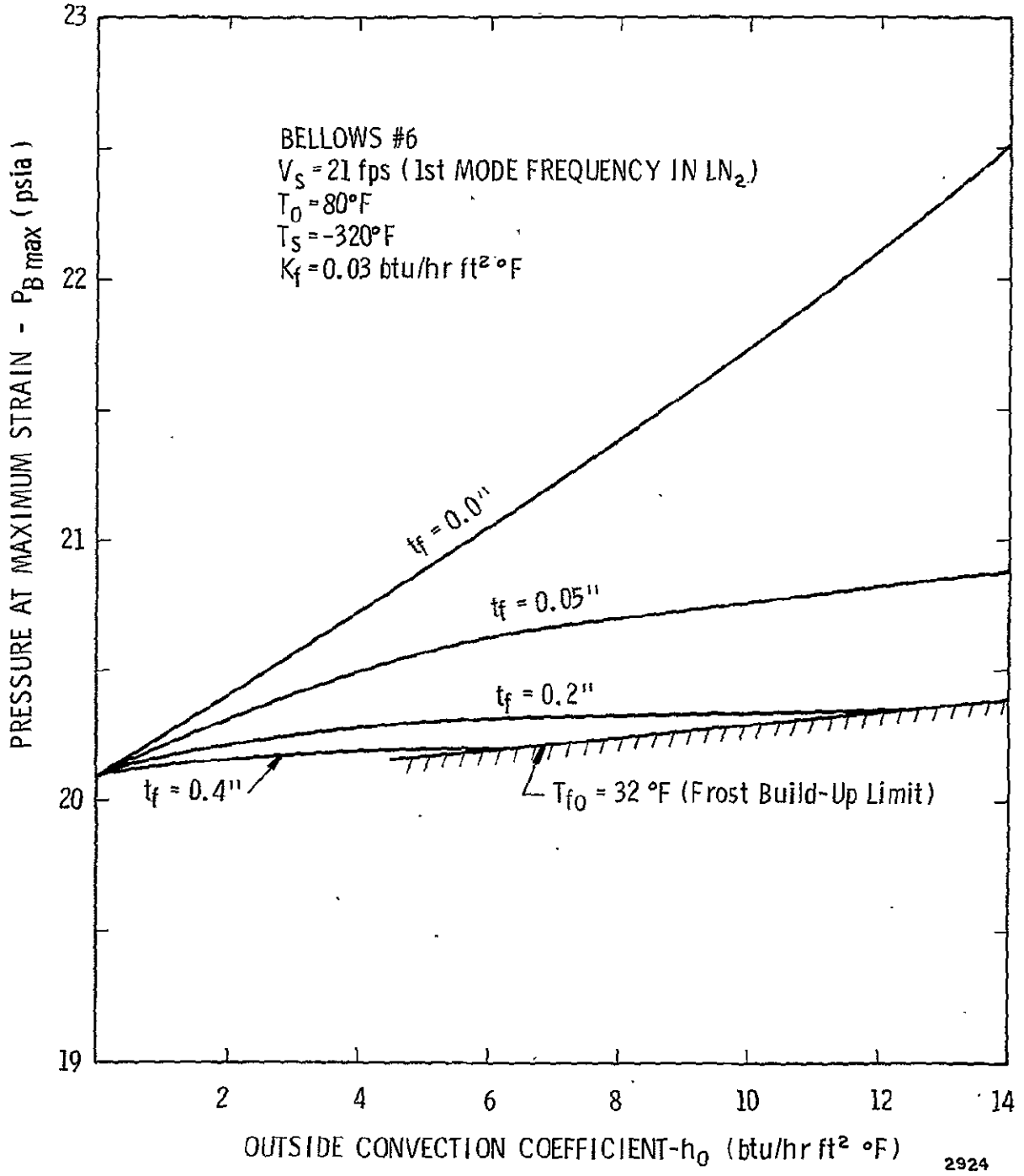

Figure 36. Bellows Pressure At Maximum Strain With Frost Build-Up

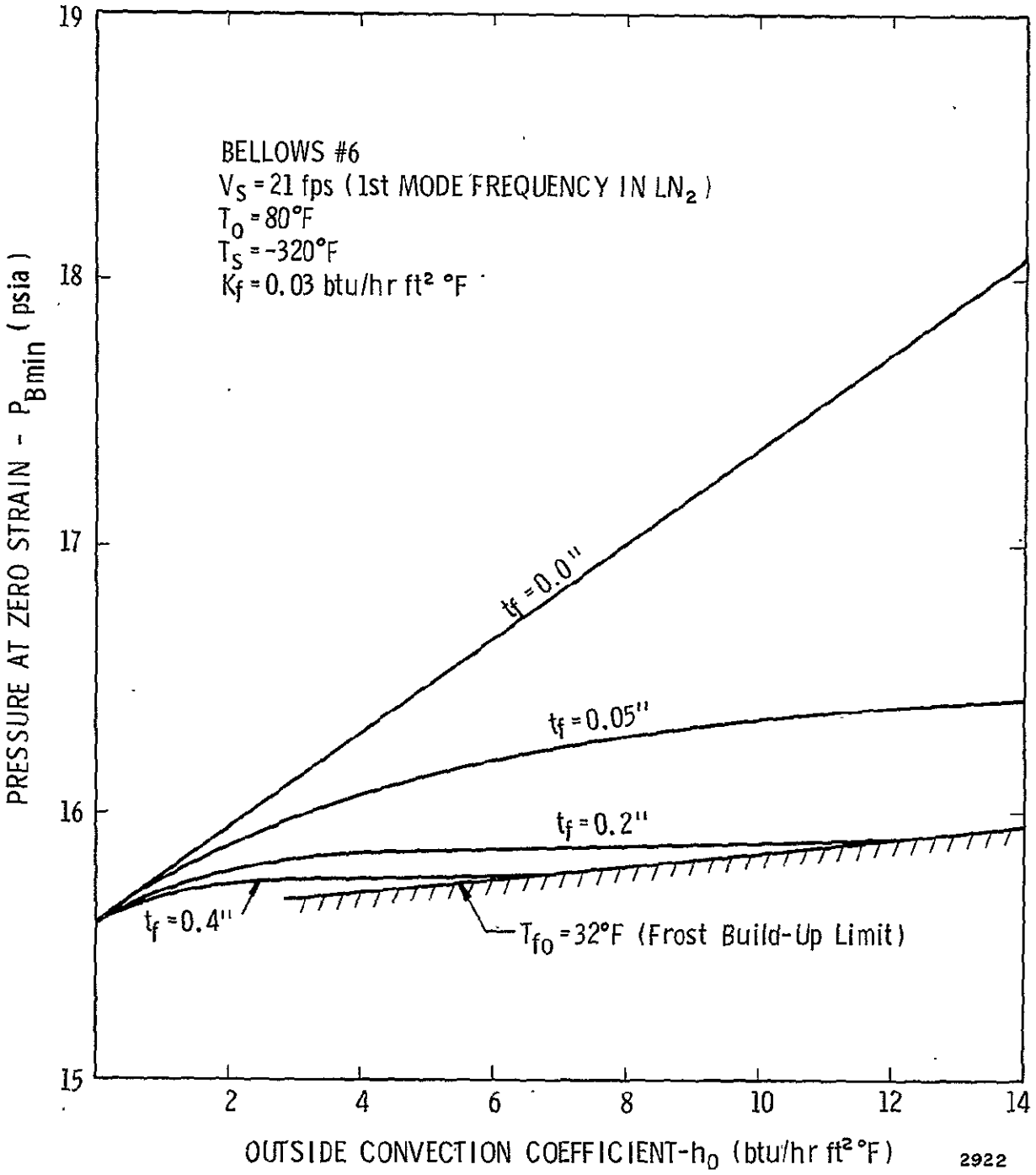

Figure 37. Bellows Pressure At Zero Strain With Frost Build-Up

transfer, Q, as determined from the environmental and stream conditions. This maximum thickness is shown in Figures 36 and 37. These results indicate that:

(a) For a given convection coefficient h_o, frost buildup insulates the bellows, reducing P_{Bmin} and P_{Bmax}.

(b) Increasing h_o at a given frost thickness results in an increase in P_{Bmax} and P_{Bmin}.

The results of the effects of frost buildup on the operating characteristics of bellows are considered adequate to indicate the expected bellows response when frosting occurs. However, it should be pointed out that assuming a constant thermal conductivity of 0.03 Btu/hr ft ^{o}F under varying conditions of frost formation is a simplification of the problem. The nature of frost formation on cryogenic feed lines is extremely complicated and depends on the relative humidity, the temperature and other factors. Experimental values of frost thermal conductivity vary, and the choice of the frost conductivity was made after a review of the literature, and is considered to be adequate for this analysis.

Geometric Effects

An examination of the heat transfer model presented in this report will show the effects of bellows geometry on the combined heat transfer/cavitation phenomena that alters bellows flow induced response. Consider Equations (11) and (15) for determining the heat transfer and bellows inside wall temperature, respectively. If the heat transferred per unit wall area is based on the inside wall area, A_{wi}, then Equation (11) becomes

$$\frac{\dot{Q}^*}{A_{wi}} = \frac{T_o - T_s}{A_{wi}\,\Sigma R} \tag{24}$$

and Equation (15) can be written as

$$T_{wi} = T_s + \frac{\dot{Q}^*}{A_{wi}}\, R_4\, A_{wi} \tag{25}$$

If $\dot{Q}^*/A_{wi}$ and $R_4 A_{wi}$ are dependent on bellows geometry then T_{wi} and P_v will also depend on geometry.

First, examining the term $R_4 A_{wi}$, we find

$$R_4 A_{wi} = \frac{1}{h_i} \tag{26}$$

Therefore, $R_4 A_{wi}$ is independent of geometry except as h_i is altered by changes in convolute shape.

Next, examine $\dot{Q}^*/A_{wi}$

$$\frac{\dot{Q}^*}{A_{wi}} = \left(\frac{T_o - T_s}{A_{wi}}\right)\left\{\frac{1}{A_{wo}h_o} + \frac{1}{2\pi\ell}\left[\frac{1}{K_f}\ln\left(\frac{r_m + t_f + t_w}{r_m + t_w}\right) + \frac{1}{K_w}\ln\left(\frac{r_m + t_w}{r_m}\right)\right] + \frac{1}{A_{wi}h_i}\right\}^{-1} \tag{27}$$

for the case of a thin walled cylinder where the thickness is such that

$$\frac{r_2 - r_1}{r_1} < 0.1 \tag{28}$$

then $\ln(r_2/r_1)$ can be estimated within 5 percent by $(r_2 - r_1)/r_1$.

Therefore, the wall and frost resistances can be estimated by

$$R_2 = \frac{t_w}{K_w A_{wi}} \tag{29}$$

$$R_3 = \frac{t_f}{K_f A_{wo}} \tag{30}$$

if condition (28) is valid. Condition (28) is valid for 2-inch diameter bellows with frost thickness of 0.1 inch or less, and the assumption becomes more accurate for larger diameter bellows at greater frost thicknesses.

Utilizing R_2 and R_3 as given by Equations (29) and (30) yields

$$\frac{\dot{Q}^*}{A_{wi}} = \left(\frac{T_o - T_s}{A_{wi}}\right)\left\{\frac{1}{A_{wo}h_o} + \frac{t_w}{A_{wi}K_w} + \frac{t_f}{A_{wo}K_f} + \frac{1}{A_{wi}h_i}\right\}^{-1} \tag{31}$$

and since

$$A_{wo} \cong A_{wi} \qquad \text{for condition (28)}$$

then

$$\frac{\dot{Q}^*}{A_{wi}} = (T_o - T_s)\left\{\frac{1}{h_o} + \frac{t_w}{K_w} + \frac{t_f}{K_f} + \frac{1}{h_i}\right\}^{-1} \tag{32}$$

the expression for heat transfer through a slab of area A_{wi}.

Since the wall resistance (t_w/K_w) is negligible compared to the other resistances and t_w is small for most bellows, the resulting expression for $\dot{Q}^*/A_{wi}$ is independent of bellows geometry and is only a function of the environmental conditions. Therefore, the inside wall temperature used to determine the vapor pressure will be strongly dependent on the bellows inside and outside conditions (i.e., T_0, T_s, t_f, K_f, h_i and h_o) and only a weak function of bellows geometry. This will be true only if the simplifying assumption of heat transfer to a thin walled cylinder is an accurate model and if the bellows is small enough to prevent sufficient heat transfer from producing an appreciable temperature drop between bellows inlet and exit. The restriction on constant stream temperature between the bellows entrance and exit should be valid for short bellows under the low rates of heat transfer represented by the environmental conditions considered.

Next, the effect of geometry on P_{Bmax} and P_{Bmin} must be considered. Solving (21) and (22) for P_{Bmax} and P_{Bmin} yields

$$P_{Bmax} = P_{v@T_{wi}} + \sigma_m \, q_\infty \tag{33}$$

and

$$P_{Bmin} = P_{v@T_{wi}} + \sigma_o \, q_\infty \tag{34}$$

The effect of bellows geometry on P_v was shown to be minor, leaving only σq_∞ to be analyzed. No experimental data is available on cavitation numbers at maximum and minimum strain except for the 2-inch bellows. It is assumed that σ_o and σ_m will not change drastically with bellows geometry changes. However, the bellows velocity at which vortex shedding occurs is dependent on bellows geometry and the different modes of vibration will occur at different velocities. This change in velocity with geometry and vibrational mode will change the σq_∞ terms in Equations (33) and (34) resulting in changing the values of P_{Bmax} and P_{Bmin}. The results of geometry effects can be summarized as follows:

(a) Bellows geometry differences for short bellows will produce negligible changes in the calculated vapor pressure for a given set of environmental and flow conditions. Therefore, results presented in Figures 34 to 37 for a 2-inch bellows should be valid for other diameters flowing LN_2 at 21 fps and -320°F.

(b) Bellows geometry differences will change the estimate of P_{Bmax} and P_{Bmin} since geometry affects the velocity for a given vibrational mode.

General Remarks

All results are presented for velocities corresponding to the first vibrational mode. No data has been taken at higher mode frequencies to confirm the accuracy of this analysis. Also, Equation (15) used to determine h_i will be affected by changes in Reynolds number through changing V_∞ and D_m. When forced convection on the outside wall of the bellows becomes severe enough, the inside wall temperature will exceed the point where boiling heat transfer can be ignored. Under these unusual conditions, Equations (16) and (17) should be used only as an order of magnitude estimate of h_i as they do not directly apply to cryogenic flow in a pipe. Also, the validity of Equation (6) is questionable at Reynolds numbers much above 10^6 as the data this equation was based on covers an Re range up to 10^5.

In general, the analysis should be adequate to yield an accurate estimate of operating pressures to insure that cavitation does not occur under a given environmental situation.

VI. EXTERNAL DAMPING

VI.1 Introduction

The prior discussions in this report have been devoted primarily to one type of mechanism which can suppress bellows flow excitation where cryogenic liquids are the flow media. This suppression was caused by vapor formation in the flowing liquid which directly affected the vortex shedding phenomena, and reduced the magnitude of the periodic force. Another possible suppression mechanism where cryogens are the flow media is the extra damping introduced by the external buildup of some combination of ice, frost, or condensed air. Experiments have been conducted to determine the damping introduced by these three types of external media, and the results are described in the following discussions.

VI.2 Frost and Ice Damping

Frost buildup alone on a bellows with an internal cryogen flow has a minor to negligible effect on the amplitude of flow-induced vibrations. Several experiments were conducted to determine if the vibration was suppressed by frost formation, and in all cases where frost alone was present, no truly significant reduction was noted. This was true even for heavy frost buildups. Figure 38 illustrates frost conditions typical of those for which tests were conducted.

The fact that frost alone yielded negligible external damping is understandable since this media has a very low mass, based on total volume occupied, and may be easily "crushed". Therefore, when bellows vibrations occur, the built-up frost offers negligible resistance to convolute motion.

External ice buildup with internal cryogen flow may or may not cause suppression of the flow-induced vibrations. As might be expected, if the ice buildup is of sufficient magnitude so that the spaces between the convolutes are largely filled with ice, then no vibrations will occur.

When thinner ice coatings are present, low energy vibrations are completely suppressed, but high energy level vibrations cause the ice coating to crack and fall off so that the original or undamped (external damping) vibration amplitude is restored. Figure 39 illustrates this phenomena. The top strain-velocity curve illustrates flow-induced vibrations of a bellows with no external damping media. Figure 39b illustrates the behavior of a bellows with a light ice buildup. Note that the first mode (lower energy level mode)

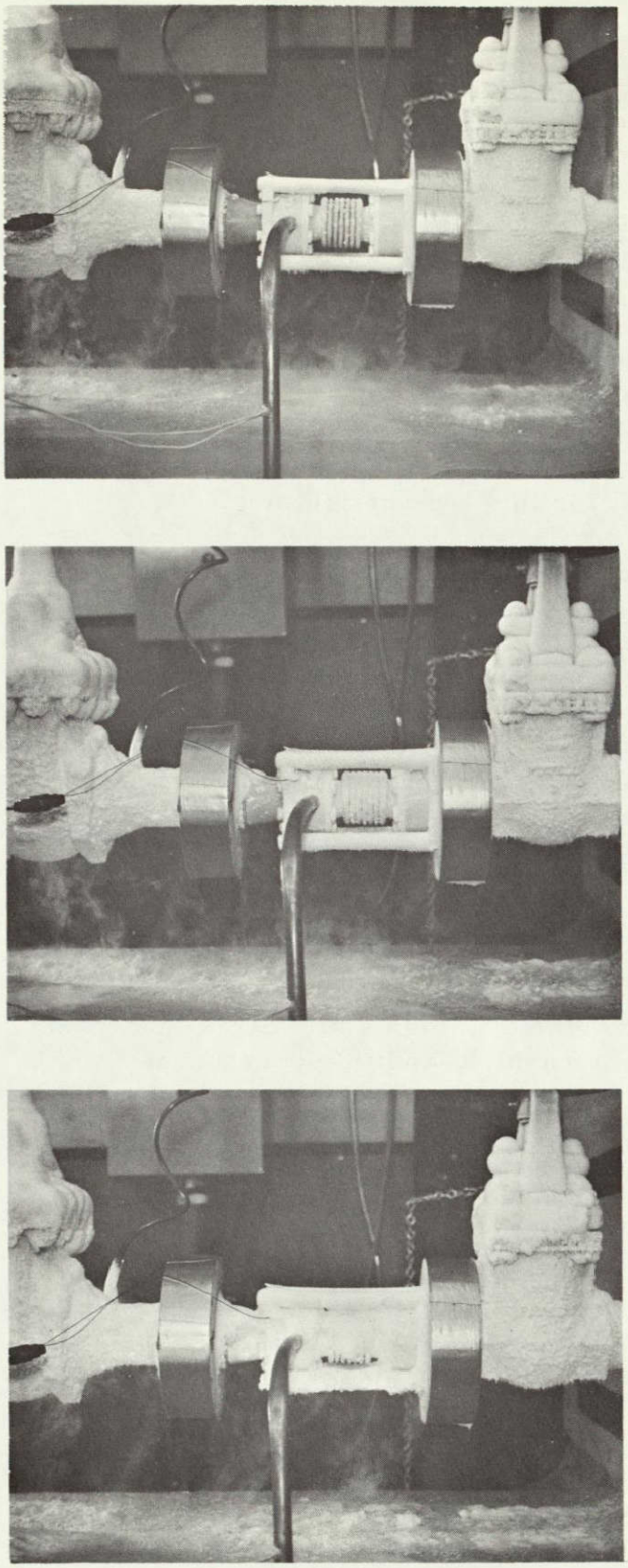

Figure 38. Photographs Of Frost Builtup On Test Bellows With Internal LN_2 Flow

is completely suppressed. The second mode, however, is only suppressed up to a certain maximum velocity where breakup of the ice occurs and the original vibration amplitudes are thereby restored.

VI.3 External Liquid Damping

Experiments conducted in the laboratory revealed that bellows damping, because of the presence of an external liquid, can be quite significant. Since such a condition generally occurs only where liquid hydrogen or helium is the flow media, our experiments were conducted under simulated conditions employing external water damping on bellows flowing water and air. In conjunction with these experiments, an analysis was performed to develop a mathematical model for this type of damping.

Figure 40 illustrates the mechanism believed to be responsible for damping of a bellows covered on the outside by a liquid. As shown, vibratory motion of the convolutes causes the external liquid to be periodically forced in and out of the space between convolutes. Estimates of the Reynolds number typical for this periodic motion show that a transient turbulent situation likely exists. Therefore, it is reasonable to expect that this external periodic fluid motion will produce a damping force on the vibrating convolutes. This force, because of the turbulent dissipation mechanism, will be proportional to the convolute relative velocity to the second power.

Based on the above hypothesis for external liquid damping, a mathematical model has been developed for the convolute vibrations for a case where external damping alone is present (no conventional damping). The results have been formulated in terms of a Stress Indicator equation, to be compatible with earlier results, and this equation is

$$SI_e = \frac{\epsilon\, \delta\, t E N_p}{f h^3} \sqrt{\frac{C_F\, p_d}{\rho_e}} \quad , \epsilon \approx 0.25 \qquad (35)$$

where

SI_e = Stress Indicator for external damping alone
ϵ = Empirical constant, $\epsilon \approx 0.25$
E = Young's modulus for bellows material
t = Bellows wall thickness per ply
δ = Space between convolute tips
N_p = Number of plys
f = Bellows vibration frequency
h = Convolute height
C_F = Vortex force coefficient
p_d = Internal dynamic fluid pressure
ρ_e = External media mass density

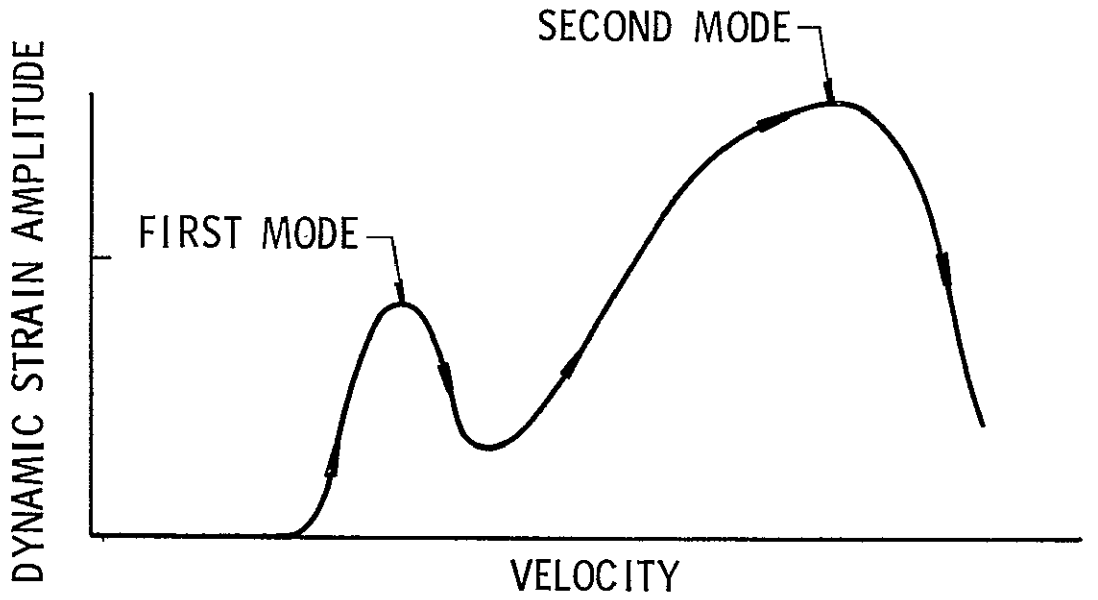

(a) STRAIN-VELOCITY PLOT WHERE NO EXTERNAL ICE IS PRESENT

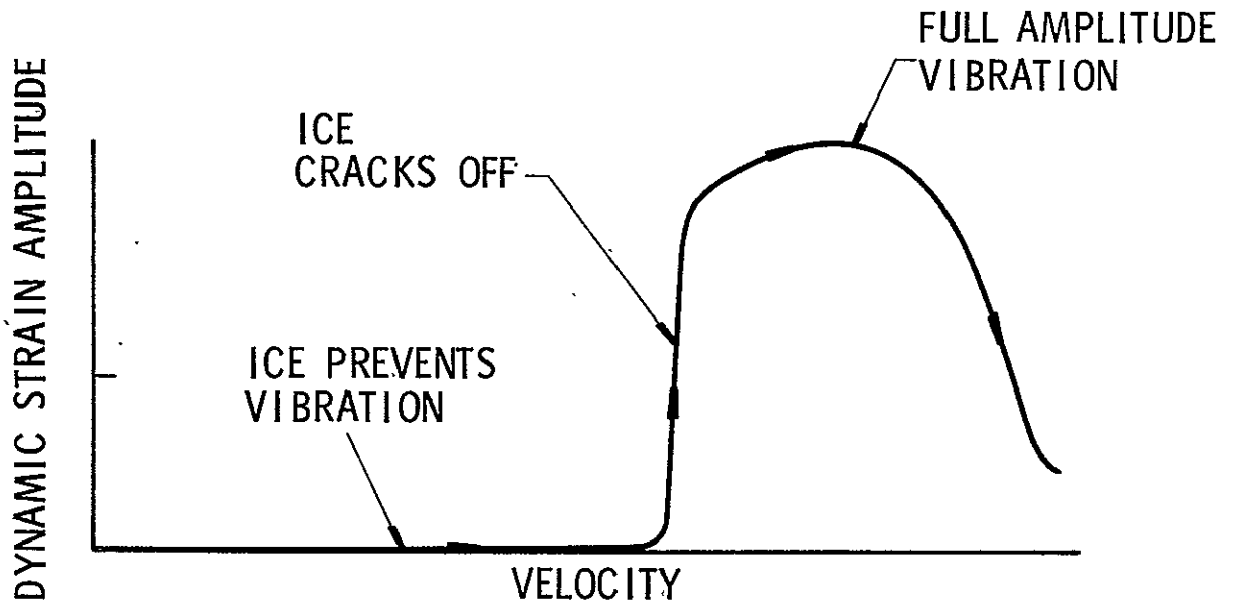

(b) STRAIN-VELOCITY PLOT WHERE THIN ICE COAT IS PRESENT

2927

Figure 39. Illustration Of Bellows Flow-Induced Vibration With And Without External Ice Builtup For Velocity Upsweep

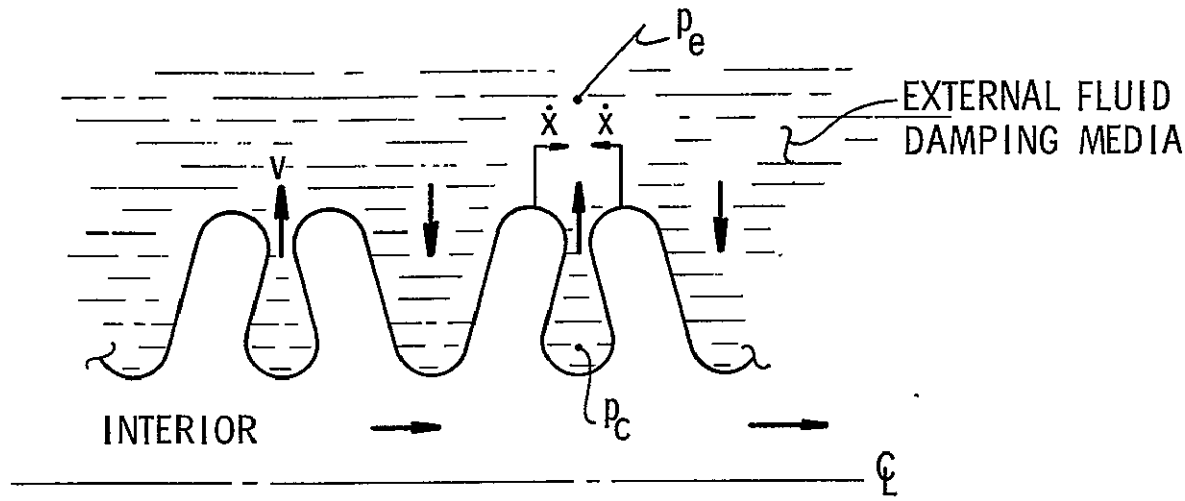

- CONVOLUTE RELATIVE VELOCITY $2\dot{x}$ GIVES DISCHARGE VELOCITY OF

$$v \approx \frac{\dot{x}h}{\delta}$$

- THIS FLUID MOTION, IF TURBULENT, GIVES A PRESSURE DIFFERENTIAL OF

$$|p_c - p_e| \approx \epsilon_1 \rho v^2$$

WHERE ϵ_1 IS AN EMPIRICAL CONSTANT

- THIS PRESSURE DIFFERENTIAL MAY BE INTERPRETED AS A FLUID DAMPING FORCE

$$F_d = (\pi D_m h)(\epsilon_1 \rho v^2) = b\dot{x}^2$$

2930

Figure 40. Illustraion Of External Fluid Damping Mechanism

Since some conventional damping is always present, Equation (35) does not indicate the true bellows flow-induced stress level, but only the external damping limited part. To get the true or correct Stress Indicator, it is necessary to combine the conventional value and the external damping value. This may be done by the expression below, or

$$SI_c = \left\{ \frac{1}{\frac{1}{SI} + \frac{1}{SI_e}} \right\} \tag{36}$$

where

SI = Stress Indicator for Conventional Damping (see Reference 1)

SI_e = Stress Indicator for External Damping Alone (see Equation (35)).

In order to judge the severity of bellows vibrations from a calculation of SI_c, the results given in Figure 48 of Reference 1 apply; this figure has been reproduced as Figure 4 in this report. It must be emphasized that the empirical constant ϵ in Equation (35) was obtained from a limited amount of experimental data, and therefore the value indicated above is tentative.

VII. APPLICATION OF RESULTS

VII.1 Summary of Use of Results

This report has described results of an investigation of bellows flow-induced vibrations where a cryogen is the flow media. It has been demonstrated that the phenomena is predictable by the method presented in Reference 1, except for two important limiting cases. First, if boiling and/or cavitation occurs in the bellows, then the vortex shedding, hence vibrations, will be suppressed. Second, the presence of an external buildup of frost, ice or condensing liquid can also suppress the vibrations. The data in Reference 1 provides an upper-limit prediction of vibration amplitudes, and the phenomena described herein are vibration suppression mechanisms.

From the standpoint of a designer or test engineer, it is important that these possible suppression mechanisms be recognized so that the worst-case condition is examined in any design or test activity. The case history reported in Reference 2 is dramatic evidence of the importance of recognizing these suppression mechanisms.

As an aid to the reader, the following sections have been prepared summarizing a procedure which might be followed in predicting these flow-excitation suppression effects.

Suppression by Internal Vapor Formation

Utilizing the heat transfer analysis presented in this report to determine when flow excitation of a bellows will be suppressed proceeds as follows:

(a) Using the results of Reference 1, determine the flow velocity where flow excitation is expected.

(b) Calculate the internal heat transfer coefficient h_i from Equation (15) by determining the Reynolds number Re_d and Prandtl number P_r at the stream conditions, and friction factor ratio f*/fo* from Reference 1. Base the Nusselt number Nu on D_o, and base Re_d on D_i for a conservative h_i estimate.

(c) Determine the external heat transfer coefficient h_o from a knowledge of bellows environmental conditions. Use Equation (19) for forced flow over the bellows or any other suitable expression for the expected bellows environmental condition, (i.e., natural or forced convection or condensation). If frost is present, estimate its thickness and conductivity.

(d) Calculate the overall heat transfer from Equation (32).

(e) Calculate the bellows inner wall temperature T_{wi} from Equation (25).

(f) Determine the cryogen vapor pressure P_v at temperature T_{wi} from Equation (23) for LN_2 or an appropriate expression for other cryogenics.

(g) Using the cavitation number limits σo and σm of 0.4 and 2.25, respectively, calculate the operating pressures P_{Bmin} and P_{Bmax} from Equations (33) and (34). These defining cavitation numbers resulted from LN_2 experimental data but should be adequate for predicting strain suppression with other liquids as the flowing medium.

(h) If the bellows operating pressure is above P_{Bmax}, flow-induced response is possible and predictable by the method of Reference 1. If the operating pressure is between P_{Bmax} and P_{Bmin} some damping of the response is expected. If the operating pressure is below P_{Bmin}, no flow-induced response will occur.

External Damping Vibration Suppression

The damping effect of frost alone can be neglected. Thus, for liquid oxygen and liquid nitrogen flows where a buildup of frost alone is usually the case, the results of Reference 1 apply but the possibility of internal vapor formation exists, and must be examined by the above procedure.

Ice formation may or may not produce a damping effect, depending on the level of buildup. In the laboratory, ice occurred only by deliberately pouring water on the bellows, or by periodic melting of the frost layer with external heating. Ice buildup should be treated as a very special case, the effect of which can only be accurately determined from laboratory testing.

External liquid (air) condensation will generally occur only for liquid hydrogen or cold helium flows. An estimate of the vibration severity with this damping mechanism present may be made by the procedure given in Section VI.3 of this report.

Realistic Testing

It should be evident from the results in this report that in performing flow-induced vibration tests on a bellows with internal cryogenic liquid flows, one must properly allow for possible vapor formation or external damping. If the bellows is to be operated under conditions where no external heating or damping media buildup is possible, such as in a vacuum, then the bellows should be tested under the same conditions. The only possible shortcut found in the laboratory was to use an external purge of the cold boil-off gas from the test to minimize heating and external damping effects. This means use cold GN_2, GOX or GH_2 where LN_2, LOX or LH_2 are the flow media, respectively. Practical difficulties may make it easier to go ahead and provide an external vacuum environment rather than use this procedure, however.

For monitoring flow-induced vibrations of bellows, experience has shown that only convolute strain measurements are absolutely reliable. Other monitoring methods such as duct vibration, internal pressure measurements, and external acoustic emission have been evaluated. In general, these other methods are undesirable, except for providing qualitative information, because they give output signals with an unrealistic frequency content. Examination of the spectral content of a duct acceleration signal, for example, often shows vibrational energy at the actual bellows frequency plus several harmonics of this frequency. A convolute strain signal from the same bellows will only reveal significant energy at the actual bellows frequency.

Because of the high frequencies involved, and the severity of the vibrations, proper mounting of strain gages can be a problem. Thorough cleaning of the convolute surface and use of an epoxy for mounting the gages has resulted in reliable installations in our laboratory. Only very fine lead wires (≈ 0.005 inch) should be soldered directly to the convolute strain gages. These fine wires should be attached to the main signal leads at terminal strips cemented on the duct adjoining the bellows. A fine coat of rubber cement should be put on the small lead wires to provide some damping and help prevent wire fatigue failures. Care must be taken to ensure that the output instrumentation has adequate frequency response for the signals anticipated.

VII.2 Example Situation

Reference 2 discussed bellows flow induced response changes with changing environmental conditions, and resulted from an investigation into the failure of a braided bellows (J-2 engine, ASI line) carrying LH_2 with an external vacuum environment. The failure was attributed to the bellows

being qualification tested in a normal atmospheric environment which created suppression of the flow-induced vibrations, hence, did not allow maximum vibratory strain to occur. The authors of Reference 2 indicated that air condensing between the convolutes and the braid caused suppression of the bellows vibrations. However, the authors seem to relate this to a heat transfer effect, which is highly unlikely. By their own calculations the bellows wall temperature with film condensation was -396°F with the hydrogen flowing at -400°F and 1000 psia (our own analysis confirms this). A 4° change in temperature between the wall and bulk flow at 1000 psi was too small to cause a density gradient sufficient to influence the vortex shedding.

The mechanism responsible for the reduced response under these conditions was most likely the added damping action of the external liquid air. Application of the external liquid damping model (see Section VI.3) to this ASI line case, indicates that this particular suppression mechanism could have reduced the flow-induced vibrations to about 20 percent of the vibration level observed with an external vacuum.

In Reference 2, the conclusion that heat transfer caused the vibration suppression of the ASI line was based, in part, on a test where hot helium gas at a mean temperature of 285°F was blown over the bellows surface. It appears from the figures in Reference 2 that this forced heating created a fluid temperature in the convolutes of -330°F compared with -400°F in the bulk flow. This type of temperature change could have produced a sufficient density gradient in the convolutes to suppress the vortex shedding and reduce the vibrational response. However, the amount of heat transferred with the hot helium was about 17 greater than for the case with condensing air, assuming the inside wall heat transfer coefficient didn't change. Therefore, the two cases were not analogous, and the reduced bellows response, in our judgment, was created by a different phenomena for each case. That is, with condensation, liquid air damped the response, while for the hot helium test a density gradient in the convolutes probably suppressed the vortex shedding.

It should be noted that, since the tests in Reference 2 were performed at pressures above the critical pressure (1000 versus 188 psia), the state of the hydrogen in the bellows was not well defined in terms of being a liquid or vapor. At super-critical pressures a liquid and vapor phase cannot exist simultaneously, and any large temperature difference that exists between the bellows wall and bulk flow as the result of heat transfer will only cause a density reduction of the fluid in the convolutes which could lead to a change in the vortex shedding.

VIII. CONCLUSIONS AND RECOMMENDATIONS

VIII.1 Conclusions

A number of conclusions have been derived from the study reported herein; these are:

(a) Vibrations excited in bellows by the internal flow of a cryogenic liquid are caused by the same fluid-elastic instability reported in Reference 1 for internal water and air flows.

(b) Where no internal boiling or phase change occurs, and where no frost, ice or condensed liquid appears on the bellows exterior, the flow-induced vibration with an internal cryogen is predictable by the method reported in Reference 1.

(c) If a phase change of the flowing media occurs and/or external frost, ice or condensed liquid is allowed to form, then the bellows vibration amplitudes, hence, the dynamic strain levels, will be reduced from the condition of (b).

(d) The conditions under which an internal phase change will produce suppression of the bellows flow-excitation are predictable. An analysis for making this prediction is presented in this report.

(e) The presence of frost on a bellows can produce a negligible reduction of the vibration amplitudes by virtue of some added damping.

(f) If built up prior to the initiation of flow, a heavy ice layer can completely suppress flow-induced vibrations of bellows. If, however, the ice is formed after flow-excitation is initiated, the convolute vibrations will prevent large buildups by causing the ice to crack and fall off. Ice buildup on a bellows is generally a rare occurrence unless water is purposely poured over the cold convolutes.

(g) Condensation of significant quantities of gas constituents from the ambient surroundings can produce a significant damping of the bellows flow-induced vibrations. This condensation would be most pronounced for internal liquid hydrogen or cold helium flows. A model for predicting vibration amplitudes when an external liquid is present is given in this report.

VIII. 2 Recommendations

We have several recommendations to make regarding the results of this report:

(a) Each application of a bellows where an internal cryogen is involved should be carefully examined to determine the possibility of flow-induced vibrations in all operating environments expected.

(b) Where no heat transfer effect or external damping is anticipated, the results in Reference 1 should be used for prediction purposes.

(c) Where heat transfer and/or external media effects are anticipated, the results given in the present report should be used.

APPENDIX A

LIST OF SYMBOLS

LIST OF SYMBOLS

A_p	=	Projected convolute area ($\pi D_m h$)
A_{wi}	=	Inside wall area
A_{wo}	=	Outside wall area
C_F	=	Vortex force coefficient
C_m	=	Bellows vibration mode factor
C_p	=	Specific heat at constant pressure
D_i	=	Inside bellows diameter
D_m	=	Mean bellows diameter
D_o	=	Outside bellows diameter
f^*	=	Bellows friction factor
f_o	=	Bellows reference frequency
f_o^*	=	Smooth pipe friction factor
h	=	Convolute height
h_{fg}	=	Enthalpy of vaporization
h_i	=	Inside convection coefficient
h_o	=	Outside convection coefficient
K_A	=	Bellows spring rate
K_f	=	Thermal conductivity of frost
K_v	=	Thermal conductivity of vapor
K_w	=	Thermal conductivity of wall
ℓ	=	Bellows length for heat transfer model
m	=	Bellows elemental mass
N	=	Bellows vibration mode number

List of Symbols...Cont'd.

N_c	=	Number of convolutes
N_p	=	Number of plys in bellows wall
N_u	=	Nusselt Number
P_B	=	Bellows Pressure
P_{Bmax}	=	Bellows pressure at maximum strain
P_{Bmin}	=	Bellows pressure at zero strain
P_r	=	Prandtl number
P_T	=	Tank pressure
q_∞	=	Stream dynamic pressure
Q	=	Dynamic amplification factor, a measure of damping
Q^*	=	Heat transfer
r_m	=	Mean bellows radius
R	=	Resistance to heat transfer
Re_d	=	Reynolds number
t	=	Bellows ply thickness
t_f	=	Frost thickness
t_w	=	Wall thickness
T_{fo}	=	Outside frost temperature
T_o	=	Environmental temperature
T_s	=	Stream temperature
T_w	=	Wall temperature
V	=	Flow velocity

List of Symbols...Cont'd.

μ_ℓ = Viscosity of Liquid

ν = Kinematic Viscosity

σ = Convolute width

σ_m = Cavitation number at maximum strain

σ_o = Cavitation number at zero strain

ρ_e = External media density in damping model

ρ_ℓ = Liquid density

ρ_v = Vapor density

τ = Surface tension

APPENDIX B

HEAT TRANSFER COMPUTER PROGRAM

Heat Transfer Program Listing

```
      PROGRAM N2HEAT(INPUT,OUTPUT)
    1 READ 2,V,DI,DO,SIG,FNC,TS,FF,FLW,Z,FKF                  Read: Flow Velocity, Bellows Inside and Outside Diameter
    2 FORMAT(10F6.4)                                          Convolute Width, Number of Convolutes, Stream Temp,
      DD=(DI+DO)/2.                                           Bellows Friction Factor, Wall Thickness and Frost Conductivity
      FLL=2.*FNC*((DO-DI)/2.)+(2.*FNC-1.)*SIG                 — Mean Diameter
      AW=(3.14*DD*FLL)/144.0                                  — Wall Equivalent length
      FKW=10.0                                                — Wall area
      AA1=6.28*FLL*FKW/12.0                                   — Wall Conductivity
      AA2=6.28*FLL*FKF/12.0
      RR=DD/2.0
      R3=(ALOG((RR+FLW)/RR))/AA1                              — Wall Resistance
      DN=50.4                                                 — LN2 Density
      VISN=3.2E-06                                            — LN2 Viscosity
      CPN=.475                                                — LN2 Specific Heat
      FKN=.0789                                               — LN2 Thermal Conductivity
      RE=(DN*V*DI)/(12*32.2*VISN)                             — Flow Reynolds No.
      FO=.015                                                 — Smooth Pipe Friction Factor
      FPR=(VISN*CPN/FKN)*3600*32.2                            — Prandtl No.
      FPR=(FF/FO)*FPR                                         — Modified Prandtl No.
      A=1.5/(FPR**.167)
      B=FPR-1.0
      RNU=(.0384*(RE**0.75)*FPR)/(1.0+(A/(RE **.125)) * B)    — Nusselt No.
      FHI=(FNU*FKN*12.0)/DD                                   — Inside Convection Coefficient
      R4=1.0/(FHI*AW)                                         — Inside Resistance
      PRINT 36,FHI,   R3,R4
   36 FORMAT(30X,F10.4,2F10.6)
      A1=0.527805
      A2=-305.07339
      A3=.16441101
      A4=-.00313892
      A5=2.9857103E-05
      A6=-1.4238458E-07
      A7=2.7375282E-10
      CAV01=0.0                                               — Cavitation Number Range at
      CAV02=1.5                                               — Zero Strain
      CAVM1=1.6                                               — Cavitation Number Range
      CAVM2=3.0                                               — at Maximum Strain
      DP=(50.4*V**2)/(64.4*144.)                              — Dynamic Pressure
      FLF=0.0                                                 — Initial Frost Thickness
    5 TO=-249.0                                               — Initial Environmental Temp
    7 FHO=2.0                                                 — Initial Outside Convection Coefficient
    3 R1=1.0/(FHO*AW)
      R1=R1*(RR/(RR+FLW+FLF))                                 — Outside Resistance
      R2=(ALOG((RR+FLW*FLF)/(RR+FLW)))/AA2                    — Frost Resistance
      R=R1+R2+R3+R4                                           — Total Resistance
      Q=(TO-TS)/R                                             — Heat Transfer
      TF=TO-Q*R1                                              — Outside Frost Temp
      TWI=TS+Q*R4                                             — Inside Wall Temp
      TR=TWI+459.6
      TK=TR/1.8
      ATM=A1+A2/TK+A3*TK+A4*TK**2+A5*TK**3+A6*TK**4+A7*TK**5
      FPV=14.69*(10.0**ATM)                                   — Vapor Pressure at TWI
      FP01=FPV+CAV01*DP                                       — Pressure Range at
      FP02=FPV+CAV02*DP                                       — Zero Strain
      FPM1=FPV+CAVM1*DP                                       — Pressure Range at
      FPM2=FPV+CAVM2*DP                                       — Maximum Strain
      PRINT40,TO,TS,FHO,R1,R2,R,Q,TF,TWI,FPV,FP01,FP02,FPM1,FPM2
   40 FORMAT(2F10.2,4F10.6,3F13.6,5F6.2)
      FHO=FHO+2.0                                             — Change Outside Convection Coefficient
      IF(FHO-20.0)3,3,4
    4 TO=TO+40.0                                              — Change Environmental Temperature
      IF(TO-300.0)7,7,8
    8 FLF=FLF+0.05                                            — Change Frost Thickness
      IF(FLF-0.5)5,5,9
    9 IF(Z-1.0)1,6,6
    6 CONTINUE
      STOP
      END
```

REFERENCES

1. Gerlach, C. R. and Schroeder, E. C., "Study of Minimum Pressure Loss in High Velocity Duct Systems," Interim Technical Report No. 1, Contract NAS8-21133, Southwest Research Institute, July 1969.

2. Daniels, C. M. and Fargo, C. G., "Fatigue Failure in Metal Bellows Due to Flow-Induced Vibrations," Technical Support Package (TSP 69-10071) for NASA Tech. Brief 69-10071.

3. Nunner, W., and Wärmeübergang and Druckabfall in rauhen Rohren, VDI-Forschungsheft, p. 455, 1956.

4. Rohsenow, W. M. and Clark, J. A., Heat Transfer and Fluid Mechanics Institute, Stanford University Press, Stanford, Calif., pp. 193-207, 1951.

5. Bromley, L. A., et al., "Heat Transfer in Forced Convection Film Boiling," Industrial and Engineering Chemistry, p. 2639, 1953.

6. Strobridge, T. R., "The Thermodynamic Properties of Nitrogen from 64 to 300°K Between 0.1 and 200 Atmospheres, NBS TN 129, p. 4, January 1962.

7. Fand, R. M., "Mechanism of Interaction Between Vibrations and Heat Transfer," Journal of the Acoustical Society of America, 34, 12, p. 1887, 1962.

8. Vance, R. W., Editor, Cryogenic Technology, John Wiley and Sons, Inc., New York, 1963, p. 177.